BINARY ALLOY SURFACES.

SURFACE SEGREGATION AND THE EFFECTS OF ION BOMBARDMENT ON THE SURFACE COMPOSITION OF Cr-Mo ALLOYS

By

SABINO A. PETRONE, B.Sc.

A Thesis

Submitted to the School of Graduate Studies

in Partial Fulfilment of the Requirements

for the Degree

Doctor of Philosophy

McMaster University

© April 1987

BINARY ALLOY SURFACES

DOCTOR OF PHILOSOPHY (1987) McMASTER UNIVERSITY
(Chemistry) Hamilton, Ontario

TITLE: Binary Alloy Surfaces: Surface Segregation and the Effects of Ion Bombardment on the Surface Composition of Cr-Mo Alloys

AUTHOR: Sabino A. Petrone, B.Sc. (McMaster University)

SUPERVISOR: Professor P.T. Dawson

NUMBER OF PAGES: xvii, 216

ABSTRACT

This thesis reports on a comprehensive investigation of the relationship between binary alloy surface composition and the externally controllable parameters of irradiating conditions, temperature and bulk composition.

The Cr-Mo binary system was used as the model system as it provides appreciable differences in the driving forces considered to play a significant role in surface segregation: atomic interaction energy and size. The Unified Segregation Model, adopted for theoretical analysis, predicted a cross-over in the segregating element from one end of the composition range to the other.

Quantitative surface analysis was performed using Auger Electron Spectroscopy. A major limitation to the accuracy attained was identified with differences in surface roughness between the alloy and elemental standards. An investigation was carried out to establish a correlation between sputtering, crystal orientation and surface roughness. The effect of surface roughness on the detected Auger current was quantified and procedures established for its minimization.

Surface compositional modifications of thirteen Cr-Mo alloys, subject to 2 KeV argon ion bombardment, have been established. A preferential sputtering of Cr has been observed across the entire composition range. The results have been interpreted in terms of a phenomenological

preferential sputtering model yielding a sputter rate constant ratio $K = 1.73 \pm 0.04$ in good agreement with theoretical prediction and the ratio of the sputter yields of the pure metals.

The surface segregation phenomenon has been investigated across the entire composition range. In the temperature range of 875-1075 K, the results reveal non-equilibrium effects which can occur when using sputter-cleaned alloys for segregation studies. A kinetic analysis of the segregation has yielded an insight into the activated processes that occur upon annealing a sputter-modified surface and the corresponding activation energies for diffusion.

Layer calculations, using a monolayer segregation model, have been used to determine the outer monolayer composition from that averaged over the finite escape depth of the Auger electrons. The calculated compositions have provided a qualitative and a quantitative test of the theoretical segregation model. The results have also yielded an enthalpy of segregation and an experimental estimation of the inelastic mean-free paths of the Auger electrons used in the analysis.

ACKNOWLEDGEMENTS

I would like to thank the technical staff in the Institute for Materials Research. In particular, J.D. Garrett, P. Hammond, and J.M. Hudak, whose suggestions and assistance with sample preparation and characterization is appreciated.

Special thanks go to C. Schonfeld and J.I.A. Thompson for their valuable advice and assistance with electronic related aspects of the research.

I would like to thank Professors J.A. Morrison and D.S. Wilkinson for their valuable suggestions over the course of this study and in the preparation of this thesis.

Above all, I am indebted to Professor P.T. Dawson, my research supervisor. His guidance and encouragement is gratefully appreciated. To the many discussions that I've held with Professor Dawson, I owe my growing interest in and knowledge of the field of Surface Science. His criticisms and suggestions of this work have been invaluable in the preparation of this thesis.

This research was supported by grants from the Natural Sciences and Engineering Council of Canada. Financial support from the McMaster University Department of Chemistry is gratefully appreciated.

TABLE OF CONTENTS

CHAPTER 1: INTRODUCTION

1.1. Alloy Surfaces 1

1.2. Scope of Thesis. 3

CHAPTER 2: EXPERIMENTAL METHODS

2.1. Sample Preparation and Characterization. 6

2.1.1. Alloy Preparation 6

2.1.2. Compositional Characterization by X-ray Diffraction 7

2.1.3. Crystal Orientation Determination by Laue Backscattering 9

2.1.4. Grain Structure and Surface Morphology Characterization. 9

2.2. Surface Preparation and Analysis 11

2.2.1. Surface Analysis by Auger Electron Spectroscopy. 11

2.2.2. System Development and Microprocessor Interfacing of Apparatus 18

2.2.3. Experimental Procedure. 21

CHAPTER 3: QUANTITATIVE AES

3.1. Introduction 23

3.2. Calculation from First Principles 26

3.3. Measurements Using Relative Elemental Sensitivity Factors. 27

3.3.1. Using a Published Data set. 27

3.3.2. In Situ Determination 29

3.3.3. Summary 33

3.4. Measurements Using External Reference Standards 35

3.5. Monolayer Calculation 40

3.6. Summary 45

CHAPTER 4: THE VARIATION OF AUGER CURRENT WITH SURFACE ROUGHNESS

4.1. Introduction 46

4.2. Fundamentals 49

4.3. Experimental Procedure 55

4.4. Results and Discussion 58

4.5. Summary 69

CHAPTER 5: ION BOMBARDMENT MODIFICATIONS OF ALLOY SURFACES

5.1. Introduction 71

5.2. Fundamentals 73

5.2.1. Radiation-Induced Processes 73

5.2.2. Radiation Damage Recovery 76

5.2.3. Ion and Damage Range Calculations 77

5.2.4. Damage Rate Calculations 82

5.3. Experimental Results 84

5.3.1. Steady-State Sputtered Surface Composition 84

5.3.2. Surface Composition as a Function of Analyzed Depth 84

5.3.3. The Effect of Ion Flux 92

5.3.4. Room Temperature 'Relaxation' of the Sputtered Surface 94

5.4. Discussion 96

5.4.1. A Phenomenological Model of the Sputtering Process 96

5.4.2. Comparison with Sigmund Theory of Alloy Sputtering 100

5.4.3. Comparison with Elemental Sputter Yield 101
5.4.4. The Homogeneity Question. 103
5.4.5. The Effect of Ion Flux and the Room Temperature 'Relaxation' of the Sputtered Surface. 108
5.4.6. A Unified Picture of the Sputtering Process 111

CHAPTER 6: SURFACE SEGREGATION IN Cr-Mo ALLOYS

6.1. Introduction 113
6.2. A Theoretical Analysis of the Segregation Phenomenon: The Unified Segregation Model 117
6.3. The Impurities Problem: Attaining a Binary System 120
6.4. Surface Segregation in Mo-Rich Cr-Mo Alloys 122
6.4.1. Theoretical Prediction 122
6.4.2. Experimental Results. 124
6.4.3. Discussion. 129
6.4.4. Summary 135
6.5. Limitations of the Monolayer Calculation and an Experimental Determination of IMFP Values 137
6.6. Summary 143

CHAPTER 7: A KINETIC ANALYSIS OF THE SURFACE SEGREGATION PHENOMENON IN A SPUTTER-MODIFIED Mo-RICH ALLOY

7.1. Introduction 145
7.2. Experimental Results. 147
7.3. A Kinetic Analysis of the Surface Segregation Phenomenon. 152
7.4. Discussion. 160
7.5. Summary 167

CHAPTER 8: EQUILIBRIUM SEGREGATION IN Cr-RICH Cr-Mo ALLOYS

8.1. Introduction 169

8.2. Theoretical Prediction 170

8.3. Experimental Results. 172

8.4. Discussion. 176

8.5. Summary 183

CHAPTER 9: SUMMARY AND CONCLUSIONS

9.1. Quantitative AES 185

9.2. Ion Bombardment Modifications of Alloy Surfaces. 188

9.3. Surface Segregation 191

9.3.1. Surface Segregation in Mo-Rich Cr-Mo Alloys 191

9.3.2. Experimental Determination of IMFP Values 194

9.3.3. Surface Segregation in Cr-Rich Cr-Mo Alloys 195

9.4. Suggestions for Future Work 197

9.4.1. The Effect of Surface Roughness on Quantitative AES 197

9.4.2. Compositional Modifications of Alloy Surfaces 197

9.5. Concluding Remarks 201

APPENDIX

1. Estimation of the 'Mobile Depth' from a Conservation of Mass Analysis 203

REFERENCES. 205

LIST OF FIGURES

Figure 2.1 Crystal lattice parameter as a function of bulk composition for the Cr-Mo binary alloy system.

Figure 2.2 Schematic representation of electron scattering processes in AES. After Seah [1983a].

Figure 2.3 Schematic representation of the Auger process. The radiationless XYZ Auger transition shown after primary electron excitation gives rise to the major Cr transition used in this study. The electronic energy levels are listed on the left as the binding energy in eV relative to the Fermi level. The X-ray and atomic notations are given on the right. The Auger electrons emitted by this process have a kinetic energy of 529 eV and are labelled Cr(529): $L_3M_{2,3}M_{4,5}$ ($2p_{3/2}$ $3p_{1/2,3/2}$ $3d_{3/2,5/2}$).

Figure 2.4 The dependence of the IMFP in monolayers (λ_m) on electron energy in pure elements. After Seah and Dench [1979].

Figure 2.5 An Auger spectrum collected in the dN(E)/dE mode of an annealed 83.4 at.% Cr-Mo alloy. The major Mo and Cr transitions are shown along with the contaminants that posed severe problems in the segregation studies of the binary system.

Figure 2.6 A schematic representation of the experimental apparatus indicating AES, ion bombardment and annealing capabilities. The complete system is under microprocessor control. The modifications and additions made by this author are enclosed by the dashed lines.

Figure 4.1 The profile of an arbitrary surface from Fadley [1976]. Both the experimental angles and resulting angles for emission are shown. Complete shadowing of the primary and emitted electrons is assumed, so that only the surface area shown with cross-hatching is active in contributing to the detected electron current. Additionally, a variation in the local normal from the average sample normal is shown resulting in a change in the depth sampled by electrons with a given trajectory.

Figure 4.2 The cone-shaped surface roughness assumed in the Monte Carlo calculations of De Bernardez et al. [1984].

Figure 4.3 (a) The grain structure of the pure Mo sample used in the surface roughness investigation. (b) A schematic representation of the two grains used for the investigation with their corresponding orientation as determined by Laue backscattering; the area used for the AES line scans in y-direction is also indicated in units of mm (magnification x6.7).

Figure 4.4 (a) and (b) SEM micrographs at 4200X magnification of grains A and B, respectively, indicating a uniform and featureless surface after polishing.

Figure 4.5 AES line scan as shown in Fig. 4.3b indicating the variation in APPH as a function of sample position for different fluence. In the very early stages of ion bombardment (t= 1 hr.) an essentially constant APPH is observed across both grains. At high fluence (t=36 hrs.), a large difference exists for the two orientations.

Figure 4.6 The evolution of the variation in APPH detected from the two grains as a function of sputtering time (fluence).

Figure 4.7 (a) and (b) SEM micrographs at 4200X magnification of grains A and B, respectively, indicating considerable difference in the surface morphology of the two grains after ion bombardment for 36 hours.

Figure 4.8 SEM micrograph at 4200X exemplifying the gross difference in surface morphology as present at the grain boundary.

Figure 4.9 SEM micrographs of the Mo sample coated with a thin film of Au to enhance contrast. (a) Grain boundary at 10000X magnification; (b) Grain A at 20000X magnification revealing a fine structure consisting of 'furrows' overlapped on the 'hills and valleys' in the direction of the ion beam.

Figure 5.1 A schematic representation of radiation damage showing a depleted zone and the surrounding environment in a (001) plane of an fcc crystal lattice. The primary knock-on atom impinges from the left and comes to rest at the position denoted P. After Seeger [1962]

Figure 5.2 Ion range and damage distributions reconstructed from a one-dimensional Edgeworth expansion and appropriate moments from Winterbon's compilation [1975] for (a) Mo and (b) Cr targets.

Figure 5.3 The surface Cr concentration, x_s^{cr}, for sputtered Cr-Mo alloys plotted as a function of the bulk Cr concentration, x_b^{cr}. x_s^{cr} has been calculated from the normalized APPH's using both the Cr(529) and Mo(186) transitions according to eq. (3.25b). Based on a phenomenological preferential sputtering model, the dotted line shows a theoretical curve plotted according to eq. (5.8) using K= 1.73.

Figure 5.4 (a) Steady-state sputtered surface spectrum of the low energy region (20-50 eV) from an 83.4 at.% Cr-Mo alloy. The best fit simulation obtained by the computer grid search technique using eq. (5.3) is shown (dotted) and corresponds to fractions of the pure element spectra shown in (b) of f_{Cr} = 0.720 and f_{Mo} = 0.288.

Figure 5.5 (a) Steady-state sputtered surface spectrum of the medium energy region (100-240 eV). The best fit simulation obtained by the computer grid search technique is shown (dotted) and corresponds to fractions of the pure element spectra shown in (b) of f_{Cr} = 0.736 and f_{Mo} = 0.269.

Figure 5.6 (a) Steady-state sputtered surface spectrum of the high energy region (425-580 eV). The best fit simulation obtained by the computer grid search technique is shown (dotted) and corresponds to fractions of the pure element spectra shown in (b) of f_{Cr} = 0.746 and f_{Mo} = 0.255.

Figure 5.7 The average surface composition is plotted as a function of the IMFP, calculated according to eq. (3.31), and the median energy of the energy window used in the simulation procedure. The average surface composition was determined for each of five independent data sets consisting of a total of 210 best fit simulations per energy region. The alloy bulk composition is shown as dotted lines. The average at each median energy is joined solely to aid the eye. The results indicate that the compositional modifications due to preferential sputtering are much greater than the small gradient in composition suggested by the data.

Figure 5.8 Surface composition as a function of ion flux for (a) low, (b) medium and (c) high energy regions. The vertical dotted

line designates the time after which a steady-state sputtered condition was attained with the standard flux ($\sim 4.1 \cdot 10^{14}$ ions/cm^{2}sec) and then reduced to $\sim 1.9 \cdot 10^{13}$ ions/cm^{2}sec.

Figure 5.9 Surface composition as a function of relaxation time for (a) low, (b) medium and (c) high energy regions. The vertical dotted line designates the time after which a steady-state sputtered condition was attained with the standard flux ($\sim 4.1 \cdot 10^{14}$ ions/cm^{2}sec) and then terminated.

Figure 5.10 A logarithmic plot of eq. (5.8) for 13 Cr-Mo alloys.

Figure 5.11 Calculated Cr composition profiles of a steady-state sputtered surface of the 83.4 at.% Cr alloy (from Table 5.2). These profiles represent an inhomogeneity in depth such that the calculated surface composition using layer calculations is consistent with the experimentally determined composition from the three energy regions: (1) a linear variation with depth; and (2) a concentration spike at x_1 and a sub-surface different from the bulk. The alloy bulk composition is shown as a dotted horizontal line. The depth scale was calculated using the $a_0/2$ estimation of the layer thickness. The dotted vertical line represents the sampled depth corresponding to the average IMFP of the high energy region.

Figure 5.12 A schematic approximation of the composition profile in a refractory alloy where only athermal 'ballistic' processes are considered to play a significant role in establishing the steady-state surface composition.

Figure 6.1 The variation in Cr and Mo APPH's for a sputtered 59.8 at.% Mo alloy with annealing time. Panel (a) shows the results for an annealing temperature of 920 ± 5 K whereas (b) is for a temperature of 1075 ± 5K. The Cr APPH's have been multiplied 2.5X.

Figure 6.2 Auger spectra of (a) a sputtered 59.8 at.% Mo alloy surface and (b) an equilibrated surface at 1075 K.

Figure 6.3 An experimental estimation of IMFP's according to eq. (3.28b) using the appropriately weighted Auger surface composition, $\bar{x}_s$ and assuming a pure monolayer of Cr at the surface as calculated with confidence from the USM for the Mo-rich alloys used in this study.

Figure 7.1 The variation in Cr and Mo APPH's for a sputtered 89.8 at.% Mo alloy with annealing time. Panel (a) shows the results for an annealing temperature of 920 ± 5 K whereas (b) is for a temperature of 1025 ± 5K. The experimental annealing time allowed before impurity interference is much longer in this alloy due to an extensive 'cleaning' treatment. The Cr APPH's have been multiplied 2.5X.

Figure 7.2 Kinetic data obtained from the 89.8 at.% Mo alloy plotted as a ratio of the two elements' major peaks as a function of annealing time. The alloy ratios are multiplied by a ratio of the corresponding pure elemental peaks (as per eq. 3.25b) so as to correct for differences in elemental sensitivity. The annealing time does not include the 15 sec required to attain target temperature. The data indicate two asymptotic plateaus at low (920 K) and high T (1025 and 1075 K). Continued annealing at 1075 K leads to evaporation losses becoming detectable.

Figure 7.3 Kinetic data from the same 89.8 at.% Mo alloy obtained at an intermediate temperature of 950 K over a period of 5 hours. The results indicate that the low temperature plateau in Fig. 7.2 does not represent an equilibrium condition.

Figure 7.4 A logarithmic plot according to eq. (7.7) of the characteristic times for diffusion (t_X) in the temperature range 950-1025 K where greater than 50% completion was attained. The error in abscissa is shown for the lowest temperature data in the bottom right-hand corner.

Figure 7.5 A logarithmic plot according to eq. (7.7) of the characteristic times for diffusion (t_X) in the temperature range 875-970 K where $\leq$ 50% completion was attained or, for intermediate temperatures, the time could be determined accurately. The same scale expansion in both directions has been used for a direct comparison with slopes in Fig. 7.4. The error in the abscissa is shown for the lowest temperature data in the bottom right-hand corner.

Figure 7.6 A plot of the apparent activation energy in the higher percent completion regime, Q^H, as a function of percent completion. If there were no systematic errors associated with the experimental results, the slope of this plot is expected to be zero.

Figure 8.1 The appropriately weighted surface composition, $\bar{x}_s^{Mo}$, in the medium energy region (100-240 eV) determined by the simulation procedure as a function of the electron energy using a 30 eV window and plotting the median energy. The data reveal a concentration gradient within the energy range consistent with a surface enrichment of Mo. The bulk composition is indicated as a solid line. The theoretical dotted line was calculated according to eq. (3.28a) using the experimentally determined monolayer composition and IMFP's.

Figure 8.2 The appropriately weighted surface composition, $\bar{x}_s^{Cr}$, in the high energy region (425-580 eV) determined by the simulation procedure as a function of the electron energy using a 30 eV window and plotting the median energy. Unlike the medium energy region, the data reveal a scatter within this energy range due to a much smaller variation in the contribution from the first layer as a function of energy. These data are also consistent with a surface enrichment of Mo. The bulk composition is indicated as a solid line. The theoretical dotted line was calculated according to eq. (3.28a) using the experimentally determined monolayer composition and IMFP's.

LIST OF TABLES

Table 3.1 Atomic density and interplanar distance in bcc metals.

Table 5.1 Steady-state sputtered surface composition of an 83.4 at.% Cr-Mo alloy determined by the simulation procedure.

Table 5.2 Estimation of the inhomogeneity in the steady-state sputtered surface of an 83.4 at.% Cr-Mo alloy through layer calculations.

Table 6.1 Normalized Auger data for three Mo-rich Cr-Mo alloys.

Table 6.2 Monolayer compositions of annealed Mo-rich alloys.

Table 6.3 IMFP's in monolayers (λ_m) calculated from experimental results and literature data.

Table 7.1 Experimentally determined activation energies of diffusion.

Table 8.1 Normalized Auger data, monolayer calculations and enthalpy of segregation results for an 83.4 at.% Cr-Mo alloy.

Table 8.2 Theoretical predictions of the Unified Segregation Model using Seitz radii for an 83.4 at.% Cr-Mo alloy at 1054 K.

GLOSSARY

AES	Auger Electron Spectroscopy
APPH	Auger Peak-Peak Height
HWHM	Half-Width at Half-Maximum
IMFP	Inelastic Mean-Free Path
ISS	Ion Scattering Spectroscopy
LSS	Lindhard, Scharff and Schiott Theory
RCS	Replacement Collision Sequence
RED	Radiation-Enhanced Diffusion
RFA	Retarding Field Analyzer
RIS	Radiation-Induced Segregation
SEM	Scanning Electron Microscopy
SIMS	Secondary Ion Mass Spectrometry
SNMS	Secondary Neutral Mass Spectrometry
USM	Unified Segregation Model
WSS	Winterbon, Sigmund and Sanders theory

CHAPTER ONE

INTRODUCTION

1.1. ALLOY SURFACES

The atoms at the surface of an alloy experience an environment quite different from that in the continuum of the bulk. More than a century ago, Gibbs [collected works 1961] established the thermodynamic formalism predicting that under equilibrium conditions, the surface composition of an alloy may be quite different from that of the bulk. This phenomenon has become known as surface (Gibbsian, equilibrium) segregation (enrichment, adsorption). Since most materials are alloys either by design through the addition of alloying elements for improving properties, or by impurities remaining after processing or by contamination from the surface environment, this phenomenon has enormous consequence in many areas of materials science. For example, in using a metal alloy as a heterogeneous catalyst, the catalytic process may be enhanced or suppressed by the enrichment of an alloying component at the surface. In corrosion science, passivation of the surface by suitable protective coatings will depend on the surface composition. Electronic devices employing thin film technology will be strongly dependent on surface properties for adhesion and integrity. Of course, the analogous phenomenon of grain-boundary segregation, i.e., segregation to an internal surface rather than a free surface, can have drastic effects leading to the failure of steel components. Associated with

this general phenomenon are temper brittleness, creep embrittlement and some forms of intergranular stress corrosion cracking.

The compositional inhomogeneity between the surface and bulk phase is not limited to equilibrium conditions. It has long been established that such inhomogeneities are also present under non-equilibrium conditions where thermodynamic equilibrium is not attained between surface and bulk. For example, fusion reactor walls are subjected to a continuous flux of different particles (ions, neutrons, etc.) with a wide range of kinetic energy; inert ion bombardment is routinely used in conjunction with numerous surface analytical techniques either to establish a clean surface or for depth profiling. Generally, the compositional modifications that arise under such non-equilibrium conditions are very complex as numerous processes may be activated under the irradiating conditions and target material properties.

The control of materials' performance for applications dependent on surface properties is based on the knowledge of the relationship between externally controllable parameters such as alloy composition and irradiating conditions, and the resulting surface properties such as chemical composition and activity, structure, etc. It has been through the advent of surface analytical techniques over the last two decades with the necessary surface sensitivity that has allowed this relationship to be investigated. Indeed, it has been the focus of great research efforts in numerous interdisciplinary fields to characterize and predict surface compositional modifications under different experimental conditions.

1.2. SCOPE OF THESIS

The purpose of this research is two-fold. First, the empirical relationship between the surface and bulk compositions across the entire composition range of a binary alloy system is determined under both equilibrium and non-equilibrium conditions. Second, the experimental results are compared with appropriate theoretical model predictions. The ultimate goal being the understanding of the phenomena that lead to compositional modifications of surfaces.

In order to achieve the first objective, the accuracy, precision and limitations of an analytical technique with the necessary surface sensitivity are established so as to be able to probe any inhomogeneity in a sample with depth. The technique chosen is one of the most widely and routinely used methods of surface analysis: Auger Electron Spectroscopy (AES). Although severe problems are often encountered in quantitative AES, it is the opinion of this author that given the techniques available, AES is suitable for this type of investigation and that adequate accuracies can be obtained through careful and often very tedious procedures for calibration of the instrumental technique. As with most surface analytical techniques, the use of inert gas ion bombardment as a routine method of obtaining clean surfaces and depth profiling dictates that any investigation utilizing this process must require a thorough understanding of the radiation-induced modifications in the composition and defect profiles that result. Finally, the surface segregation phenomenon is investigated such that the segregation behaviour in the experimentally accessible temperature range is established under both equilibrium and non-

equilibrium conditions.

The second objective, involving a comparison of current theoretical model predictions and experimental results, is the ultimate test in the understanding of the observed and documented phenomena. If the alloy system studied is appropriately chosen, then significant contributions can be made toward understanding the relationship of the externally controllable parameters and the surface properties that result in many practical applications.

The Cr-Mo binary alloy system was chosen for a number of reasons. First, both elements are technologically important, for example, as alloying additives and fusion-reactor wall candidates [Gold and Harrod 1979]. Second, Cr and Mo form a continuous series of solid solutions across the entire composition range and hence all have the same structure [Hansen 1958, Elliott 1965, Shunk 1969, Rudy 1969]. Third, from a quantitative analysis point of view using AES, both components have well separated Auger transitions in the surface sensitive energy region of 20-600 eV. Additionally, those matrix effects which individually can impose significant limitations on the accuracy of the technique are expected to have a negligible composite effect in this alloy system. This is attributable to the individual matrix effects acting in opposite directions and hence leading to a compensation of their overall effect. Fourth, of the major driving forces presently considered for surface segregation, namely, differences in atomic interaction energies and atomic size, this alloy system exhibits appreciable differences in both parameters and hence provides adequate driving forces for both effects. The magnitudes of these driving

forces can be illustrated with appropriate literature data. The difference in atomic interaction energy is proportional to the difference in the pure element sublimation enthalpies ($\Delta H^{Mo}_{SUB} - \Delta H^{Cr}_{SUB}$) which is equal to 62.3 kcal/mole [Hultgren et al. 1973a]. The difference in atomic radii, as estimated using Seitz radii, is equal to 9% [King 1966]. Finally, it is an appropriate follow-up to an earlier investigation of the Mo-W alloy system [Dawson and Petrone 1981] where only the driving force due to differences in atomic interaction energies was present as exemplified by a difference in the sublimation enthalphies of 45.7 kcal/mole [Hultgren et al. 1973a]. Mo and W have nearly identical atomic radii with a difference of < 0.1% in the Seitz radii [King 1966].

Despite the above reasons that make the Cr-Mo system an interesting model system for surface compositional modifications studies, severe experimental problems with non-metallic impurity segregation and the high vapour pressure of Cr account for the absence of data on this system. This investigation then, is the first of this system.

CHAPTER TWO

EXPERIMENTAL METHODS

2.1. SAMPLE PREPARATION AND CHARACTERIZATION

2.1.1. Alloy Preparation

A total of thirteen Cr-Mo alloys were prepared from pure Chromium (Materials Research Corporation, Marz Grade, 99.996 % purity) and Molybdenum (Johnson Matthey, Puratronic grade, 99.985 % purity). Sufficient stock material was used to produce 0.5 cm^3 boules of the target composition, degreased ultrasonically with acetone and then pre-melted to remove any volatile impurities before weighing.

The basic method of preparation involved co-melting of the pure elements on a cold-hearth mono-arc melter which had been evacuated to 10^{-5} torr and backfilled with Ar. In the early stages of the research, an Ar pressure of ~ 0.5 atm was used. After establishing that the preparation process was a major source of non-metallic impurities, the preparation chamber was modified by this author so as to allow sample preparation under an Ar pressure of ~ 1.2 atm.

Slices of the alloy boules ca. 1 cm in diameter and 1 mm in thickness were obtained and polished by standard metallographic techniques. Unless otherwise indicated, the general procedure involved an initial stage using silicon carbide paper of 220 grit followed by 400 and then 600 and for

the next stage, diamond paste was used with a particle size of 6 and 1 μm, successively.

Due to the relatively high vapour pressure of Cr at the melting point, large weight losses were observed during preparation of the five Mo-rich alloys. For these alloys, the bulk composition was determined to within 1.5 at.% by measuring the lattice parameters using X-ray diffraction and published lattice parameter data, as discussed below. Minimal weight losses were observed during preparation of the Cr-rich alloys thereby allowing bulk compositions to be accurately determined to within 1.0 at.% from the weight of the starting materials.

2.1.2. Compositional Characterization by X-ray Diffraction

X-ray measurements can be used effectively to determine the lattice parameter of metals and alloys [Pearson 1958]. If the lattice parameter versus composition curve has been established throughout a homogeneous-phase region of an alloy system, then the composition of an alloy of unknown composition can be determined from a measurement of its lattice parameter. The accuracy attained will depend on the variation of lattice parameter with composition in that alloy system. This procedure is only applicable to binary alloys [Cullity 1956, Pearson 1958].

Considerable data are available in the literature from numerous investigations of the Cr-Mo binary system. The data have been compiled by Pearson [1958, 1967] and Rudy [1969] and is summarized in Fig. 2.1; where necessary, measurements in kX units were converted to nanometers. Additionally, the lattice spacing measurements determined for the alloys used in this investigation are plotted against the nominal composition. The

nominal compositions were calculated from the accurately determined weights of starting materials and the assumption that any observed weight loss was due to Cr because of its much greater vapour pressure at the melting point. An analysis of the pure elements' vapour pressure data reveals that this is a reasonable assumption. For example, at the melting point of a 50 at.% Cr-Mo alloy of ~ 2400 K [Rudy 1969], the vapour pressures of the pure elements are P_{Cr} = 30.3 torr and $P_{Mo} = 1.42 \cdot 10^{-4}$ torr [Hultgren et al. 1973a]. The difference in vapour pressure is greater than five orders of magnitude. In all cases, good agreement is observed between the experimentally determined alloy lattice parameter as a function of nominal composition and literature results.

The experimental measurements were obtained using a Cu X-ray source operated at 30 KeV and 20 mA; 2θ diffraction peaks were scanned in the region 38^{o} to 140^{o}. The best value for the alloy parameter was assigned from the values obtained for each reflection observed according to standard methods [Nelson and Riley 1945]. Additionally, the half-width at half-maximum (HWHM) of the peaks was used as a measure of the homogeneity of the alloy. In all cases differences were small and no systematic trends were observed between the alloy data and those from the pure elemental standards that had been prepared by the same procedure.

A test of whether the X-ray measurements should be made with the alloy maintained stationary, i.e., over a fixed volume of sample, or whether the analysis should be averaged over the entire sample, was performed by mechanically rotating the alloy at a speed faster than 2θ was being scanned. Negligible differences were found in the lattice parameter obtained

by the two procedures. The results indicated that given the small crystallite size of the alloys, an appropriate value of the lattice parameter can be obtained without the tedious procedure of rotating the sample and, that the alloy was homogeneous to within the resolution of the technique.

2.1.3. Crystal Orientation Determination by Laue Backscattering

The orientation of some large single crystals in a polycrystalline Mo sample was determined by the back-reflection Laue method [Cullity 1956, Barrett 1966]. A Mo X-ray source was used as the source of white radiation operated at 50 KeV and 12 mA with a beam size ca. 1 mm in diameter. Laue photographs were obtained at specimen to film distances of 3 and 5 cm with typical exposure times of 50-60 minutes.

2.1.4. Grain Structure and Surface Morphology Characterization

Grain structure, where necessary, was determined using an optical microscope with polarized light capability [ASM 1985]. Using Nomarski differential interference-contrast illumination it was also possible to obtain limited information of the surface morphology up to a magnification of 400X.

Characterization of surface morphology was carried out using a Scanning Electron Microscope (SEM) [Goldstein et al. 1981, Reimer 1985, ASM 1985]. The instrument was operated in the secondary-electron mode with a typical primary beam energy of 20 KeV and a beam diameter of 20 nm. In order to improve the contrast, the sample was coated, where indicated, with a thin film of Au [Goldstein et al. 1981, ASM 1985] because of its relatively high coefficient of secondary-electron emission.

Figure 2.1: Crystal lattice parameter as a function of bulk composition for the Cr-Mo binary alloy system.

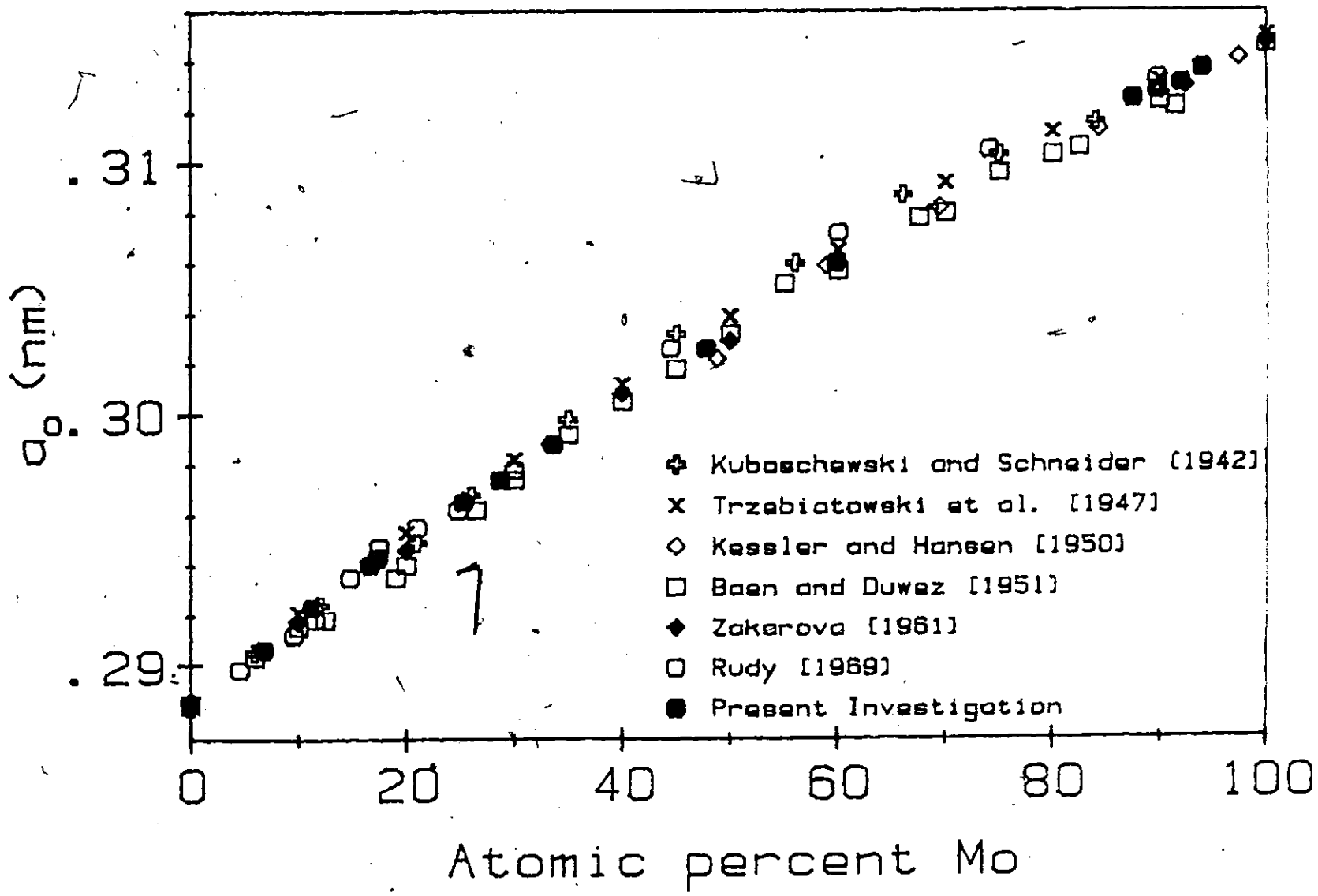
.31
.30
.29
a_o (nm)
0
20
40
60
80
100
Atomic percent Mo
Kubaschewski and Schneider [1942]
Trzebiatowski et al. [1947]
Kessler and Hansen [1950]
Baen and Duwez [1951]
Zakerova [1961]
Rudy [1969]
Present Investigation

2.2. SURFACE PREPARATION AND ANALYSIS

2.2.1. Surface Analysis by Auger Electron Spectroscopy

Surface analysis was performed by Auger Electron Spectroscopy (AES) [Seah and Briggs 1983, Thompson et al. 1984]. In AES, the incident electron beam strikes the target, penetrates with both elastic and inelastic scattering and eventually comes to rest at a depth of 1-2 μm. The process is shown schematically in Fig. 2.2.

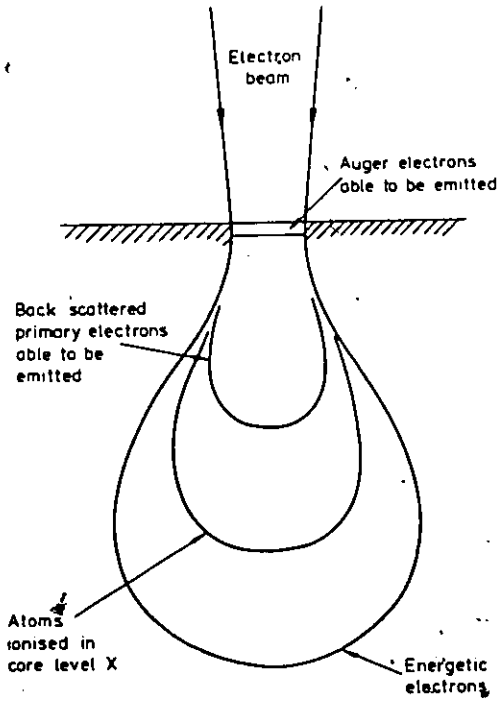

Figure 2.2: Schematic representation of electron scattering processes in AES. After Seah [1983a].

The fundamental mechanism which leads to the Auger process is shown schematically in Fig. 2.3 for the major Cr transition used in this study. In general, an atomic core level X is initially ionized by a primary beam electron or a sufficiently energetic secondary electron. The atom

subsequently decays by filling level X with an electron 'falling' from level Y with the excess energy released as either an X-ray photon or through the emission of an electron from level Z. The latter process is known as a radiationless XYZ Auger transition.

As the Auger electron diffuses from its source, it can undergo numerous scattering events. If its trajectory is such that it escapes into the vacuum, it can be detected with an electron spectrometer. Its energy will depend on the scattering events that it underwent. The energy losses associated with excitations of lattice vibrations or phonon losses are small and of the order of a few tens of meV. The energy of an Auger electron that undergoes only elastic and phonon scattering is not significantly altered and the measured energy, E_{XYZ}, is approximately given by the expression:

$$E_{XYZ} = E_X - E_Y - E_Z - \Phi_A,$$

where Φ_A is the work function of the analyzer material. For example, the transition depicted in Fig. 2.3 for Cr yields Auger electrons with a measured kinetic energy of 529 eV. In X-ray and atomic notation [Chang 1974, Prutton 1975], this transition is labelled $L_3M_{2,3}M_{4,5}$ and ($2p_{3/2}$ $3p_{1/2,3/2}$ $3d_{3/2,5/2}$), respectively. Similarly, the major Mo transition used in this study, Mo(186), is denoted $M_5N_{2,3}N_{4,5}$ ($3d_{5/2}$ $4p_{1/2,3/2}$ $4d_{3/2,5/2}$).

Auger electrons that undergo inelastic scattering events lose sufficient energy that they are no longer detected at the energy appropriate to the XYZ transition and constitute part of the secondary electron background. Inelastic scattering can occur by excitation or

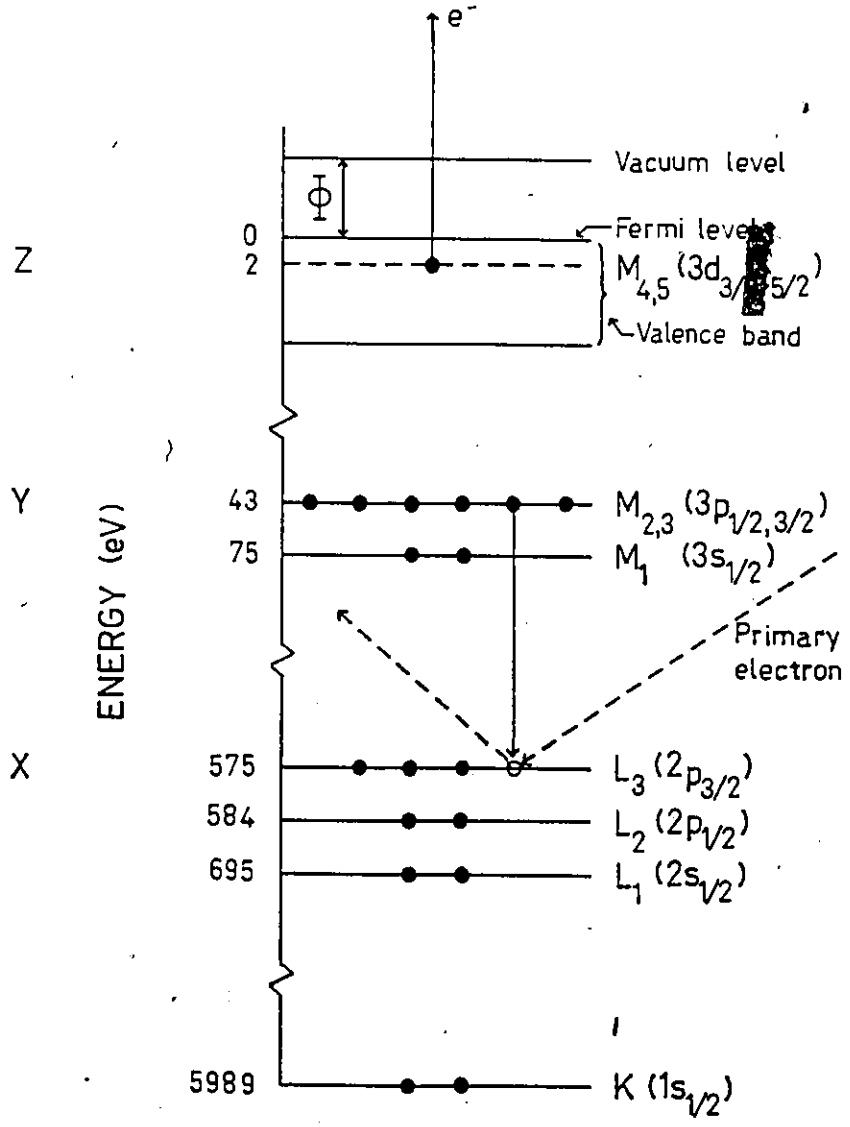

Figure 2.3: Schematic representation of the Auger process. The radiationless XYZ Auger transition shown after primary electron excitation gives rise to the major Cr transition used in this study. The electronic energy levels are listed on the left as the binding energy in eV relative to the Fermi level. The X-ray and atomic notations are given on the right. The Auger electrons emitted by this process have a kinetic energy of 529 eV and are labelled Cr(529): $L_3M_{2,3}M_{4,5}$ ($2p_{3/2}$ $3p_{1/2,3/2}$ $3d_{3/2,5/2}$).

ionization of inner shell and valence electrons. The collective excitation of the valence electrons making up the electron gas in a metal leads to plasmon losses. The inelastic scattering events are quite severe and are the basis for the surface sensitivity of the technique. The inelastic mean free path (IMFP) is defined as the characteristic distance travelled in a solid before a flux of Auger electrons with a given kinetic energy is reduced to 1/e of the original value through inelastic scattering events. The value of the IMFP depends both on the matrix and the Auger electron energy. A compilation of existing experimental literature data due to Seah and Dench [1979] is shown in Fig. 2.4. The data reveal that the energy window used in this study of 20-600 eV represents the most surface sensitive region of the energy spectrum.

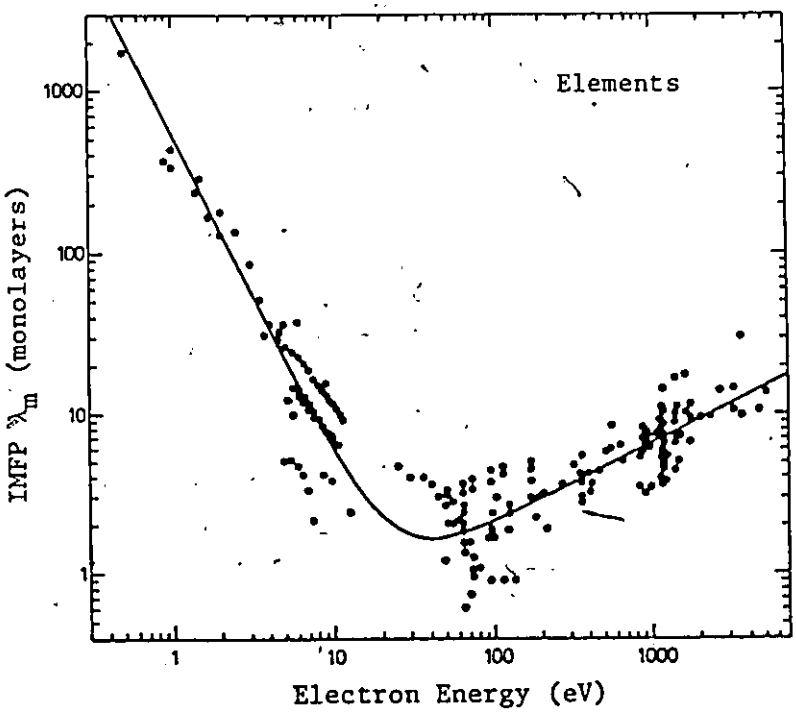

Figure 2.4: The dependence of the IMFP in monolayers (λ_m) on electron energy in pure elements. After Seah and Dench [1979].

Auger electron energy analysis was performed using a four-grid retarding-field analyzer (RFA) [Ertl and Kuppers 1974, Chang 1974, Thompson et al. 1984]. Details of the analyzer and use of the phase-sensitive detector technology may be found in the references indicated and references therein. A schematic representation of the apparatus is shown in Fig. 2.6. Auger spectra in this study were collected in the dN(E)/dE mode where N(E) represents the total energy distribution function. The differentiation was accomplished electronically by imposing a sinusoidal modulating voltage on the retarding voltage and synchronously detecting the collector current at the second harmonic of the modulating frequency using a lock-in amplifier.

For the Cr-Mo alloy system, both elements have numerous non-overlapping transitions in the region 100-600 eV as shown in Fig. 2.5 for an annealed 83.4 at.% Cr-Mo alloy. One can also see that the major contaminants, namely C, N, and O, are also sufficiently separated that they could be accurately monitored. It should be pointed out that a great effort of this research thesis concentrated on developing procedures which could successfully remove (reduce) the non-metallic impurites which are observed to segregate strongly upon annealing (Fig. 2.5).

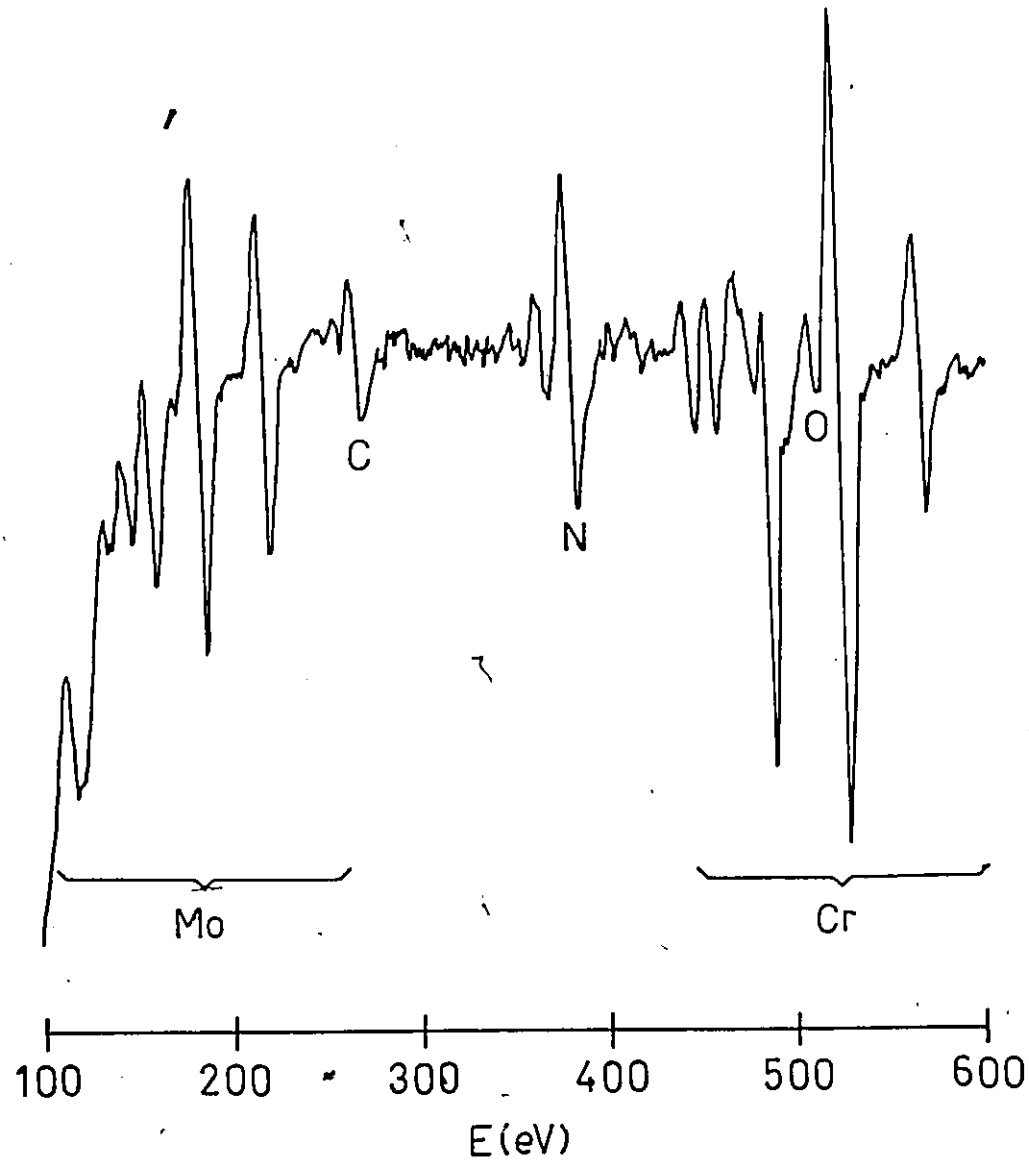

Figure 2.5: An Auger spectrum collected in the dN(E)/dE mode of an annealed 83.4 at.% Cr-Mo alloy. The major Mo and Cr transitions are shown along with the contaminants that posed severe problems in the segregation studies of the binary system.

Figure 2.6: A schematic representation of the experimental apparatus indicating AES, ion bombardment and annealing capabilities. The complete system is under microprocessor control. The modifications and additions made by this author are enclosed by the dashed lines.

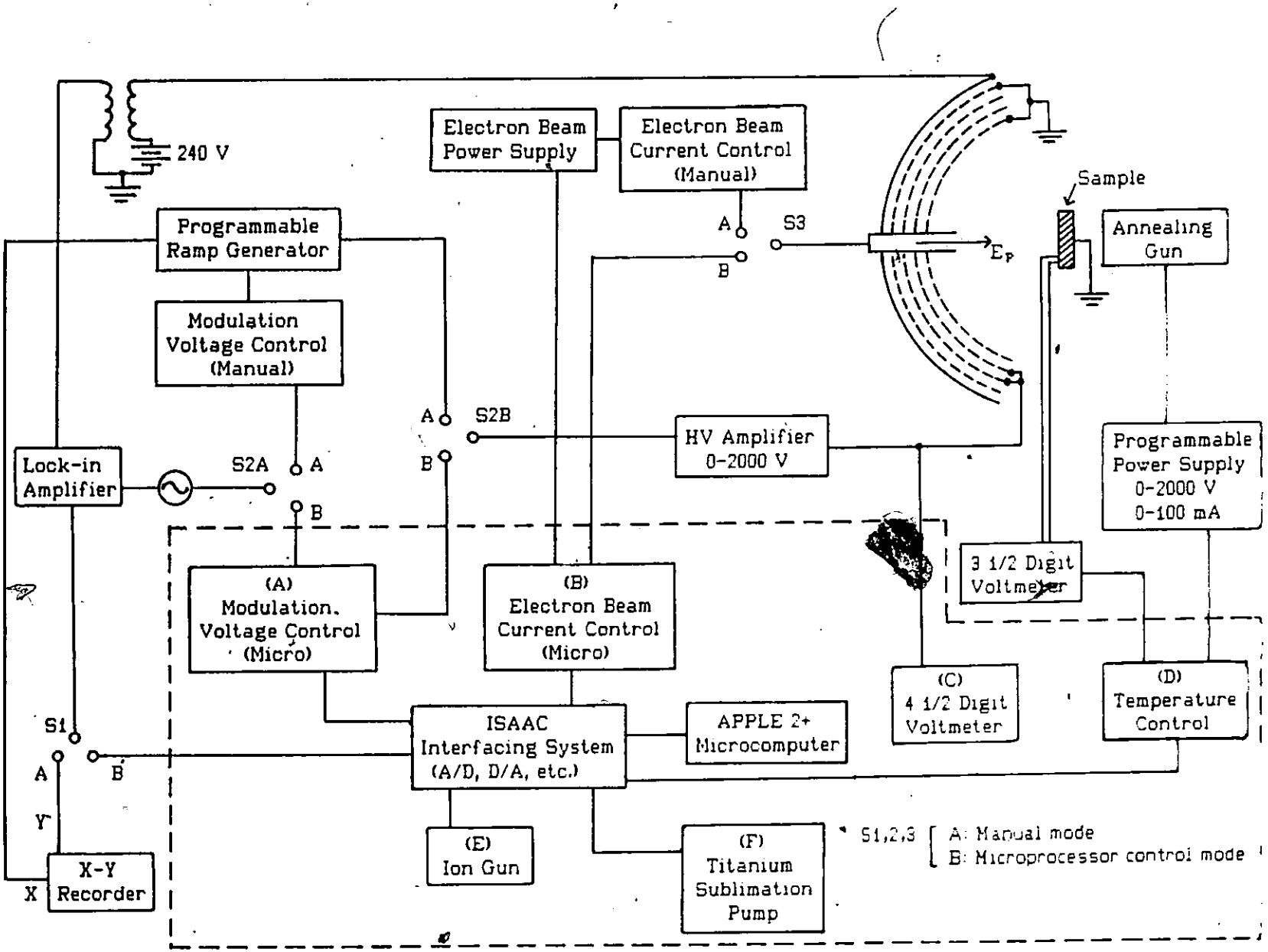
240 V
Electron Beam Power Supply
Electron Beam Current Control (Manual)
Sample
Annealing Gun
Programmable Ramp Generator
A
B
S3
E_p
Modulation Voltage Control (Manual)
A
B
S2B
HV Amplifier 0-2000 V
Programmable Power Supply 0-2000 V 0-100 mA
Lock-in Amplifier
S2A
A
B
(A) Modulation Voltage Control (Micro)
(B) Electron Beam Current Control (Micro)
3 1/2 Digit Voltmeter
(C) 4 1/2 Digit Voltmeter
(D) Temperature Control
S1
A
B
Y
X
X-Y Recorder
ISAAC Interfacing System (A/D, D/A, etc.)
APPLE 2+ Microcomputer
(E) Ion Gun
(F) Titanium Sublimation Pump
S1,2,3
A: Manual mode
B: Microprocessor control mode

2.2.2. System Development and Microprocessor Interfacing of Apparatus

The AES apparatus was originally under complete manual control. The need for digitally collected data and automated control of most functions prompted complete hardware and software interfacing to a microprocessor. The modifications and additions to the existing apparatus instituted by this author are discussed below and are represented schematically in Fig. 2.6.

The system interfacing was based on an APPLE 2+ microcomputer using a 6502 microprocessor and an ISAAC interfacing system consisting of analog-to-digital (A/D) and digital-to-analog (D/A) converters, binary switches, etc.

In order to collect Auger spectra digitally over a large range of energies consecutively, it was necessary to be able to control and switch the appropriate modulating voltage. The necessary circuitry was built and implemented (labelled (A) in Fig. 2.6) so as to take a reference sinusoidal waveform (2.8 V p-p, 1 Khz) and with an appropriate voltage divider circuit and an analog multiplexer (Intersil IH6108 one of 8 channel CMOS multiplexer using three line binary decoding with TTL or CMOS logic inputs), the correct modulating voltage could be chosen and overlapped onto the retarding voltage at the analyzer.

Control of the primary electron beam was essential and achieved as follows: The unit is shown as (B) in Fig. 2.6. A voltage proportional to the primary beam current is amplified and continually monitored using a 12 bit A/D in ISAAC. Control of the beam current is accomplished in manual mode by varying the voltage applied across a W filament floating at the

primary beam voltage (2 KeV) with a variable resistor. Microprocessor control was accomplished by using opto-isolators to replace the manually controllable variable resistor. The opto-isolator used (Clairex Photomod CLM4006A) consists of two separate components: One component is a lamp whose intensity output at an appropriate wavelength is proportional to the voltage applied across its inputs. These inputs are connected to a 12 bit D/A in ISAAC thereby allowing a digitally controlled voltage at the lamp inputs and hence, the lamp intensity. The other component of the opto-isolator is a photoconductive cell made of either CdS or CdSe whose resistance is proportional to the photon flux from the lamp. In essence then, the opto-isolator unit allows for a digitally controllable variable resistance which in turn can vary the voltage across the W filament and hence the primary beam current. The circuitry implemented could energize and maintain the primary electron beam to within ± 0.1 μa in an acceptable period of time (seconds). Appropriate safety measures were also implemented to prevent filament damage.

Microprocessor control of the retarding (sweep) voltage was also essential. The necessary circuitry was built and implemented so as to attain a resolution of 0.15 V. Additionally, an appropriate voltage divider circuit and a high-accuracy 4 1/2 digit voltmeter were built which allowed calibration of the retarding voltage to within 0.1 V (labelled (C) in Fig. 2.6).

Temperature control of the sample was achieved as follows: The sample temperature is determined using a thermocouple spot-welded to the sample surface. The thermocouple voltage, proportional to the sample temperature, is connected to the temperature control unit labelled (D) in

Fig 2.6 This input voltage is appropriately amplified and compared to a pre-determined reference voltage which depends on the target temperature required. Any difference is amplified and sent to a programmable power supply (0-2000V, 0-100 mA) and an appropriate variation in the power at the annealing gun behind the sample is instituted. The temperature control unit could generate a ramp with a pre-determined slope to a target experimental temperature. The unit was used with a heating rate of approximately 3200 K/min in the experimental temperature range of 875-1075 K. This allowed the target temperature to be reached within 15 sec and maintained constant to within ± 5 K. The unit was also interfaced for appropriate microprocessor control.

The ion bombardment apparatus (PHI 04-191) was modified by converting a square xy variable rastering capability to a rectangular raster with individually controlled x and y dimensions. This allowed a more efficient use of the ion flux given the sample dimensions. The apparatus was also interfaced to the microprocessor for control of appropriate functions (labelled (E) in Fig. 2.6).

Additionally, the Ti sublimation pump was also interfaced (labelled (F) in Fig. 2.6) so as to deposit periodically a getter film thereby cleaning the backfilled UHV chamber when the ion pumps were not in use.

In order to solve the greatest experimental problem of this investigation, i.e., segregation of non-metallic bulk impurities upon annealing, a code was written (IBACON) which made use of the microprocessor control of the ion bombardment and annealing apparatus. The code allowed for a flexible and time-varying procedure for removing

the impurities over extended periods of time with limited operator input by using pre determined knowledge of the kinetics of the impurities' segregation and appropriate sputter rates.

The system development that has been described, together with data collection software written by K. Tzatzov, essentially allows complete automated control of the entire apparatus.

2.2.3. Experimental Procedure

The Auger spectra were generated with a 2 KeV, 25 μa primary beam ca. 1 mm in diameter at normal incidence. In analog data aquisition, the 100-600 eV region of the energy spectrum encompassing the major transitions due to Mo (100-240 eV) and Cr (465-570 eV) along with most contaminants (C,N,O,S,P,Cl) was continually monitored. The surface composition was determined from a statistical analysis performed on the two elements' major peaks: Mo(186) and Cr(529). Other regions of the spectrum, namely 70-100 eV and 600-1000 eV, were also periodically checked for the presence of other contaminants. The phase-sensitive detector output was also processed using a microcomputer for the data aquisition. Appropriate energy windows in the region 20-600 eV were swept consecutively taking 16 samples at each energy with the data averaged over 3 sweeps. The more surface sensitive low energy transitions (20-50 eV) were monitored with a sweep resolution of 0.2 eV and a modulation voltage of 1 V peak-peak. The transitions at higher energy (> 100 eV) were monitored with a sweep resolution of 0.5 eV and a modulation voltage of 10 V peak-peak. Appropriate windows were used for monitoring contaminant levels. The digitized data obtained by this procedure provided the means

for performing simulations of unknown spectra by linear combinations of standard spectra.

Sputtered surfaces were generated by rastering a 2 KeV Ar^+ ion beam (P_{Ar} = 5.0 · 10^{-5} torr) over most of the sample surface ca. 1 cm in diameter. The standard ion flux used, as determined with a Faraday cup, is ~ 4.1 · 10^{14} ions/cm^2sec. Unless otherwise stated, the sputtered alloy compositions were determined after a steady-state ion bombardment condition was reached; ion sputtering was continued during the analysis.

Annealed surfaces were produced by electron bombardment heating of the reverse side of the sample (from that analyzed) which was suspended on 0.005 inch diameter W wires for thermal isolation. Temperature calibration was performed using a W/Re thermocouple spot-welded to the sample surface. For some experiments, where indicated, the temperature control circuit described earlier was used.

The base pressure in the UHV chamber was typically 3-5 · 10^{-10} torr. The geometry was such that any combination of ion bombardment, annealing and AES analysis could be performed without moving the sample. The analyzer used in this study collected electrons emitted from the sample surface with trajectories relative to the surface normal from approximately $\theta = 5^o$ to $\theta = 60^o$. The azimuthal angle ϕ, which together with θ defines the solid angle subtended at the analyzer, ranges from 0 to 360^o.

CHAPTER THREE

QUANTITATIVE AES

3.1. INTRODUCTION

Auger electron spectroscopy is one of the most widely used analytical techniques for obtaining the chemical composition of solid surfaces. It is clear that the detected Auger current is proportional to the atomic concentration in the surface region. However, from the initial publications of AES as an analytical technique [Harris 1969], the question of how the observed intensity can be converted to an elemental concentration has been a major concern. Although qualitative and semi-quantitative AES analysis can be routinely performed, quantitative analysis is still difficult due to the many parameters that affect the detected Auger current. In fact, considerable scepticism still exists in regard to the use of AES for quantitative surface analysis. The question posed should not be whether or not the technique is routinely quantitative, but rather, what analytical procedure and necessary calibration are required to attain a desired accuracy? If an understanding of the relevant parameters is obtained and appropriate steps taken to control them or account for their effect, then the technique has the potential of yielding accuracies difficult to obtain by other surface analytical techniques.

As a basis for the formalism of quantitative AES, an analytical expression is required that relates the detected Auger current, I_A, to the

atom density, N_A, of element A in the surface region. For the process depicted schematically in Fig. 2.3, it is generally accepted that the Auger current I_A arising from an XYZ Auger transition of kinetic energy E_A in a matrix m is a complex function of many parameters and is given by [Seah 1983b]:

$$I_{A,XYZ} = I_P \sec\alpha \, \sigma_{A,XYZ}(E_A,E_P) \, \gamma_A(XYZ) \, R \, (1 + r_m(E_A,E_P,\alpha)) \, T(E_A) \, D(E_A) \cdot \int \int N_A(z) \exp(-z / \lambda_m(E_A) \cos\theta) \, dz \, d\Omega , \quad (3.1)$$

where I_P is the primary electron beam current incident at an angle α to the surface normal; $\sigma_{A,XYZ}(E_A,E_P)$ is the ionization cross-section of the core level X; $\gamma_A(XYZ)$ is the probability that an excited atom will decay through an XYZ Auger transition; R_A is a roughness factor which will be discussed in Chapter 4; $(1+r_m(E_A,E_P,\alpha))$ is a backscattering correction factor; $T(E_A)$ is the analyzer transmission efficiency; $D(E_A)$ is the detector efficiency; $N_A(z)$ is the atom density of A atoms at depth z; $\lambda_m(E_A)$ is the inelastic mean-free path (IMFP) of Auger electrons in the matrix m emitted at angle θ with respect to the local normal at the sample surface; and Ω is the solid angle subtended by the analyzer.

In the above formalism a number of assumptions are made [Shimizu 1983]. The sample is assumed homogeneous in element A in the plane parallel to the surface (xy) but the concentration varies with depth z. The Auger electron emission is considered isotropic with the Auger electron undergoing random inelastic scattering; the absorption effect along its path s represented using the IMFP λ_m by $\exp(-s/\lambda_m)$. Any crystallographic effects and contributions from other processes such as Coster-Kronig transitions are not considered to play a role.

There are basically three approaches to quantitative analysis

1. A first-principles approach where all the parameters in eq. (3.1) are either measured or calculated.
2. Measurements using relative elemental sensitivity factors obtained from a published data set or an in situ determination.
3. Measurements using external reference standards.

All three methods have their advantages and disadvantages. In practice, a blend of the three is often used to yield the desired accuracy depending on the requirements.

In this chapter, the above three approaches will be presented with the corresponding accuracy that can be expected. Finally, the method chosen for this study is discussed with the limitations that have been established through calculations and an experimental investigation of the effect of appropriate parameters that have considerable influence on the ultimate accuracy obtained.

3.2. CALCULATION FROM FIRST PRINCIPLES

For practical quantification, eq. (3.1) can be simplified, for example, by assuming sample homogeneity with depth z. Additionally, for a spectrometer which primarily detects electrons along the direction θ to the surface normal, (3.1) reduces to:

$$I_{A,XYZ} = I_P \sec\alpha\, \sigma_{A,XYZ}(E_A,E_P)\, \gamma_A(XYZ)\, R\, (1 + r_m(E_A,E_P,\alpha))\, T(E_A)\, D(E_A) \cdot N_A\, \lambda_m(E_A) \cos\theta \qquad (3.1a)$$

A first principles approach to quantitative AES requires the measurement or calculation of all the parameters in eq. (3.1a). A major requirement for this method of quantification is the need for an accurate measurement of the Auger current I_A, which in itself, is not a trivial task [Seah 1983b]. Additionally, large errors can result due to uncertainties in many of the terms on the right-hand side of eq. (3.1a). It is evident, that a first principles approach to quantification of AES is very difficult [Joshi et al. 1975, Holloway 1977, Ferron et al. 1984]. In favorable cases, the accuracy obtained is about a factor of 2 [Werner and Garten 1984].

Mroczkowski and Lichtman [1983a, 1983b, 1985] have recently used a pseudo-first principles approach combining theoretically calculated and empirically determined parameters to calculate Auger currents for pure elements and hence obtain relative elemental sensitivity factors (discussed in section 3.3). A comparison with the corresponding experimentally determined published data set [Palmberg et al. 1972] yielded good agreement 95% of the time in cases where pure elemental standards are readily available.

3.3. MEASUREMENTS USING RELATIVE ELEMENTAL SENSITIVITY FACTORS

3.3.1. Using a Published Data Set

A procedure extensively used for semi-quantitative analysis is based on relative elemental sensitivity factors. In this method, the sensitivity of all detectable elements is related to that of an appropriate reference element (usually Ag, MNN:351 eV) [Palmberg et al. 1972, Davis et al. 1976]. If one measures the Auger current from a test sample and a reference standard, R, sequentially, then from eq. (3.1a) dropping the functional form and XYZ notation for clarity, one obtains:

$$\frac{I'_A}{I^R_R} = \frac{I_P \sec\alpha\, \sigma_A\, \gamma_A\, R'\, (1 + r'_A)\, T_A\, D_A\, N'_A\, \lambda'_A \cos\theta}{I_P \sec\alpha\, \sigma_R\, \gamma_R\, R^R\, (1 + r^R_R)\, T_R\, D_R\, N^R_R\, \lambda^R_R \cos\theta}$$

where a superscript prime denotes a matrix dependent parameter with a pure elemental matrix denoted by its symbol. Under the assumptions of equal surface roughness and instrumental response, the above equation reduces to:

$$\frac{I'_A}{I^R_R} = \frac{\sigma_A\, \gamma_A\, (1 + r'_A)\, N'_A\, \lambda'_A}{\sigma_R\, \gamma_R\, (1 + r^R_R)\, N^R_R\, \lambda^R_R} \tag{3.2}$$

isolating the atom number densities yields,

$$N'_A / N^R_R = I'_A / I^R_R\, S_A \tag{3.3}$$

where,

$$S_A = \frac{\sigma_A\, \gamma_A\, (1 + r'_A)\, \lambda'_A}{\sigma_R\, \gamma_R\, (1 + r^R_R)\, \lambda^R_R} \tag{3.4}$$

It is preferable that average values of r'_A and λ'_A be used to obtain S_A, however this is difficult in practice and it is assumed that they equal r^A_A and λ^A_A, respectively. Knowing S_A and N^R_R, one can then determine N'_A.

The need of an in situ reference standard is removed by using the relationship:

$$\sum_i x_i = 1 \tag{3.5}$$

where x_i is the mole fraction of element i defined by:

$$x_i = n_i / \sum_i n_i \tag{3.6}$$

Eq.(3.3) then reduces to

$$x_A = (I'_A/S_A) / (\sum_i I'_i/S_i) \tag{3.7}$$

where the sum is over all detected elements with one appropriate transition per element. In analyses where the Auger spectra are collected in the $N'(E)$ mode, it is convenient to use the peak height P'_A as a measure of the detected Auger current, I'_A. For a homogeneous binary alloy AB, eq. (3.7) reduces to:

$$x_A = P'_A / [(P'_A + P'_B (S_A/S_B)] \tag{3.8}$$

A major limitation in using eqs. (3.7) or (3.8) is in the accuracy to which the relative elemental sensitivity factors (S_A/S_B) are known. The use of matrix independent values neglects changes in atomic density, back-scattering factor, escape depth and peak shape with material and changes in surface roughness. For this reason this approach is considered semi-quantitative with an expected accuracy of 30-60%. Improvements can be

obtained by the in situ determination of the relative elemental sensitivity factors.

3.3.2. In Situ Determination

The Auger peak height P'_A is proportional to the concentration of that element present in the analyzed volume. The proportionality is a function of matrix effects which can vary with composition. In the formalism of Hall and Morabito [1978], the peak height from element A of a given transition is given by:

$$P'_A = x_A N'(1+r'_A) d'_A f'_A k_A \qquad (3.9)$$

where the product notation is written only in symbolic form for convenience; N' is the total number of all atoms per unit volume; $(1+r'_A)$ is the backscattering correction factor; d'_A is the electron escape depth; f'_A is a peak shape factor; and k_A is a spectrometer constant assumed independent of composition but specific to one particular transition. The spectrometer constant includes the primary beam current, the primary beam area, the ionization cross-section, the Auger transition probability, electron spectrometer transmissivity, detector efficiency, and a roughness factor.

The corresponding equation for element B is:

$$P'_B = x_B N'(1+r'_B) d'_B f'_B k_B \qquad (3.10)$$

combining (3.9) and (3.10) yields,

$$P'_{rel}(A,B) \equiv \frac{S'_A}{S'_B} = \frac{(P'_A/x_A)}{(P'_B/x_B)} = \frac{(1 + r'_A) d'_A f'_A k_A}{(1 + r'_B) d'_B f'_B k_B} \qquad (3.11)$$

Using $x_A + x_B = 1$, (3.9) and (3.10) yield,

$$\frac{P'_A}{N' (1 + r'_A) d'_A f'_A k_A} + \frac{P'_B}{N' (1 + r'_B) d'_B f'_B k_B} = 1$$

which from (3.11) yields,

$$P'_A + P'_B \cdot P_{rel} = N' (1 + r'_A) d'_A f'_A k_A \qquad (3.12)$$

Eq.(3.12) suggests one method of an in situ determination of P'_{rel}: From an AES analysis of a series of AB alloys encompassing the entire composition range, a plot of P'_A versus P'_B will yield a line whose slope at any composition is P'_{rel} for that composition. It is possible to generate a complete series of alloys from a partially interdiffused bilayer film where under ion bombardment the complete range of composition from pure A to pure B is sequentially revealed [Hall and Morabito 1978]. If the complete analysis is performed under conditions where surface roughness and instrumental response are not variable such that k_A and k_B are constant then this procedure may be acceptable. However, if either, or both, of the two conditions is not met then eq. (3.11) should be used with a plot of P'_A/P'_B versus x_A/x_B yielding P'_{rel}. Using this procedure assumes that any differences in surface roughness or instrument response will affect both peaks equally, i.e. k_A/k_B is constant.

A major concern of such analyses is the routine use of ion bombardment to obtain a clean surface and/or a depth profile. Clearly, the compositional modifications arising from this process have to be considered (Chapter 5). Hall and Morabito [1978] have addressed this problem by considering a sputter correction coefficient as another matrix effect

and introduced a sputter-corrected relative sensitivity factor P^{s}_{rel} (A,B). This treatment of the sputtering process, in keeping with the original assumption of this general method, assumes a uniform composition in the analyzed volume of the sputtered surface. It is well established that ion bombardment of alloys, even at room temperature, is a very complex process and that the above assumption will not be universally applicable. This is especially true for lower melting point alloys.

Despite these limitations, the procedure has been used in numerous systems with appropriate plots yielding an insight into the matrix effects as a function of composition. In most cases [Hall et al. 1977, Hall and Morabito 1977, 1978, Dawson and Tzatzov 1985] good linear correlations are obtained indicating that if any of the matrix effects considered change as a function of composition, there must be a change in another matrix effect so as to maintain the linearity. Additionally, for such systems the slope determined, equal to P'_{rel} or P^{s}_{rel}, allows one to calculate the appropriate surface composition of an unknown or test sample.

A third method [Hall and Morabito 1979] of determining P_{rel} is based on its evaluation in the limit of very dilute alloys where the matrix consists of almost entirely one element. In this approach, the peak heights of the pure elemental standards, obtained under identical spectrometer conditions and surface roughness, are required together with a calculable matrix correction factor. From eq. (3.10), neglecting peak shape factors, the peak height from a pure elemental standard is:

$$P^{B}_{B} = N^{B} (1 + r^{B}_{B}) d^{B}_{B} k_{B} \qquad (3.13)$$

The peak height from the same transition in the limit of pure A

is given by

$$P_B^A = x_B N^A (1 + r_B^A) d_B^A k_B \quad (3.14)$$

The value of $P_{rel}^A(A,B)$ in the limit of pure A is obtained from eq. (3.11):

$$P_{rel}^A(A,B) = (P_A^A/x_A) / (P_B^A/x_B) = P_A^A / (P_B^A/x_B) \quad (3.15)$$

Inserting (3.13) and (3.14) into (3.15) yields:

$$P_{rel}^A(A,B) = (P_A^A / P_B^B) F^A(A,B) \quad (3.16)$$

where,

$$F^A(A,B) = \frac{N^B (1 + r_B^B) d_B^B}{N^A (1 + r_B^A) d_B^A} \quad (3.17)$$

The escape depth is proportional to the IMFP [Seah 1972] in a particular matrix and can be obtained from an expression due to Penn [1976] or from a more recent empirical expression proposed by Seah and Dench [1979]:

$$\lambda_B^A = 538 (N^A)^{-1/3} E_B^{-2} + 0.41 (E_B/N^A)^{-1/2} \quad (3.18)$$

where λ_B^A is in nm and E_B in eV. For electron energies above 50 eV the second term dominates and substitution into eq. (3.17) yields:

$$F^A(A,B) = \frac{N^B (1 + r_B^B) 0.41 (E_B/N^B)^{1/2}}{N^A (1 + r_B^A) 0.41 (E_B/N^A)^{1/2}}$$

$$= \frac{(1 + r_B^B)}{(1 + r_B^A)} \left(\frac{N^B}{N^A}\right)^{1/2} \quad (3.19a)$$

similarly,

$$F^B(A,B) = \frac{(1 + r_A^A)}{(1 + r_A^B)} \left(\frac{N^A}{N^B}\right)^{1/2} \quad (3.19b)$$

There are analogous expressions for P^{B}_{rel} (A,B) and F^{B} (A,B) indicating that, in principle, it is not strictly correct to set P'_{rel} (A,B) equal to the ratio of peak heights of the pure elements as it can be quite different for dilute A and dilute B binary alloys because of matrix effects. Hall and Morabito [1979] have calculated F^{A} and F^{B} values for 4860 binary systems. Their results indicate that although values of F ranging from 0.2 to 5 are obtained, one can expect most factors to be 1.0 ± 0.5. In fact, by using Seah and Dench's [1979] IMFP empirical expression, it is found that in 86% of the binary systems $F^{A} = F^{B}$ to within 5%.

The result that these correction factors are nearly equal in a typical AB alloy system allows one to speculate that they are also the same for intermediate compositions. This can be attributed to the mutual cancellation of some of the matrix effects. For example, if the atomic density increases, it is reasonable to expect a corresponding decrease in escape depth. Similarly, a decrease in escape depth due to increased scattering is expected to be accompanied by an increase in the backscattering correction factor. The fortunate result, for quantitative AES, is that although each of the matrix effects is appreciable, their composite effect is not [Hall and Morabito 1979].

3.3.3. Summary

The use of relative elemental sensitivity factors has aquired widespread acceptance for routine qualitative and semi-quantitative AES analysis. The ultimate accuracy obtained whether using theoretically calculated or experimentally determined values from a published data set is 30-60%; an improvement can be obtained by using a locally produced

data set. It is possible to attain an accuracy approaching 15% [Werner and Garten 1984] by applying matrix correction factors [Hall et al. 1977, Hall and Morabito 1977, 1978, 1979].

In terms of applying this method to a quantitative study such as this, the above accuracies must be considered in terms of the basic assumption inherent in the method: The sample surface is assumed homogeneous over the analyzed volume. Although this assumption may be valid under numerous conditions including a steady-state sputtered surface or depth profile, it is the possibility of the existence of an inhomogeneity with sample depth that establishes the need for a quantitative surface analysis technique which can accurately probe any inhomogeneity. At present this is not possible via this method. Therefore, because of this fundamental limitation and relatively poor accuracy, this method is deemed unacceptable for this study.

3.1 MEASUREMENTS USING EXTERNAL REFERENCE STANDARDS

The most accurate method of quantifying AES involves the measurement of the signal intensity from an element in a test sample and the intensity from the same element in a reference standard of known composition, sequentially under identical experimental conditions. In this procedure, instrumental factors need not be known. The reference standard may be a pure element or an alloy; the latter being more difficult to prepare and characterize. In a study encompassing the entire composition range of an AB binary alloy system, the method developed below indicates that use of pure elemental standards can potentially yield the required accuracy.

The form of eq. (3.1) applicable to an RFA as is used in this study is [Andersen et al. 1967]:

$$I'_{A,XYZ} = I_P \sec\alpha\, \sigma_{A,XYZ}(E_A,E_P)\, \gamma_A(XYZ)\, R'\, (1 + r'_A(E_A,E_P,\omega))\, T(E_A)\, D(E_A) \cdot \int\int\int N'_A(z) \sin\theta \exp(-z / \lambda'_A(E_A)\cos\theta)\, dz\, d\theta\, d\phi\,, \qquad (3.20)$$

Many of the parameters may be removed by considering the ratio I'_A / I^A_A. It can be shown that,

$$\frac{I'_A}{I^A_A} = \frac{R'\,(1 + r'_A)\, N'_A\, \lambda'_A}{R^A\,(1 + r^A_A)\, N^A_A\, \lambda^A_A} \qquad (3.21)$$

The important parameter in eq. (3.21) is the atom number density N'_A which can give the composition of the test sample. The atom sizes a'_A and a^A_A are related to N'_A and N^A_A, respectively according to [Seah 1983b]:

$$N^A_A = (a^A_A)^{-3}, \quad \text{and} \quad N'_A = (a'_A)^{-3}\, x_A$$

such that,

$$(N'_A/N^A_A) = (a^A_A/a'_A)^3 \cdot x_A \qquad (3.22)$$

The atom size a'_A is calculated from,

$$(a'_A)^3 = M'/(\rho' N) \qquad (3.23)$$

where M' is the mean atomic weight of the matrix atoms, ρ' is the mean atomic density and N is Avogadro's number. The IMFP can be calculated from eq. (3.18) according to Seah and Dench [1979] which, in the present formalism, for E > 50 eV approximates to:

$$\lambda'_A = 0.41\,(a'_A)^{3/2}\,(E_A)^{1/2} \qquad (3.24)$$

where λ'_A and (a'_A) are in nanometers and E_A in electron volts. Substituting (3.22) and (3.24) into (3.21) yields:

$$x_A = G'_A \frac{R'}{R^A} \frac{I'_A}{I^A_A} \qquad (3.25)$$

where,

$$G'_A = \frac{(1 + r'_A)}{(1 + r^A_A)} \left(\frac{a^A_A}{a'_A}\right)^{1/2} \qquad (3.25a)$$

Eq. (3.25) is the basis for this method of analysis. For the case where both the matrix correction factor G'_A and the surface roughness ratio R'/R^A are both unity, the mole fraction of component A is equal to the ratio of detected Auger current from the test and standard sample, respectively, i.e.,

$$x_A = I'_A/I^A_A \qquad (3.25b)$$

However, this is not always the case. In order to obtain the necessary accuracy required for a quantitative study such as this, the magnitudes of the matrix factor G'_A and roughness factor R'/R^A must be realized and appropriate corrections and/or experimental conditions established so as to account for their effect in the final analysis.

Initially considering the matrix correction factor G', it is clear from its definition that for $x_A \longrightarrow 1$, $G'_A \longrightarrow G^A_A = 1$. For $x_A \longrightarrow 0$, $G'_A \longrightarrow G^B_A$, which in the formalism of Hall and Morabito [1979], $G^B_A = [F^B(A,B)]^{-1}$. It is possible to calculate G^B_A for the Cr-Mo alloy system under present investigation and hence obtain a measure of the matrix effects and any required corrections.

The backscattering correction factor $(1+r'_A)$ has been calculated by Hall and Morabito [1979] from an empirical equation given by Reuter [1972] ideally applicable to higher electron energies (>10 KeV). In this present study, a more recent expression due to Ichimura et al. [1983] applicable to the lower energies used in Auger analysis is used. For a primary electron beam at normal incidence,

$$r = [4.35 - 3.93\ (Z)^{0.1}]\ U^{-0.25} + [4.85\ (Z)^{0.1} - 5.45]$$

where Z is the atomic number and $U = E_p/E_b$ is the overvoltage ratio with E_p the primary electron beam energy and E_b the binding energy of the inititial level responsible for the transition. The ionization energies were obtained from Bearden and Burr [1967] and atomic densities from Kittel [1976]. For the Mo(186, $M_5N_{2,3}N_{4,5}$) and Cr(529, $L_3M_{2,3}M_{4,5}$), the calculated matrix correction factors are:

$G^{Cr}(\text{Mo } 186,\ x_{Mo} \longrightarrow 0) = 1.015$, and $G^{Mo}(\text{Cr } 529,\ x_{Cr} \longrightarrow 0) = 1.028$.

Thus, in going from one extreme of the composition range to the other, it is found that not only are the changes in the matrix correction factor G' small (less than 2% and 3% for the Mo(186) and Cr(529) transitions, respectively), but also that the actual values are essentially unity. This is a fortuitous result in that it allows one to assume negligible matrix effects for quantitative AES in this alloy system by the method of elemental standards.

Returning to eq. (3.25), a major concern then, is due to the effect of surface roughness. The present state of knowledge in this area is very limited; especially as it applies to surface roughness that is present or evolves under typical Auger analysis conditions. An experimental investigation was carried out in an attempt to establish limitations on the ultimate accuracy that can be attained because of this effect and experimental conditions which can be adopted so as to minimize its effect. These results are presented in Chapter 5.

In summary, the procedure of using elemental reference standards for quantifying AES results has been presented. It is shown that for a sample homogeneous over the analyzed volume, this procedure can potentially yield the accuracies required for a quantitative study such as this. The major limitations to the ultimate accuracies attained are due to matrix effects and variable surface roughness. Through appropriate calculations, it has been shown that in the Cr-Mo alloy system, for the two major Auger transitions used, the matrix correction factor G is essentially unity across the entire composition range and hence can be neglected. However,

the effect of surface roughness cannot be established through existing literature and an appropriate experimental investigation was deemed necessary. The question of quantifying sample surfaces inhomogeneous in depth is addressed in the subsequent section.

3.5. MONOLAYER CALCULATION

As discussed in the previous section, the most accurate method of quantitative AES for this study is through the use of well characterized elemental standards. However, even under ideal conditions, the ratio of detected Auger current from the unknown sample and standard yields from eq. (3.25b) a surface composition only for a sample homogeneous in depth over the analyzed volume. If any inhomogeneity exists, the composition determined reflects an appropriately weighted average surface composition $\bar{x}_S$, i.e., the homogeneous equivalent. In a study of surface segregation where the compositional modification is expected to be localized in the outermost layer (Chapter 6), it is necessary to be able to deconvolute the outermost layer composition x_1 from the apparent Auger composition $\bar{x}_S$.

In the case of a sample surface inhomogeneous in depth, the total Auger signal is considered to be a sum of contributions from each layer [Gallon 1969]. Based on the formalism of Dawson and Burke [1983], together with this author's modifications, the procedure to calculate the outermost monolayer composition can be described as follows: It is assumed that matrix effects are negligible. The total Auger current, I_A, from an unknown sample is given by:

$$I_A = \bar{x}_S^A I_A^A = x_1^A I_1 + x_b^A \sum_{i=2}^{\infty} I_i \qquad (3.26)$$

where for the mole fractions, the superscript denotes the name of the element; x_b^A is the bulk composition of element A and I_A^A is the total Auger current for pure A defined as,

$$I_A^A = \sum_{i=1}^{\infty} I_i$$

i.e., $x_i^A = 1$ for all i. Thus, from (3.26),

$$\bar{x}_S^A = [x_1^A I_1 + x_b^A \sum_{i=2}^{\infty} I_i] / \sum_{i=1}^{\infty} I_i \qquad (3.27)$$

now, using

$$x_i^A = x_b^A + \Delta x_i^A$$

and substituting into (3.27) yields,

$$\bar{x}_S^A = [\Delta x_1^A I_1 + x_b^A \sum_{i=1}^{\infty} I_i] / \sum_{i=1}^{\infty} I_i \qquad (3.28)$$

$$= \Delta x_1^A (I_1 / \sum_{i=1}^{\infty} I_i) + x_b^A \qquad (3.28a)$$

which can be rewritten to isolate Δx_1^A as,

$$\Delta x_1^A = (\bar{x}_S^A - x_b^A) \cdot (\sum_{i=1}^{\infty} I_i / I_1) \qquad (3.28b)$$

The Auger current must be integrated over the collection angle of the analyzer which from eq. (3.20) is given by:

$$I_i = C \int \sin\theta \exp [(i-1) / \lambda_m \cos\theta] \, d\theta \qquad (3.29)$$

where C is a constant which includes instrumental and sample parameters and all other parameters have been previously defined. I_i is defined so that Auger electrons originating from the first layer undergo no attenuation and the value I_1 is independent of E.

The IMFP's in nanometers, λ_{nm}, are calculated using eq. (3.18) developed by Seah and Dench [1979] from a statistical analysis of all the published measurements of electron IMFP's in solids for energies 0-1000 eV, which restated in their formalism is:

$$\lambda_{nm} = \lambda_m \, a \tag{3.30}$$

where for elements, the IMFP in monolayers, λ_m, yielding the lowest scatter is shown in Fig. 2.4 and is given by:

$$\lambda_m = 538 \, E^{-2} + 0.41 \, (a \, E)^{1/2} \tag{3.30a}$$

with 'a' being the average monolayer thickness in nanometers calculated using eq. (3.23) restated in its expanded form:

$$(a^3) = \frac{(x_b^A \, M^A + x_b^B \, M^B)}{(x_b^A \, \rho^A + x_b^B \, \rho^B) \, N} \cdot 10^{24} \tag{3.30b}$$

where the variables are as defined earlier and ρ is in units of kg m^{-3}.

For the Cr-Mo system, the monolayer thickness calculated from eq. (3.30b) yields for the pure metals a_{Cr} = 0.229 nm and a_{Mo} = 0.250 nm. If one defines a monolayer as the distance between two nearest-neighbor atomic planes, the data shown in Table 3.1 [Dieter 1976] can be obtained. The data reveal that the greater the atomic density of the plane, the greater is the planar spacing for that orientation. Higher index planes will generally have a lower atomic density and smaller inter-planar spacing than indicated in Table 3.1 [Robinson 1981]. The unweighted average of the three low-index planes is approximately equal to the (100) planar spacing. Clearly, the monolayer thickness calculated from Seah and Dench's eq. (3.30b) is too large in that it approaches the crystal lattice parameter a_o of the pure metals, i.e., a bilayer. For this reason, the (100) $a_o/2$ inter-planar spacing is considered a reasonable approximation for bcc metals and is used to convert the IMFP in nanometers (λ_{nm}) calculated from eq. (3.30) to monolayers according to the relationship:

$$\lambda_m' = \lambda_{nm} / (a_o/2) \qquad (3.31)$$

where λ_m' is denoted modified Seah and Dench.

Table 3.1 : Atomic density and interplanar distance in bcc metals.

Crystal Plane	Atomic Density (atoms/unit area),	Distance Between Planes bcc Metals	Cr (nm)	Mo (nm)
(110)	$2/\sqrt{2}a_o^2$ (= $1.4142/a_o^2$)	$a_o/\sqrt{2}$ (= $0.7071\ a_o$)	0.2039	0.2225
(100)	$1/a_o^2$	$a_o/2$ (= $0.5000\ a_o$)	0.1442	0.1574
(111)	$1/\sqrt{3}a_o^2$ (= $0.5774/a_o^2$)	$a_o/2\sqrt{3}$ (= $0.2887\ a_o$)	0.0833	0.0909
Average	$0.9972/a_o^2$	$0.4986\ a_o$	0.1438	0.1569

Crystal lattice data from Dieter [1976].
a_o^{Cr} = 0.2884 nm ; a_o^{Mo} = 0.3147 nm [Pearson 1958,1967, Rudy 1969].

In summary, a procedure has been presented to deconvolute the outermost monolayer composition x_1 from the appropriately weighted average composition $\bar{x}_s$ determined by AES. This is accomplished through the monolayer calculation with a knowledge of the sub-surface (bulk) composition, an appropriate value of the Auger electron IMFP and an experimentally determined value of $\bar{x}_s$. The calculation has been successfully applied in segregation studies of the Mo-W alloy system [Dawson and Burke 1983]. Its extension to the Cr-Mo alloy system of this study, with the

modifications instituted by this author, provides a further test of the procedure. It is expected to yield the necessary accuracy and precision in the determination of x_1 to warrant appropriate comparisons with theoretical predictions.

3.6. SUMMARY

The methods used to quantify AES results have been presented with their inherent problems and limitations. Due to the complexity of the quantification, the discussion was initially limited to analysis of sample surfaces homogeneous over the analyzed volume. Quantification from first principles or through the use of relative elemental sensitivity factors is, at best, semi-quantitative. It was shown that through the use of well characterized elemental standards, the potential exists to attain the necessary accuracy for this study. The major limitations to the ultimate accuracy attainable by this procedure have been identified as being due to matrix effects and variable surface roughness. Of the matrix effects considered to play a significant role, it is found that they act in opposite directions in enhancing or suppressing the detected Auger current. For the Cr-Mo system, an overall compensating effect prevails such that the matrix correction factor is essentialiy unity and hence negligible. The overall effect of a variable surface roughness cannot be established using existing literature and an experimental investigation, presented in Chapter 4, is carried out.

Quantification of AES results using elemental standards has been extended to sample surfaces inhomogeneous in depth z. A monolayer calculation is developed based on a layer model which assumes that the inhomogeneity in depth is limited to the outermost monolayer, i.e., the monolayer approximation. This, in essence, has overcome a major limitation of AES due to its depth resolution being the order of several atomic layers.

CHAPTER FOUR

THE VARIATION OF AUGER CURRENT WITH SURFACE ROUGHNESS

As discussed in Chapter 3, a major limitation to quantitative AES using elemental standards is due to a variable surface roughness from sample to sample. In this chapter, the fundamental aspects of the problem, based on a literature survey, are summarized and the results of an experimental investigation presented. The investigation was carried out to quantify this effect as it exists under typical AES analysis conditions and establish appropriate experimental procedures so as to minimize the limitation it imposes on the ultimate accuracy of the AES technique.

4.1. INTRODUCTION

Surface analysis by AES, as in numerous other surface techniques, is routinely accompanied by inert gas ion bombardment either to obtain clean surfaces or depth concentration profiles. The process is very complex and can lead to numerous effects as will be discussed in Chapter 5. One major effect arises from the sputter removal of surface atoms which can lead to changes in the surface morphology. This area of research has been extensively studied and the subject of numerous reviews [Navinsek 1977, Auciello 1981, 1982, Carter et al. 1983, Wehner 1985].

The effect of surface morphology, or roughness, on quantitative AES can 'potentially' be accounted for by a surface roughness factor R in the analytic expression of the Auger current (eq. 3.1) [Chang 1974]; however, this is the least well defined parameter in that equation. The uncertainty in quantitative AES that can arise from this 'unquantifiable' parameter can be quite severe. Holloway [1975] used Au films deposited on substrates of different surface roughness and found that the Auger intensity can be reduced by as much as 50% with increasing surface roughness. The magnitude of the decrease was found to depend on numerous experimental parameters including type of analyzer used, and hence the collection angle, and the primary beam, sample and analyzer geometry. Wu and Butler [1982] prepared films of electro-deposited Cu of varying roughness, characterized the surface morphology by SEM, determined the surface areas according to the BET gas adsorption technique [Brunauer et al. 1938] and measured the corresponding Auger intensities. Their results indicate a strong correlation between surface area, or roughness, and Auger signal intensity: As the surface area increases, a corresponding decrease in the Auger intensity of up to 60% relative to a 'smooth' surface is observed. The importance of this effect on quantitative AES cannot be underestimated. As a comparison, although the backscattering factor varies across the periodic table by a factor of 2, it only varies at maximum by 20% for a given element in different matrices [Hall and Morabito 1978].

The procedure usually adopted in quantitative analysis is to assume that R is constant from sample to sample and hence can be ignored. This is not strictly valid in that even an appropriately polished 'smooth' or

featureless surface can evolve into a 'rough' surface under ion bombardment (for example, Hauffe 1971, Hermanne 1973, Gvosdover et al. 1976, Yamada et al. 1979, Mroczkowski and Lichtman 1983a). The characteristics of the surface morphology that develops will depend on many sample and experimental parameters. However, it should be possible to establish conditions under which the above assumption is valid and possibly limitations to the overall accuracy arising from the neglect of this effect as it applies to surface morphologies that are present and evolve under typical AES experimental conditions. Based on this premise, an experimental investigation was carried out.

4.2 FUNDAMENTALS

A primary effect of surface roughness arises due to the fact that electrons emitted from a smooth surface into a field free space will never return, whereas those from a rough surface will have a smaller probability of escape because their trajectory may intersect the surface at an adjacent elevated area and be recaptured [Chang 1974]. In principle, once the roughness dimensions are comparable to, or greater than, the IMFP of the Auger electrons ($\gtrsim$ 0.5 nm), the angular distribution of emitted electrons will be changed and any quantitative measurement which is a function of this angular distribution will be affected [Baird et.al. 1976].

It is convenient to model the effect of surface roughness phenomenologically by considering the Auger process as a combination of excitation and detection [Holloway 1975]. Fig. 4.1 shows the major effects that need to be considered. For the excitation process, the convoluted or rough surface:

1. exhibits an increase in surface area with increasing surface roughness [Wu and Butler 1982];
2. can lead to significant shadowing of some regions of the surface from excitation by the primary beam;
3. leads to variations in the primary beam incidence angle.

Because of the shadowing only a fraction ($\leq$ 1) of the increased surface area can contribute to the emitted Auger current. This effect will become more important for off-normal incidence and roughness dimensions comparable to or greater than the penetration depth of the primary beam,

i.e., 1-2 μm. Additionally, as the primary incidence angle varies from normal incidence, relative to the local normal, the number of Auger electrons produced in the near-surface region which can potentially escape before being inelastically scattered and be detected, increases, i.e., the $\sec\alpha$ dependence in eq. (3.1). In other words, although the total number of Auger electrons produced is essentially constant for a given primary beam current, the fraction which is produced in the near-surface region is greater. The net effect arising from these changes in the excitation process is then to increase the number of Auger electrons produced from the surface region.

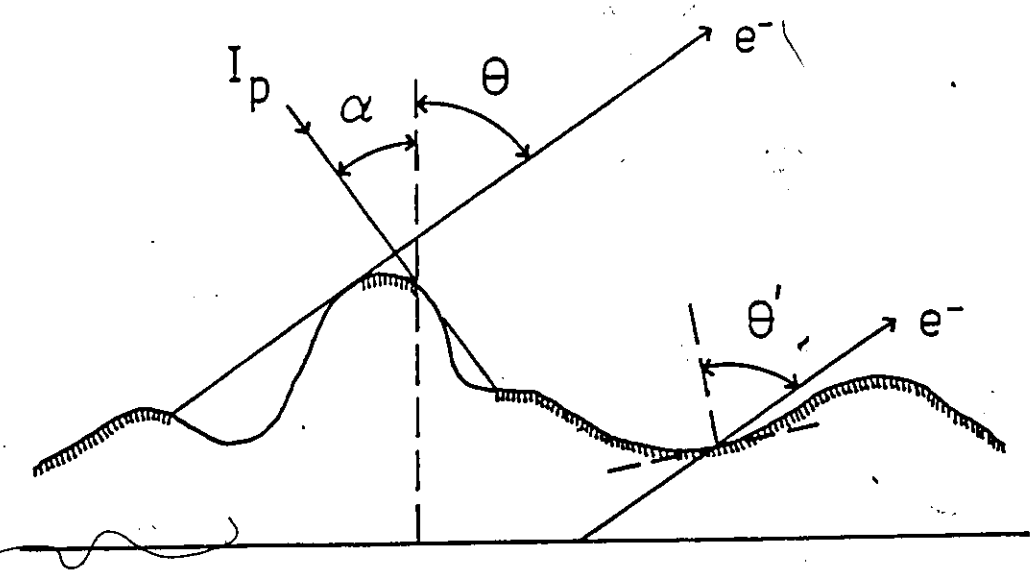

Figure 4.1: The profile of an arbitrary surface from Fadley [1976]. Both the experimental angles and resulting angles for emission are shown. Complete shadowing of the primary and emitted electrons is assumed, so that only the surface area shown with cross-hatching is active in contributing to the detected electron current. Additionally, a variation in the local normal from the average sample normal is shown resulting in a change in the depth sampled by electrons with a given trajectory.

Similarly, for the detection process, the convoluted surface

1. can lead to significant shadowing of emitted electrons whose trajectory is such that a straight line path between the excited area and the detector intersects the surface at an adjacent elevated area;
2. leads to variations in the angle between the local surface normal and the analyzer axis.

As before, the electron shadowing will also decrease the fraction of increased surface area that can contribute to the detected Auger current. The second effect is very important as it dictates the depth of the sample which can contribute to the emitted Auger current at any given point. Any variation in the local normal from the average sample normal will lead to a change in the depth sampled and hence the number of Auger electrons emitted with a given trajectory. As the angle θ between the emitted electron trajectory and the local normal increases, the sample depth from which electrons with a given IMFP can penetrate before being inelastically scattered, decreases. This effect gives rise to the $\cos\theta$ dependence of sampled depth in eq. (3.1). It is difficult to establish the overall change in the detected Auger current arising from these two effects as it will be a function of the appropriate experimental parameters.

As one can see the effect of surface roughness is very complex and depends on numerous experimental parameters including primary beam characteristics such as energy, angle of incidence and cross-sectional area, type of detector and the experimental geometry used, and surface roughness characteristics and dimensions. In addition to the above 'primary' effects, there are secondary effects that may also be considered [Holloway 1975].

Conceivably, there will be a set of experimental conditions such that the existing surface roughness, for example, leads to an increase in the excitation process with no decrease in the detection yielding an overall increase in the detected Auger current. However, the limited experimental evidence that exists in the literature deals essentially with macroscopic roughness and consistently indicates a decrease in detected Auger or photoelectron current with increasing surface roughness [Holloway 1975, Sun et al. 1980, Wu and Butler 1982, Wu et al. 1982].

Earlier theoretical models of the surface roughness effect in photoelectron spectroscopy [Fadley 1974, 1976, Fadley et al. 1974] and in AES [Holloway 1975] are difficult to apply and their practical applicability is uncertain [Holloway 1975, 1978, Webbi and Roques-Carmes 1984, Mroczkowski and Lichtman 1985]. A more recent Monte Carlo method of electron trajectory simulation [De Bernardez et al. 1984] leads to some interesting conclusions. The authors considered the case of a cone-shaped surface roughness generated by the rotation of a triangular wave around an axis. It was assumed that the topography seen is the same from any cone. The triangular wave shown in Fig. 4.2 is characterized by a wavelength, or triangle base, B, and amplitude, or triangle height, H; the surface normal, or cone axis, is defined perpendicular to B. Additionally, normal primary beam incidence was assumed with energy sufficiently high that energy losses within the analyzed volume could be neglected. Under these conditions Auger electrons are generated in depth with a constant probability per unit area perpendicular to the beam. This then leads to an electron generation probability increasing linearly in the direction normal

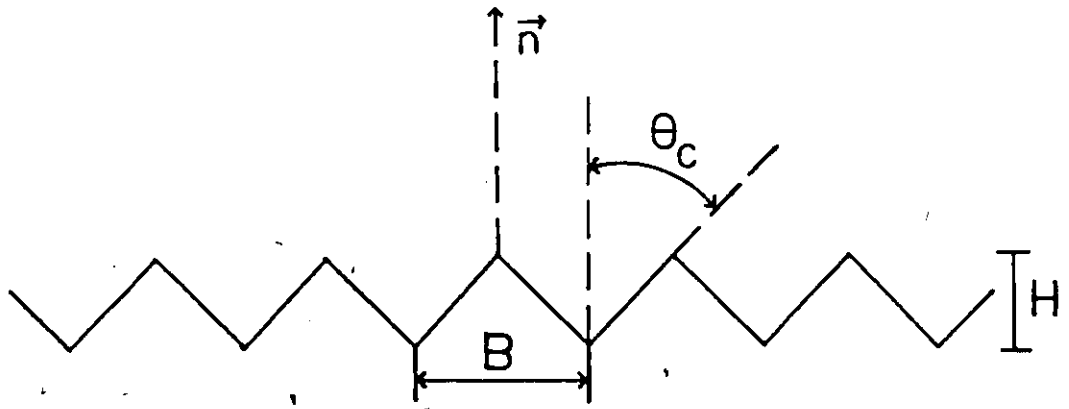

Figure 4.2: The cone-shaped surface roughness assumed in the Monte Carlo calculations of De Bernardez et al. [1984].

to the cone axis being zero at the axis, i.e., zero area, and a maximum at B/2, i.e., maximum area. The generated Auger electrons were then followed until they either arrived at the surface or lost sufficient energy to no longer contribute to the corresponding peak in the energy spectrum. Once at the surface the electrons could either be recaptured, by impinging on a neighbouring cone, or escape from the solid with a given trajectory relative to the target surface normal. The calculations were performed for different relative surface areas S, defined as the ratio between the cone tilted area and the cone base area:

$$S^2 = 1 + (2H/B)^2 \qquad (4.1)$$

A critical angle θ_c exists equal to $\tan^{-1}(B/2H)$. The electron angular distribution calculations for different relative surface areas S and constant B indicate a strong dependence on the values of S and the

corresponding critical angle θ_c. One can see from Fig. 4.2 that if the electron emission angle is greater than the critical angle θ_c, considerable shadowing of the electrons emitted from the sides of the cones will occur. The results indicate that the flat surface (S=1) exhibits the expected decrease in number of electrons $N(\theta)$ escaping from the surface with increasing θ, i.e., with decreasing sampled depth. However, for the rough surfaces (S>1) two regions can be identified:

1. for $\theta > \theta_c$, the decrease in $N(\theta)$ with increasing θ is much stronger than for the flat surface with the magnitude of the deviation increasing with increasing surface roughness;
2. for $\theta < \theta_c$ a small increase in $N(\theta)$ is observed especially for lower energy electrons.

The variation in the absolute AES signal that one would observe would then depend on the collection angle of the analyzer. It is expected that using an RFA, because the collection angle is large, the decrease in signal from (1) is much greater than the increase from (2) and hence a net decrease should be observed.

4.3. EXPERIMENTAL PROCEDURE

A 100 at.% Mo sample was prepared by the method described in Chapter 2. The grain size of the sample was much greater than 1 mm in diameter and hence satisfied the requirements of this study:

1. the ability to perform an Auger line scan across the different grains given the spatial resolution available;
2. the ability to determine the crystal orientation of the different grains through Laue backscattering.

The sample was polished using different techniques in order to obtain the desired starting surface morphology. Using a standard etch-attack technique [Samuels 1967], suggested for such refractory elements, leads to visible grain structure (Fig. 4.3). The grains possess quite different surface morphology, as observed under SEM analysis or even an optical microscope. If the standard mechanical polishing technique described in Chapter 2 is used with an additional final polish using 0.25 μ diamond paste, the desired mirror polish with no visible grain structure is obtained.

The crystal orientations of the grains of interest were determined by Laue backscattering and the surface morphology was characterized by SEM. The sample was then transferred to UHV to study the effect of ion bombardment on Auger yield as a function of crystal orientation and the evolving surface morphological differences. Upon completion of this study, the sample surface was again characterized by an appropriate SEM analysis.

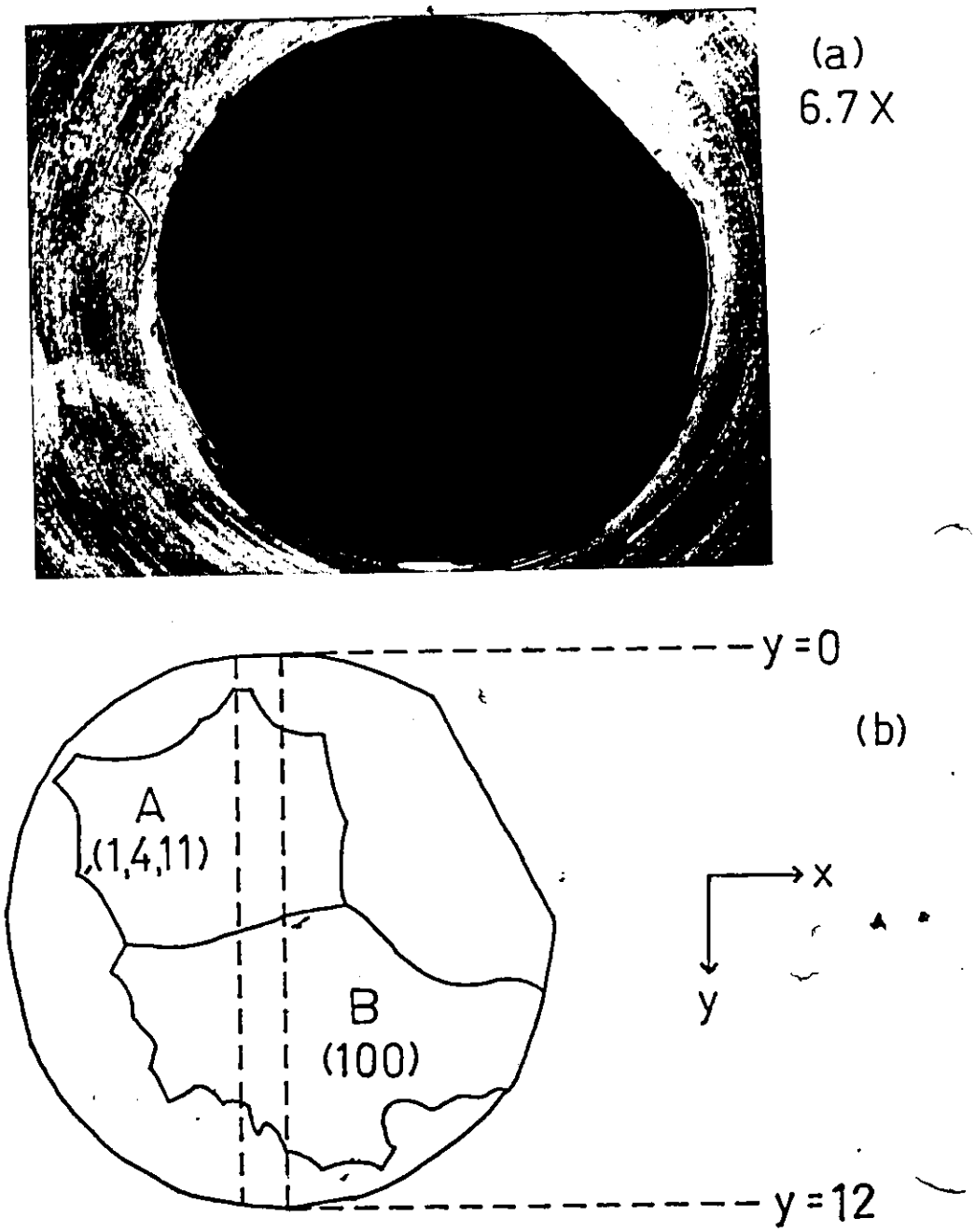

Figure 4.3: (a) The grain structure of the pure Mo sample used in the surface roughness investigation. (b) A schematic representation of the two grains used for the investigation with their corresponding orientation as determined by Laue backscattering; the area used for the AES line scans in y-direction is indicated in units of mm (magnification 6.7X).

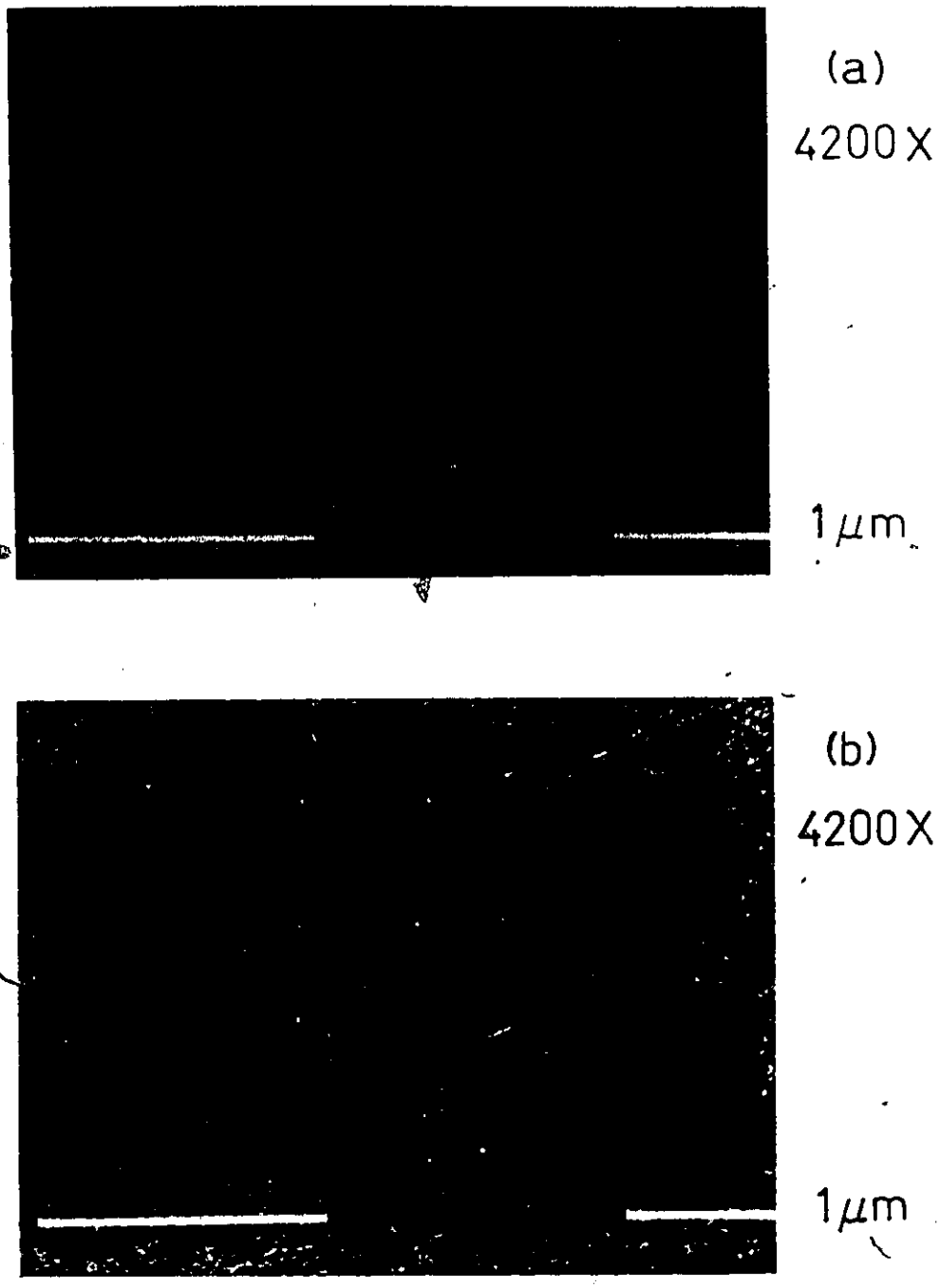

Figure 4.4: (a) and (b) SEM micrographs at 4200X magnification of grains A and B, respectively, indicating a uniform and featureless surface after polishing.

4.4. RESULTS AND DISCUSSION

The grain structure of the sample is shown in Fig. 4.3 with the grains used in this study labelled A and B. Their crystal orientation as determined by Laue backscattering is approximately 2^{o} off (1,4,11) for grain A and approximately 3^{o} off (100) for grain B. The initial surface morphology of the two grains as determined by SEM is shown in Fig. 4.4 under a magnification of 4200X indicating a uniform and relatively smooth featureless surface. This was also observed up to the highest magnification used of 16000X.

Upon commencement of ion bombardment, an Auger line scan was performed over the sample area shown in Fig. 4.3b as soon as a contaminant-free surface was obtained, i.e., in approximately 1 hour. The results shown in Fig. 4.5 indicate that the detected Auger current from the initial well polished surface is essentially constant and independent of crystal orientation. The bombardment was continued for 36 hours with an estimated total fluence of $\sim 5 \cdot 10^{19}$ ions/cm^2 and accompanied by periodic line scans until a steady-state condition was attained. A line-scan of the final sputtered state which was ultimately characterized by SEM is also shown in Fig. 4.5. The results clearly indicate a drastic and essentially constant difference of $\sim$ 18% in the detected Auger current from the two grains: The low-index grain exhibiting the greater intensity.

In addition to the relative change in detected Auger current, it is also of interest to compare absolute changes. This is made possible by using the Auger signal from a 'standard' as a monitor of any changes in instrumental response while maintaining an essentially constant surface

roughness. A second pure Mo sample was used which had been sputtered until a steady-state condition in the detected Auger current was attained. The Auger current was measured periodically, with the 'standard' sample sputtered only to obtain a clean surface, and found to be invariant over the course of the experiment. This then allows a direct comparison of the Auger peak-peak heights (APPH's) in Fig. 4.5 indicating an overall decrease of $\sim$ 5% in detected Auger current from the high-index grain (A) and an increase of $\sim$ 10% from the low-index grain (B) relative to the initial polished surface. The evolution of these changes can be seen in Fig. 4.6 showing the APPH's from one position on each grain as a function of sputter time. One can see that most of the difference in the detected Auger current from the two grains, i.e., $\sim$ 80%, develops within the first 5 hours of sputtering. This bombardment time corresponds to a total fluence of $\sim 7 \cdot 10^{18}$ ions/cm^2.

SEM analysis of the final sputtered state yields an insight into the observed changes in the detected Auger currents from the two grains. Figs. 4.7a and 4.7b obtained at 4200X are typical of the surface morphologies of the two grains. Fig. 4.8, obtained under the same conditions, exemplifies the gross morphological difference as present at the grain boundary. The figures indicate that relative to the polished surface, the low-index grain has become 'smoother', whereas, the high-index grain has developed considerable texture consisting mainly of 'hills and valleys' approaching micron dimensions. Additionally, in order to obtain better contrast, the sample was then coated with a thin Au film [Goldstein et al. 1981]. As seen in Figs. 4.9a and 4.9b under 10000X and 20000X magnification,

respectively, the texture of the high-index grain has an additional fine structure consisting of 'furrows' in the direction of the ion beam.

The results indicate, that under the experimental conditions, changes in the excitation and detection processes arising from a change in surface roughness are such that a net decrease in detected Auger current is observed with increasing surface roughness. It is possible to qualitatively discuss these results in terms of the arguments presented in the literature summary in Section 4.2 (Fundamentals). Considering the changes in the excitation process initially, because the primary electron beam was at normal incidence and the roughness dimensions are less than its penetration depth, shadowing of the primary beam can be neglected. One can then conclude, that an increase in surface roughness can only increase the Auger yield from the near surface region. The observed decrease in detected Auger current with increasing surface roughness can thus, only be attributed to changes in the detection process. These will consist mainly of changes in the extent of emitted electron shadowing and changes in the depth analysed. Individually, this amounts to an increase in the extent of electron shadowing or a decrease in the average sampled depth. However, these two variables are closely linked and it is difficult to establish their relative contribution to their overall composite effect. In summary, the results suggest that under the experimental conditions, any increase in the Auger current emitted due to an increase in the excitation process, is more than compensated by a decrease due to the detection process. Using an RFA with the experimental collection angle, leads to an overall decrease in detected Auger current with increasing surface roughness.

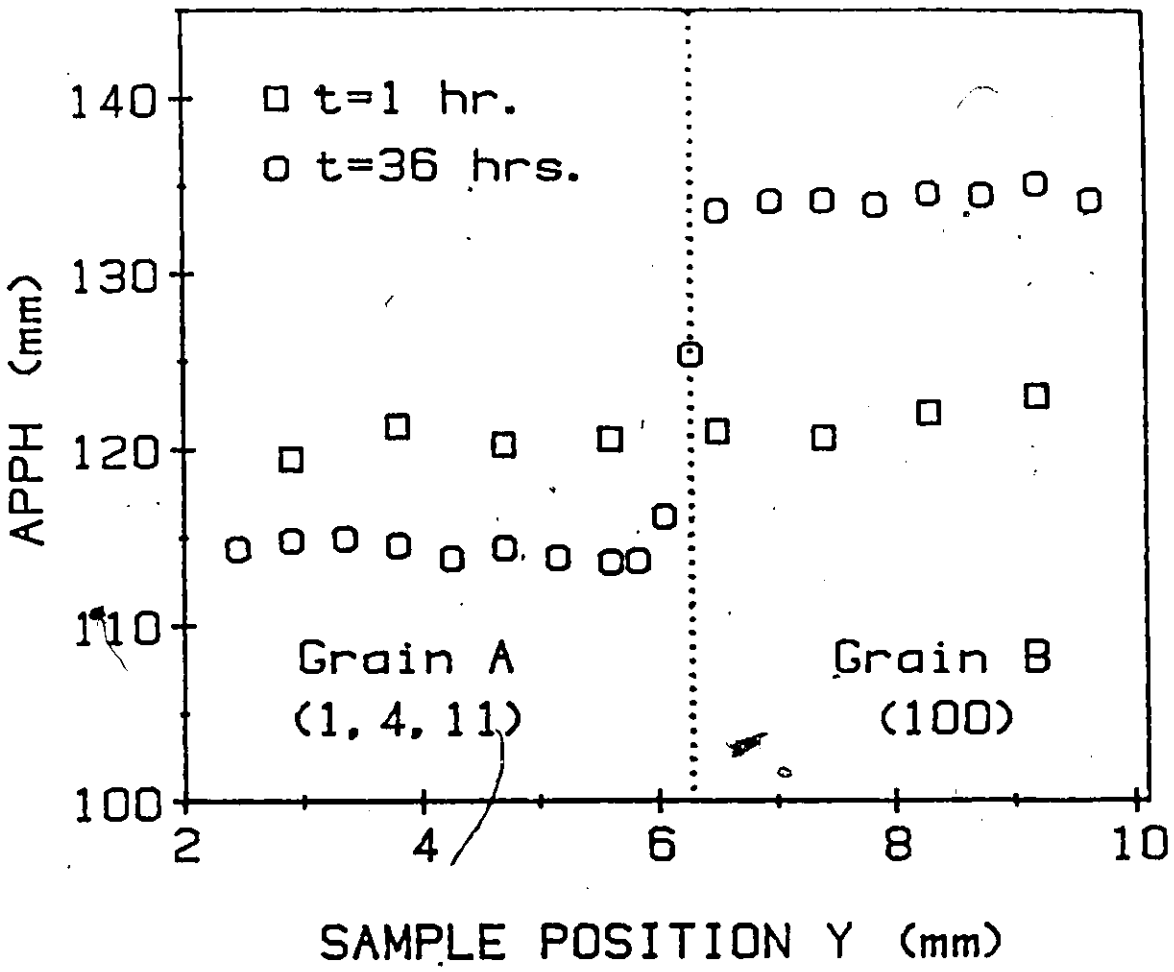

Figure 4.5: AES line scan as shown in Fig. 4.3b indicating the variation in APPH as a function of sample position for different fluence. In the very early stages of ion bombardment (t= 1 hr.) an essentially constant APPH is observed across both grains. At high fluence (t=36 hrs.), a large difference exists for the two orientations.

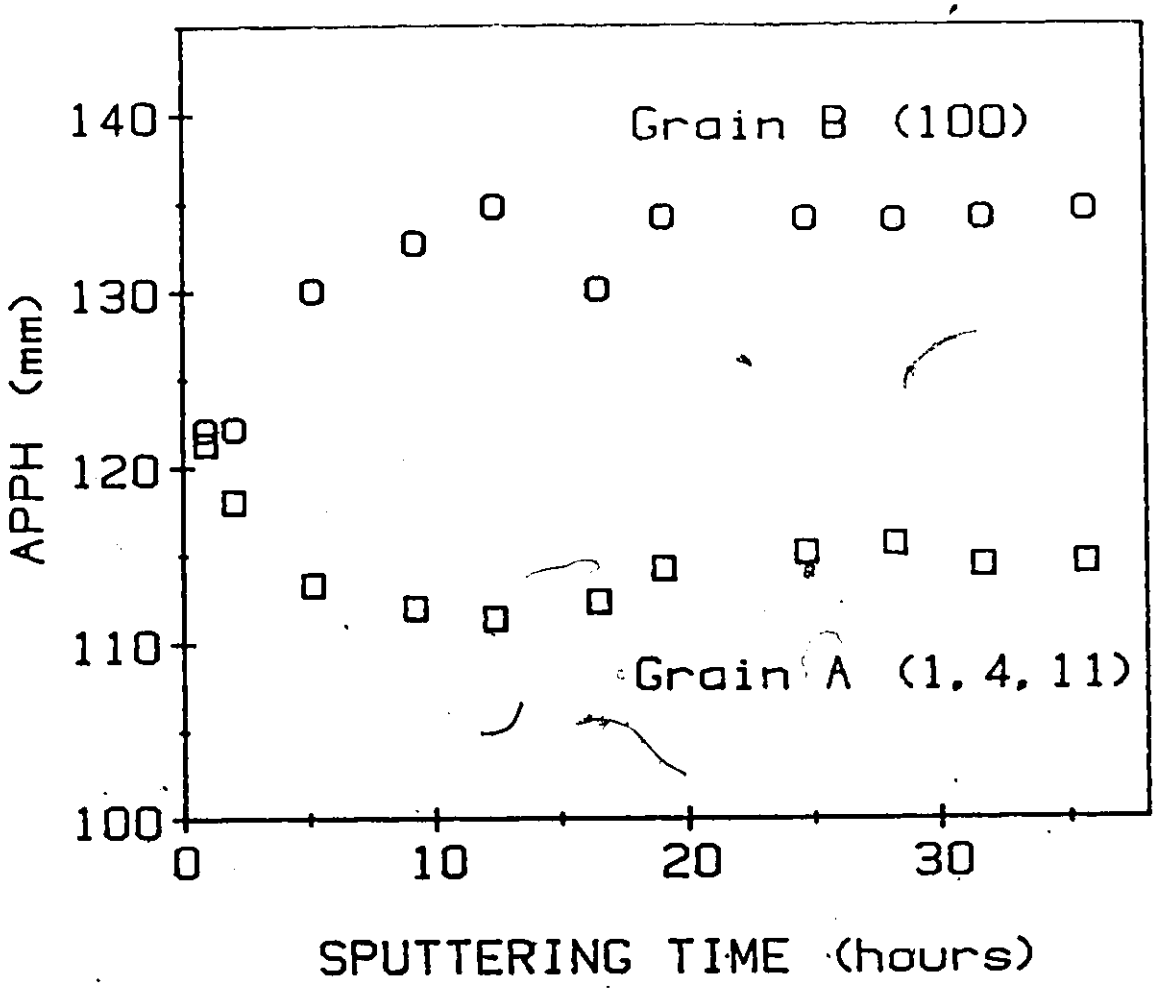

Figure 4.6: The evolution of the variation in APPH detected from the two grains as a function of sputtering time (fluence).

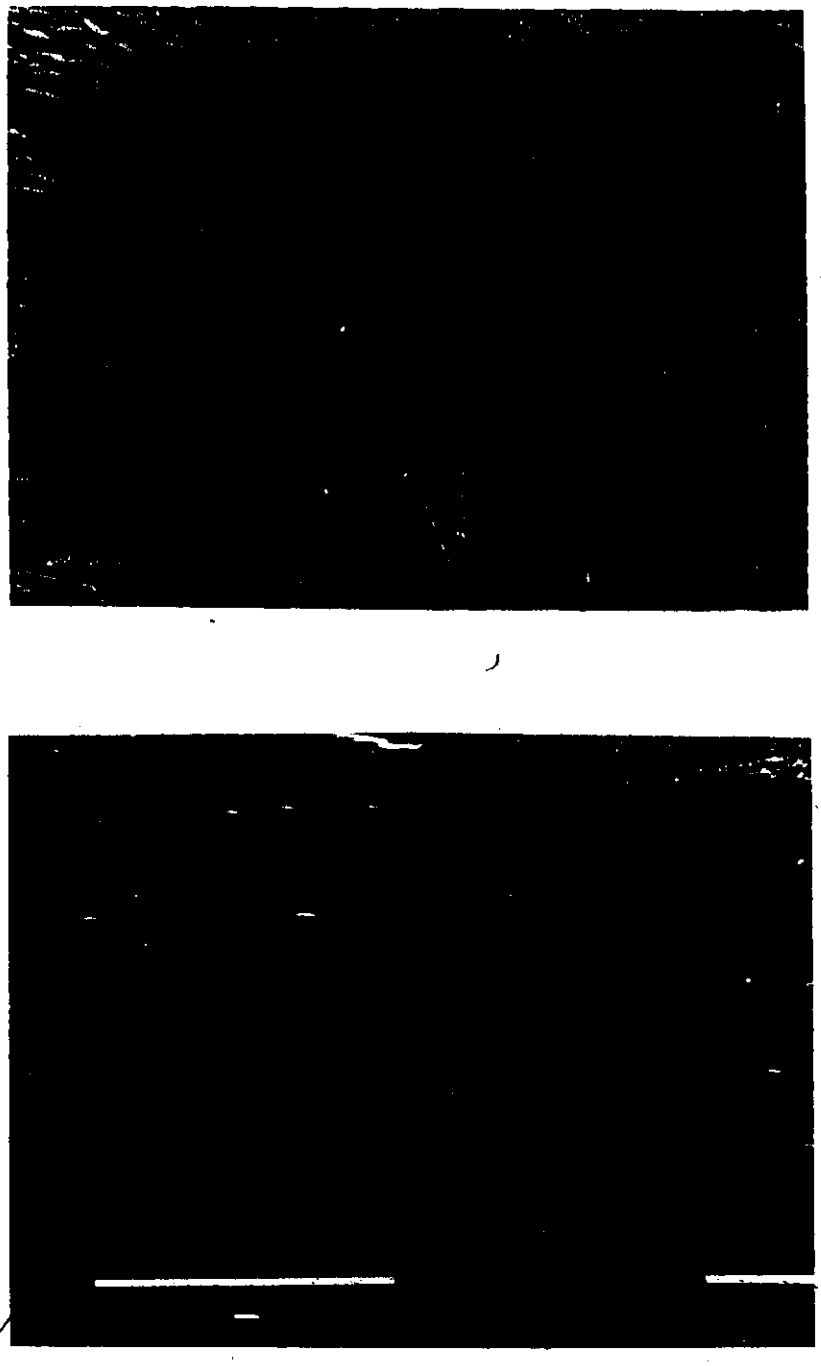

Figure 4.7: (a) and (b) SEM micrographs at 4200X magnification of grains A and B, respectively, indicating considerable difference in the surface morphology of the two grains after ion bombardment for 36 hours.

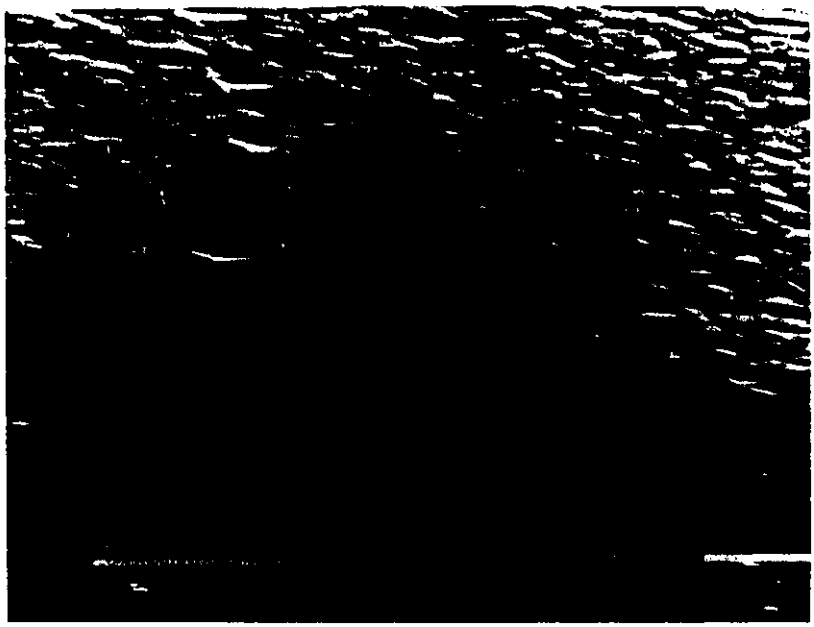

Figure 4.8: SEM micrograph at 4200X exemplifying the gross difference in surface morphology as present at the grain boundary.

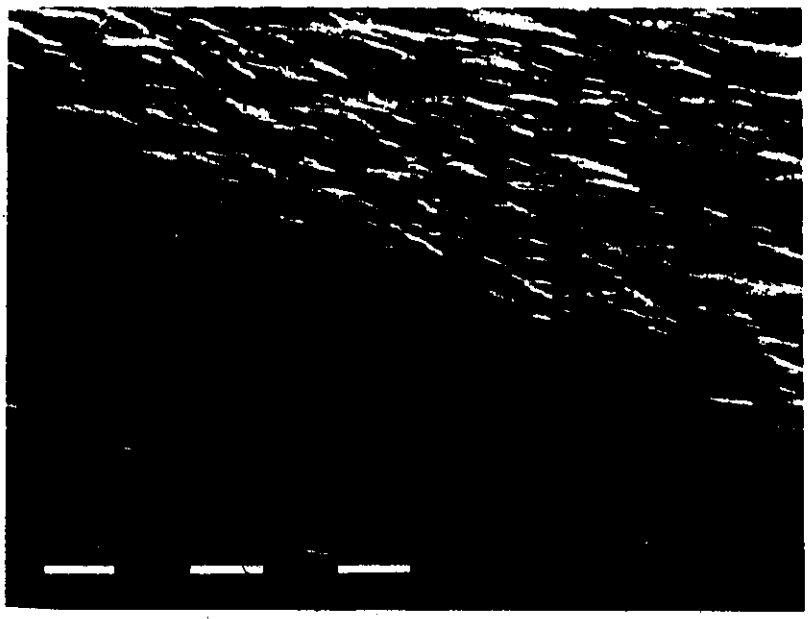

Figure 4.9: SEM micrographs of the Mo sample coated with a thin film of Au to enhance contrast. (a) Grain boundary at 10000X magnification; (b) Grain A at 20000X magnification revealing a fine structure consisting of 'furrows' overlapped on the 'hills and valleys' in the direction of the ion beam.

A second aspect of the results involves the evolution of the surface morphology as a function of ion bombardment time, or fluence, and grain orientation. Changes in surface morphology induced by ion bombardment arise mainly due to the fact that the erosion rate, or sputter yield, is not constant over the entire surface. The characteristics of the surface morphology that develops will depend on many sample and experimental parameters, including the type of target material and its initial state, crystal orientation, impurities' level, sample temperature, ion species, ion energy, angle of incidence, flux and fluence. Depending on the actual experimental conditions, one may also need to consider effects such as shadowing of certain areas from the ion beam, reflection of incident ions to other parts of the surface and the re-deposition of sputtered material onto adjacent surfaces. The process is very complex and hence, it is very difficult to predict the type of structure that will result [Wu and Butler, 1982]. Additionally, there will be a critical fluence, between $5 \cdot 10^{16}$ and $5 \cdot 10^{17}$ ions/cm^2, where the surface structure has changed so much that all surface dependent processes are significantly changed [Navinsek 1977].

In a comprehensive review of the topic Navinsek [1977] interpreted the evolution of surface morphology in terms of ion fluence. He used this parameter to establish three regions:

1. low fluence (10^{11}- 10^{15} ions/cm^2) yielding indirectly detectable damage on an atomic scale;
2. medium fluence (10^{15}- 10^{17} ions/cm^2) yielding visible damage on a microscopic scale; and,

3. high fluence (> 10^{17} ions/cm^2) leading to well developed surface structures on a macroscopic scale.

He concludes that under ion bombardment, using ions with energies less than a few KeV and a fluence less than the critical fluence, single crystals will become smoother or rougher depending on the stability of that particular orientation: Stable crystal faces will become smoother, all others will develop facets. Studies on polycrystalline materials reinforce this picture.

It has been suggested [Gvosdover et al. 1976] that structures such as cones are formed on surfaces with the 'roughest' atomic structure. Studies by Whitton et al. [1978] indicate that a dense array of cones stable under prolonged bombardment can be obtained when surfaces with particular high crystallographic indices are irradiated. The reason for this orientation selectivity is unknown.

The experimental results of this study, suggest that the initial polished surface consists of polish damage similar across the entire sample. Under ion bombardment the polish damage is slowly removed with increasing fluence and the structure that evolves is a function of the crystallographic orientation. It is expected that the atomically rougher high-index grain should exhibit quite different sputtering characteristics than the microscopically smoother low-index grain. Its tendency to facet should be greater [Farnsworth et al. 1969] and the probability of trapping a displaced surface atom ,i.e., re-deposition, should also be greater due to its rougher structure. Such a picture predicts a smaller erosion rate for the high-index plane consistent with the experimental observations shown in

Figs. 4.8 and 4.9a. Additionally, the period of time before the crystal orientation effects begin to dominate the evolving structure under increasing fluence should vary in proportion to the polish damage.

An attempt to answer the question of whether the difference in surface morphology can be removed, or reduced, was made in another set of experiments. As above, the sample was polished to the desired 'smooth' uniform featureless state and ion bombardment under the same conditions was continued until the gross difference in Auger yield attained a steady-state. The sample was then heated for one hour at temperatures of approximately 1300 and 1450 K with corresponding Auger line scans. The results indicated small changes in Auger intensities across each grain but the gross difference persisted.

4.5. SUMMARY

It is possible to prepare a polycrystalline Mo elemental standard with a uniform surface morphology across the entire sample. The Auger current measured from such a surface is found to be essentially constant at different sample positions: A property of an elemental standard which is expected and usually assumed. However, even under ion bombardment conditions typically used in AES, i.e., 2 KeV Ar^+ at glancing incidence, a surface morphology evolves as the fluence is increased to $\sim 5 \cdot 10^{19}$ ions/cm^2 that leads to gross differences in the detected Auger current of up to 18% from grain to grain. This gross difference is attributed to the extent of surface roughness that evolves which is in turn mainly dependent on the crystal orientation. It is found that relative to the polished surface:

1. A high-index grain ~ (1,4,11) develops considerable texture of macroscopic dimensions consisting mainly of 'hills and valleys' with a 'furrowed' fine structure in the direction of the ion beam yielding a net decrease in detected Auger current.
2. A low-index grain ~ (100) becomes smoother yielding a net increase in the detected Auger current.

It is clear that for quantitative AES an elemental standard exibiting the initial properties of the Mo sample used in this investigation, is appropriate. A 'standard' exibiting the final properties is unacceptable. However, one can minimize this effect due to surface roughness as follows:

1. An initial well polished surface with uniform morphology over the entire sample must be used.

2. Total fluence must be maintained to a minimum.

3. The analyzed area must be such that the detected Auger current is averaged over numerous grains. This can be accomplished with a defocussed primary electron beam and/or using a sample with small grain size.

Once a critical fluence is attained, as exemplified by a varying detected Auger current at different sample positions, a severe decrease in accuracy can arise from use of that 'standard'. Since it has not been possible to negate the effect of surface roughness by annealing the sample to approximately half its melting point, the sample(s) will have to be repolished once again to a uniform featureless surface.

This investigation has documented the problems that can arise in the quantification of AES using elemental standards. In terms of this study, it is concluded that in order to attain accurate AES results, both the elemental standards and alloy surfaces must, not only possess a uniform morphology, but also an identical one. In practice, such surfaces are difficult to attain given some of the severe processing used to obtain impurity-free alloys. For this reason, all the quantitative results presented in this study were obtained after appropriate processing was complete and all surfaces repolished to a uniform and similar morphology. Additionally, the procedure suggested for minimizing the effect of surface roughness has been adopted.

CHAPTER FIVE

ION BOMBARDMENT MODIFICATIONS OF ALLOY SURFACES

The use of inert gas ion bombardment as a routine method of obtaining clean surfaces and depth profiling dictates that any investigation utilizing this process must require a thorough understanding of the radiation-induced modifications in the composition and defect profiles that result. In this chapter, an investigation of the processes that play a significant role in establishing such modifications, is presented. An appropriate review of the literature is summarized to establish the necessary fundamentals, as they pertain to this study, and the results of an experimental investigation of the Cr-Mo system are presented. This investigation establishes the state of the surface prior to initiating any of the segregation experiments presented in the subsequent chapters.

5.1. INTRODUCTION

Ion bombardment modifications of alloy surfaces are not limited to the evolution of surface morphologies as presented in the previous chapter. It is now well established that bombardment with energetic ions can lead to perturbations in both the composition and defect profiles of the near-surface region through at least six distinct processes [Wiedersich 1983, 1985, Lam et al. 1985]. These can be grouped as those being essentially

athermal 'ballistic' processes: preferential sputtering, displacement mixing and recoil implantation; and those requiring the thermally activated motion of atoms/defects: Gibbsian segregation, radiation-induced segregation (RIS) and radiation-enhanced diffusion (RED). The contribution of each of these effects to the state of a surface under a particular set of experimental conditions is very difficult to discern in most systems: It will depend mainly on the species, energy and flux of the bombarding ion and on the target material and its temperature. However, the latter set is expected to play a minor, if not a negligible role at room temperature in refractory alloys such as those used in this study.

5.2. FUNDAMENTALS

5.2.1. Radiation Induced Processes

Irradiation under the experimental conditions used in this study, falls in the linear cascade regime where collisions are considered to occur with stationary target atoms [Sigmund 1981, Behrisch 1983]. Vacancy-interstitial pairs, or Frenkel pairs, are created by the displacement of target atoms from their equilibrium sites through a collision with either the projectile or a target atom that had been set in motion. If sufficient energy is transferred to a target atom such that its kinetic energy component normal to the surface is greater than the surface binding energy, the atom will be sputtered causing an erosion of the target surface. The sputtered flux of atoms originates from the topmost few layers of a target [Sigmund et al. 1982, Dumke et al. 1983, Shapiro et al. 1985, Lam et al. 1985] with the majority having energies in the lower eV range [Sigmund 1981, Kelly 1984a]. Thus only a small fraction of the incident particle's energy is consumed in sputtering events, the remainder ends up as heat and bulk radiation damage. When a multicomponent target is subjected to ion bombardment, the constituent elements are sputtered at different rates because of differences in surface binding energies and in the efficiency of energy transfer, i.e., a mass dependence. This phenomenon has become known as preferential sputtering and has been well reviewed [Coburn 1979, Betz 1980, Andersen 1982, Betz and Wehner 1983, Kelly 1978, 1980, 1984b, 1984c, 1985].

The maximum energy E_{MAX} transferred to a target atom of mass M_1 by an ion of kinetic energy E_o and mass M_2 is given by

$E_{MAX} = 4E_0M_1M_2/(M_1 + M_2)$. If E_{MAX} exceeds some critical energy (~1 KeV) displacement cascades are formed consisting of vacancy-rich centres, or depleted zones, with the interstitials ejected into the surrounding lattice by replacement collision sequences (RCS) along close packed atomic rows and channeling [Eyre 1973]. The vacancy density of the depleted zones may be sufficiently high that their spatial distribution is unstable. The vacancies may then collapse into energetically more stable clusters at temperatures far below those at which mono-vacancies migrate by thermal activation [Wilkens 1975]. The steady-state defect profiles will be quite complex and will be determined by the mobility and interactions of the different defects formed with each other and existing sinks such as the surface, grain boundaries, immobile clusters, etc. A schematic two-dimensional representation of radiation damage in a crystal lattice as envisioned by Seeger [1962] is shown in Fig. 5.1.

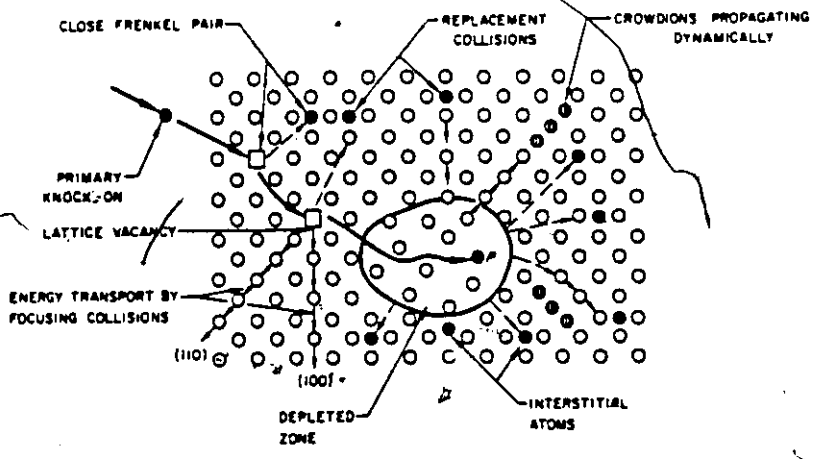

Figure 5.1: A schematic representation of radiation damage showing a depleted zone and the surrounding environment in a (001) plane of an fcc crystal lattice. The primary knock-on atom impinges from the left and comes to rest at the position denoted P. After Seeger [1962]

The violent passage of the incident ion through the alloy gives rise to collisional (ion-beam, ballistic) mixing comprised of displacement mixing and recoil implantation. Displacement mixing can be considered as a random-walk process of the recoiling atoms set in motion in the collision cascade. Recoil implantation is a result of lighter atoms being preferentially transported in the beam direction relative to the heavier components because of preferential momentum transfer [Sigmund 1979]. However, because the energy transfer from recoiling atoms to other atoms is rapid, most of the relocation of atoms in energetic cascades leads to isotropic mixing rather than recoil implantation [Wiedersich 1985]. To a good approximation, recoil implantation and displacement mixing can be considered temperature-independent since the recoil energies are much greater than the thermal activation energies. Additionally, since the sputter yield of materials is relatively temperature independent up to temperatures approaching the melting point [Andersen and Bay 1981], and definitely at room-tempearture in refractory alloys, it too can be grouped with the collisional processes as being an essentially athermal or ballistic process.

At elevated temperatures, the radiation-induced defects, vacancy and interstitial type, become mobile and migrate until they annihilate either through recombination with their anti-defect or at sinks. If their concentration is sufficiently higher than dictated by equilibrium conditions, then their mobility can lead to radiation-enhanced diffusion since the diffusion coefficients of the alloy components are a function of the defect concentrations. If during irradiation, the production and/or annihilation of defects is non-uniform, defect-fluxes will arise. Any preferential

coupling of an alloy component with a defect flux can lead to radiation induced segregation. Finally, at sufficiently high temperatures surface (Gibbsian) segregation will occur so as to lower the total free energy of the system. This last process, describing equilibrium compositional modifications, is presented in Chapter 6.

5.2.2. Radiation Damage Recovery

An insight into the steady-state sputtered condition of the system can be obtained from radiation damage recovery experiments. A rich literature and numerous review articles exist on this research area (Seeger et al. 1970, Eyre 1973, Schilling and Sonnenberg 1973, Seeger 1973, Seidman 1973, Wilkens 1974, Young 1975, Robinson and Young 1975, Smallman and Harris 1977, Balluffi 1978, Peterson and Siegel 1978). Studies on this subject have involved numerous defect distributions depending on the energetic particle, i.e., electron, neutron, ion, etc., and irradiation conditions used. Of the group VIa refractory elements, Mo has been the most widely studied with much less work performed on Cr. The complexities introduced by the presence of substitutional solute atoms and non-metallic interstitial impurities are beyond the scope of this study. An interpretation of literature results is given mostly in terms of the element Mo, i.e., the solvent in the alloys used in this study for the investigation of non-equilibrium effects.

STAGE I recovery is associated with the long-range migration of interstitials and for both Mo (Eyre 1973) and Cr (Biget et al. 1975) lies well below room temperature. The long range mobility of these defects can lead to the formation of clusters as observed by Eyre (1972) in neutron

irradiated Mo at 77 K. The vacancy type defect, most likely mono vacancy, becomes mobile and can undergo long-range migration in Stage III. The temperature associated with this stage is very dependent on the type of irradiation used and sample purity. Values ranging from 425-650 K have been observed [Eyre 1973, Evans 1975, Evans and Eldrup 1975, Balluffi 1978]; the best value obtained on a very pure specimen from a quenching experiment is 645 K [Suezawa and Kimura 1973]. Once a vacancy is mobile it can undergo recombination with its anti-defect or annihilate at fixed sinks such as the surface, grain boundaries and immobile clusters. Migration to vacancy-type clusters leads to cluster growth which then anneal out at much higher temperatures. Positron annihilation [Peterson et al. 1974, Eldrup et al. 1975, Evans 1975, Evans and Eldrup 1975], TEM [Wilkens 1970, Eyre 1973, Eyre and English 1974, Bentley et al. 1975] and resistivity measurement [Moteff 1967] studies in Mo indicate that temperatures of at least 875 K are required for the thermal emission of mono-vacancies from small clusters. If the sink density, other than immobile vacancy-type clusters, is low then further growth of these types of clusters is possible at appropriate nucleation sites which then anneal out at even higher temperatures.

5.2.3. Ion and Damage Range Calculations

The linear collision-cascade regime has been treated in most detail theoretically. In this regime, the theoretical description of the slowing down of energetic particles in a target is based on the work of Lindhard et al. [1963a, 1963b, 1968] and has become known as LSS theory. Calculations of collision-cascade effects proceed mostly from transport theory using

a Boltzmann transport equation. It is assumed that an amorphous, infinite target, with an imaginary surface plane embedded in it, is used and that both particle-target and target-target collisions occur between a moving and a stationary particle. The initial kinetic energy of the incident particle is considered to be shared between inelastic energy processes, i.e., excitation and ionization of target electrons, and as kinetic energy transferred to a large number of target atoms through elastic collisions. Analytical solutions to the Boltzmann equation can only be obtained by assuming that the inelastic processes are negligible. This assumption can be by-passed by use of numerical methods. A standard approach for obtaining these distributions is based on using a moments expansion of the equation followed by a final reconstruction of a distribution from its moments. Winterbon et al. [1970] have applied LSS theory to determine the spatial distribution of ion, and elastic and inelastic energy deposition ranges. This work has become known as WSS theory and a compilation of moments of numerous ion-target combinations with various irradiating energies is available [Winterbon 1975]. Additionally, an essentially complete review of the field has been published by Sigmund [1972a, 1972b].

In practice, the distributions of interest are reconstructed from a knowledge of the mean projected range $\langle x \rangle$, the second central moment $\langle \Delta x^2 \rangle$, and, for greater accuracy, the third and fourth central moments, $\langle \Delta x^3 \rangle$ and $\langle \Delta x^4 \rangle$, respectively. The Edgeworth expansion is one of a number of distribution functions that can be used to reconstruct the distribution of interest from the appropriate moments. Using a truncated one-dimensional Edgeworth expansion, the actual distribution C(x) is written

as a product of a Gaussian function G(x) and a polynomial function P(x) [Gibbons et al. 1975, Kelly 1984a]:

$$C(x) = G(x)\, P(x)$$

The differential concentration profile is then given by:

$$C'(x)\,dx = [\,dx / (2\pi \langle x^2 \rangle)^{1/2}\,] \cdot \exp(-\delta^2/2) \cdot [\,1 + (\beta_1^{1/2}/6)\cdot(\delta^3 - 3\delta) + (\beta_1/72)\cdot(\delta^6 - 10\delta^4 + 15\delta^2)\,] \qquad (5.1)$$

where the following notation has been used:

depth variable = $\delta \equiv (x - \langle x \rangle) / \langle \Delta x^2 \rangle^{1/2}$;

first moment ≡ mean projected range = $\langle x \rangle \equiv R_p$;

second central moment ≡ standard deviation in mean projected range ≡ x-straggling = $\langle \Delta x^2 \rangle^{1/2} \equiv (\langle x^2 \rangle - \langle x \rangle^2)^{1/2}$;

third central moment ratio ≡ skewness = $\langle \Delta x^3 \rangle / \langle \Delta x^2 \rangle^{1/2} \equiv \beta_1^{1/2}$;

fourth central moment ratio ≡ kurtosis = $\langle \Delta x^4 \rangle / \langle \Delta x^2 \rangle^{1/2} \equiv \beta_2$.

Equation (5.1) has been normalized to unit dose by dividing by the fluence (ions/cm^2) and contains the simplification suggested by Gibbons et al. [1975] for the fourth central moment, namely, $\beta_2 = 3 + 5\beta_1$. Under the assumptions of this analysis, i.e., an amorphous, uniform, infinite target under bombardment at normal incidence and in the linear cascade regime, the reconstructed distributions are expected to yield good approximations to the 'real' distributions: An accuracy of ~ 10 % has been quoted by Winterbon [1975] by using appropriate data. The problems that arise when using polycrystalline targets and off-normal incidence are discussed later.

For this study, approximate ion range and damage distributions were reconstructed from a truncated one-dimensional Edgeworth expansion and

appropriate moments interpolated from Winterbon's tables (1975). For pure Mo and Cr targets under 2 KeV Ar^+ ion bombardment, the results shown in Figs. 5.2a and 5.2b, respectively, were calculated. The results for a Mo target, predict a maximum in the ion distribution occuring at 1.7 nm with a standard deviation, or x-straggling, of 1.3 nm yielding a penetration depth, estimated equal to $\langle x \rangle + 2\langle x^2 \rangle^{1/2}$, of 4.3 nm. Similar values are obtained for the Cr target. It is expected that the similarity in the distributions for the two elements extends to the alloys of this system. This has been observed in a corresponding calculation for a 50 at.% alloy using the mean values of the appropriate parameters.

The conditions under which these calculations are valid have been described. The major differences with the experimental conditions used are due to an off-normal ion incidence and a polycrystalline target. It has been suggested [Winterbon 1975] that the off-normal incidence used ($\theta = 72^o$) can be taken into account through a cosθ dependence in the appropriate moments to yield smaller penetration depths. However, it is presently believed that under such a bombardment geometry, straggling could actually lead to an increased penetration [Davies, private communication]. The polycrystallinity of the sample will lead to a deeper penetration of the ions due to channeling [McCargo et al. 1963, Chu 1976] and the damage will also extend deeper than predicted due to defect mobility and RCS. Any enhancement in the defect concentration over the equilibrium concentration can lead to RED and hence contributes to the depth of the 'altered layer'. Therefore, at best the above calculation yields an order-of-magnitude estimate for the depth of the sputter modified sub-surface.

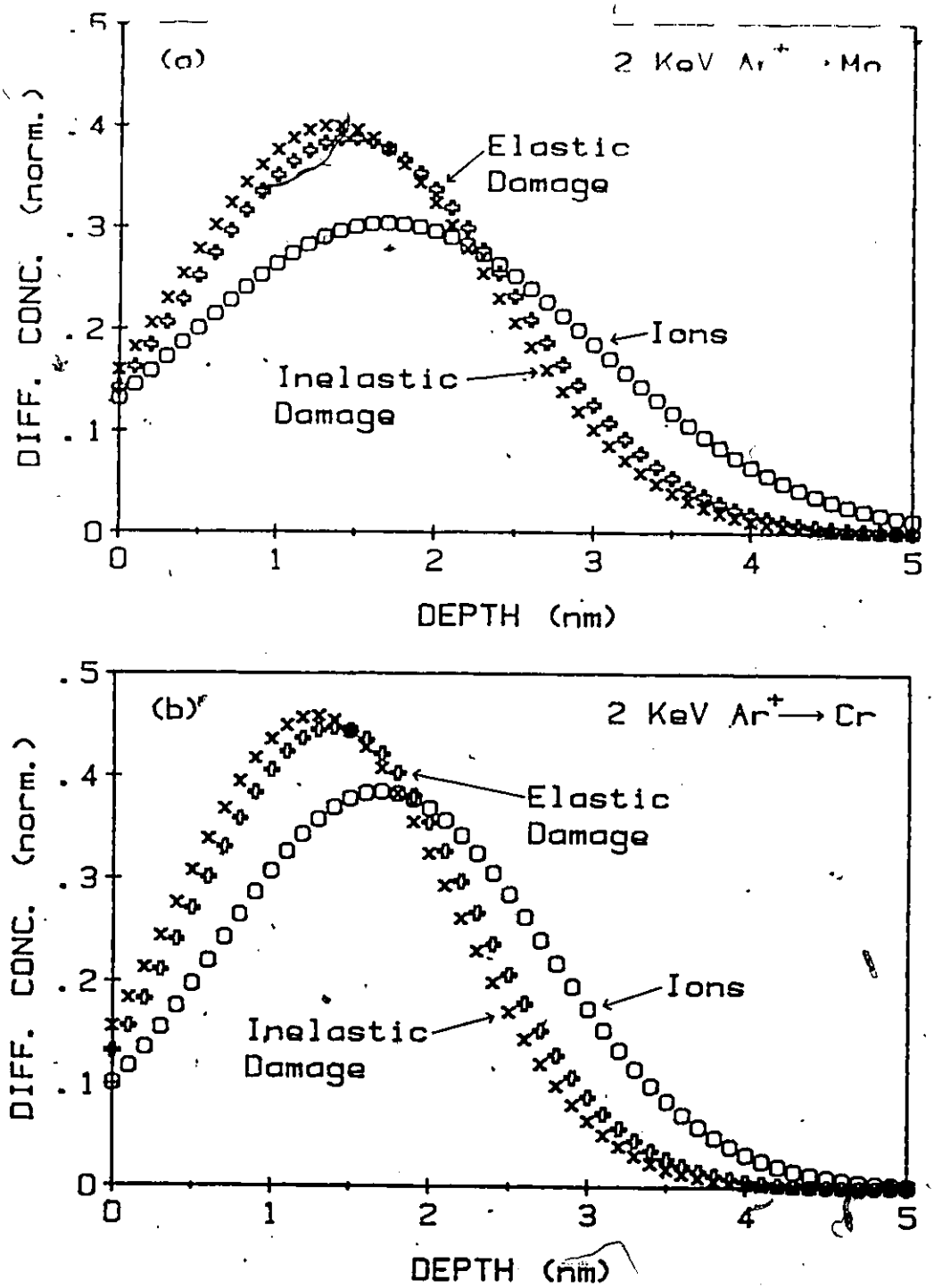

Figure 5.2: Ion range and damage distributions reconstructed from a one-dimensional Edgeworth expansion and appropriate moments from Winterbon's compilation [1975] for (a) Mo and (b) Cr targets.

5.2.4 Damage Rate Calculation

With a knowledge of the ion and damage range distributions, one can calculate other relevant effects. Of particular interest in radiation damage studies is the average number of displaced atoms that result in a collision cascade. The average number of Frenkel pairs can be calculated from the modified Kinchin-Pease equation [Sigmund 1969b]:

$$N_d(E) = 0.84\ \nu(E) \cdot E\ /\ 2E_d\ , \qquad \text{for } E >> E_d \qquad (5.2)$$

where $\nu(E)$ is the part of the incident ion energy E deposited into elastic collision processes such that $\nu(E) + \eta(E) = E$ where $\eta(E)$ is the inelastic part, E_d is the threshold displacement energy required to create a stable Frenkel pair. Merkle [1975] has suggested that for irradiations in which all crystal orientations are equally probable, the value of E_d used in eq. (5.2) should be an average threshold value which generally lie between a factor of 1.5 to 2.2 above the minimum threshold.

Another important parameter useful in damage studies is the average number of displacements per atom (dpa) which can be estimated from knowledge of the Frenkel-pair production rate, the damage distributions and the ion fluence.

It is of interest to estimate the extent of damage and the associated 'mobility' of the atoms in the surface region under the ion bombardment conditions used in this study. For Mo, using the modified Kinchin-Pease equation (5.2) with an average displacement energy E_d of 70 eV [Merkle 1975] and a fraction of the ion energy deposited into elastic damage calculated using WSS theory (Section 5.2.3) of $\nu(E) = 0.78$ yields a Frenkel

pair production rate of 9.4 displaced atoms/ion. With the standard ion flux used of $\sim$ $4.1 \cdot 10^{14}$ ions/cm^{2}sec and an effective penetration depth of 4.3 nm (Section 5.2.3) yields an average damage rate of 0.14 dpa/sec. A steady-state sputtered condition is attained within 15 min and hence, for a negligible sputter rate, one obtains $\sim$ 130 dpa. This is an overestimate as clearly, the sputter rate is not negligible but nontheless indicates a considerable mobility in the surface region under the irradiating conditions.

5.3. EXPERIMENTAL RESULTS

5.3.1. Steady-State Sputtered Surface Composition

The steady-state sputtered surface compositions of 13 alloys encompassing the entire composition range are shown in Fig. 5.3 as a function of the Cr bulk mole fraction, x_b^{cr}. For each alloy the surface mole fraction x_s^{cr} has been calculated according to eq. (3.25b) using both the Mo(186) and Cr(529) transitions. In keeping with the notation presented so far, the surface mole fraction should be denoted as the appropriately weighted value, $\overline{x}_s^{cr}$, however, as will be presented, the steady-state sputtered surface of such alloys can be adequately approximated as being homogeneous over the analysed depth and hence the former symbol is appropriate. The data indicate a depletion of Cr in the surface region, relative to the bulk concentration, across the entire composition range. Additionally, no systematic ordering is observed between the x_s^{cr} values calculated from the Mo and Cr peaks.

5.3.2. Surface Composition as a Function of Analyzed Depth

The possible existence of any sample inhomogeneity with depth in a sputtered surface under steady state conditions was further investigated in three alloys: 6.0, 83.4 and 93.2 at.% Cr. Digitally collected data from three energy regions, namely, 20-50, 100-240 and 425-580 eV, were used to probe the surface composition as a function of analyzed depth. Numerous independent data sets each comprising of alloy and elemental standards spectra collected sequentially under identical instrumental conditions, were obtained. Surface compositions were determined from the alloy spectra objectively by minimising the sum of the squares of differences between

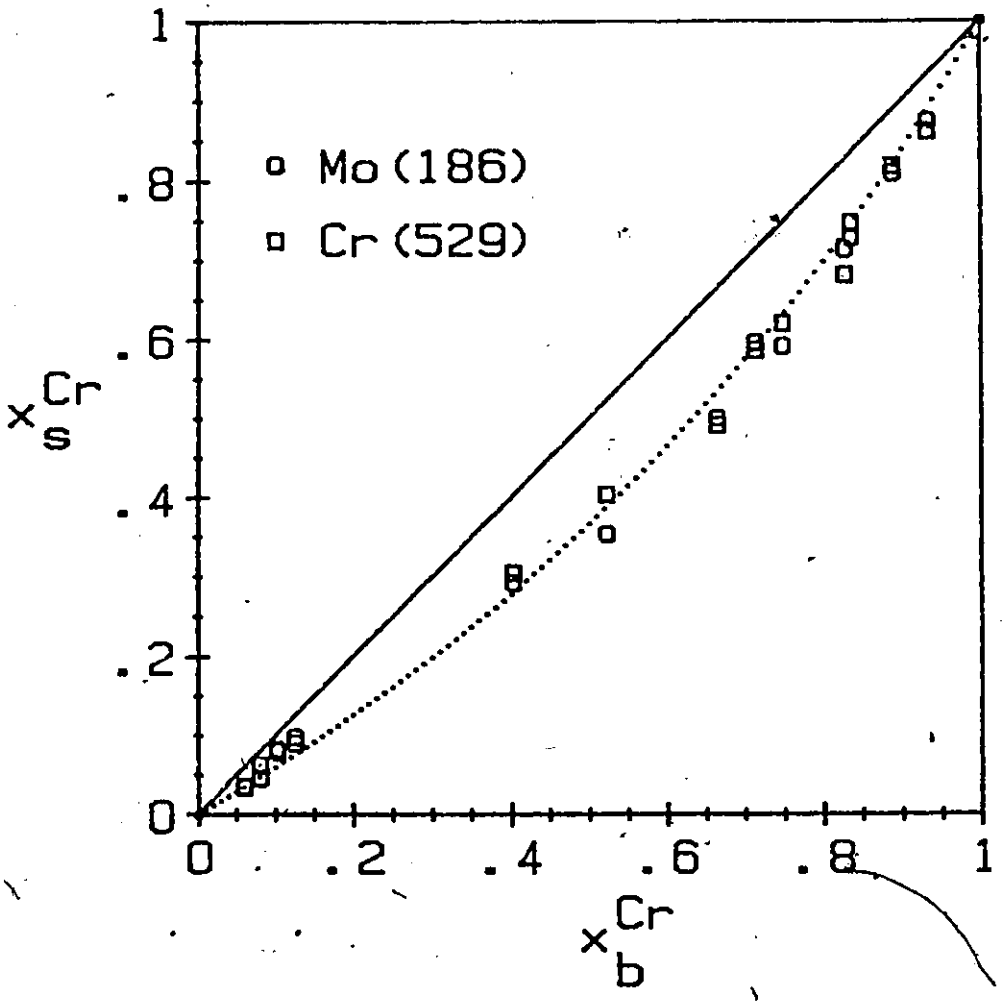

Figure 5.3: The surface Cr concentration, x_s^{cr}, for sputtered Cr-Mo alloys plotted as a function of the bulk Cr concentration, x_b^{cr}. x_s^{cr} has been calculated from the normalized APPH's using both the Cr(529) and Mo(186) transitions according to eq. (3.25b). Based on a phenomenological preferential sputtering model, the dotted line shows a theoretical curve plotted according to eq. (5.8) using K= 1.73.

the alloy spectra and simulated spectra using a computer grid search routine. The alloy spectrum was fitted by:

$$I^{AB}(E) = f_A I_A^A(E) + f_B I_B^B(E) \quad (5.3)$$

where $I^{AB}(E)$ is the intensity in the simulated spectrum; $I_A^A(E)$ and $I_B^B(E)$ are the intensities from the standard spectra, respectively; and f_A and f_B are the corresponding fractions of the pure standards. Of the three alloys investigated by this procedure, the 83.4 at.% Cr alloy exhibits the greatest deviation in composition from that of the bulk and hence provides the best test case. Typical sputtered spectra from this alloy along with the appropriate elemental standards and the resulting best fit simulations in the three energy windows are shown in Figs. 5.4, 5.5 and 5.6, respectively. The excellent simulations obtained according to eq: (5.3) are consistent with the expectations of negligible matrix effects in this alloy system for a sample surface homogeneous over the analyzed volume (Section 3.4). The average of the best fit parameters for each of five data sets are plotted in Fig. 5.7 as a function of the IMFP (analyzed depth). As discussed later, the average value of five data sets consisting of a total of 210 best fit simulations per energy region has been calculated and shown in Table 5.1. The results indicate that to within experimental error, the surface region is homogeneous over the analyzed depth. Because the sputter perturbation in the other two more dilute alloys was much smaller, the resolution of this technique could not establish whether a systematic variation also existed in these alloys.

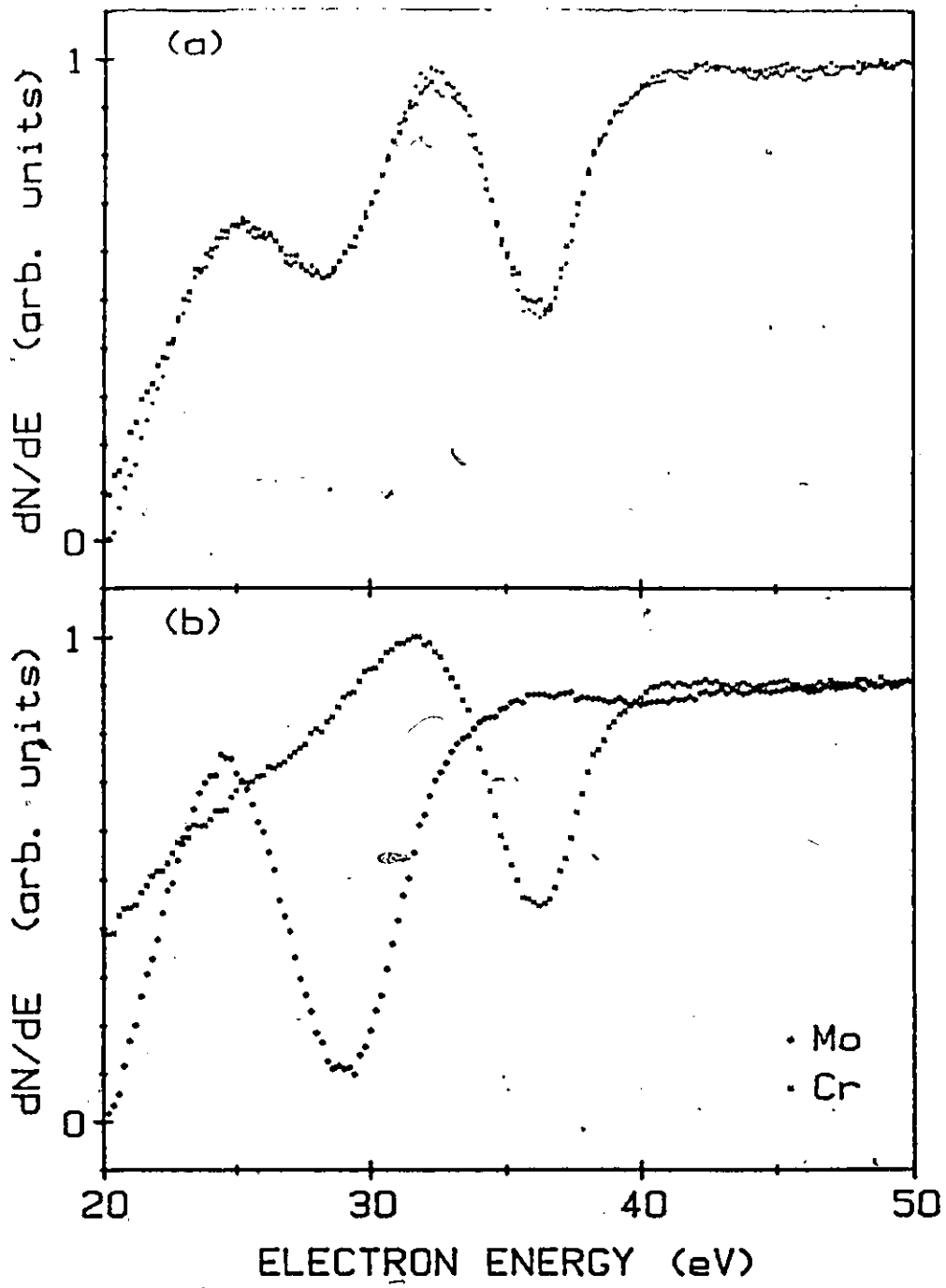

Figure 5.4: (a) Steady-state sputtered surface spectrum of the low energy region (20-50 eV) from an 83.4 at.% Cr-Mo alloy. The best fit simulation obtained by the computer grid search technique using eq. (5.3) is shown (dotted) and corresponds to fractions of the pure element spectra shown in (b) of $f_{Cr} = 0.720$ and $f_{Mo} = 0.288$.

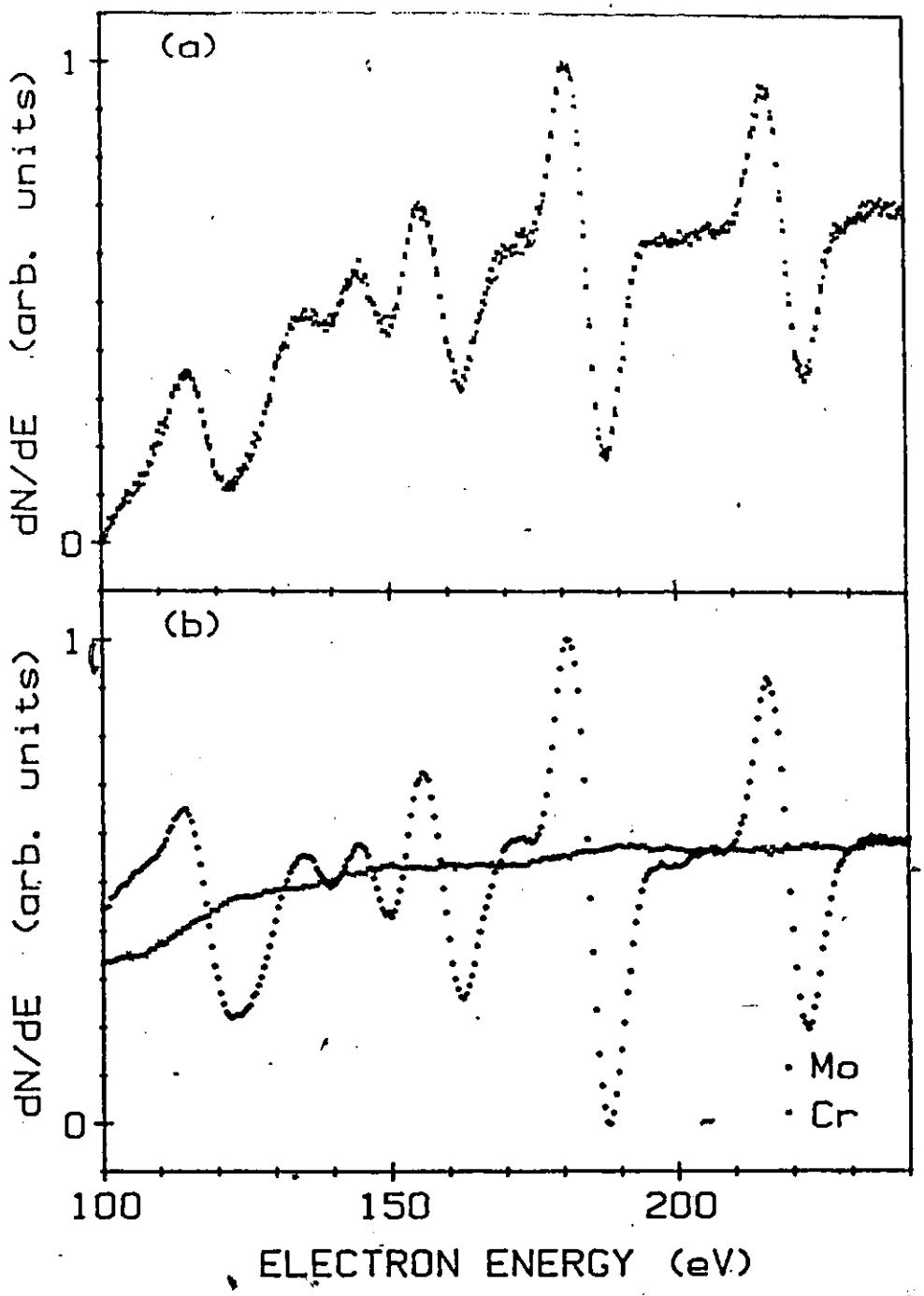

Figure 5.5: (a) Steady-state sputtered surface spectrum of the medium energy region (100-240 eV). The best fit simulation obtained by the computer grid search technique is shown (dotted) and corresponds to fractions of the pure element spectra shown in (b) of f_{Cr} = 0.736 and f_{Mo} = 0.269.

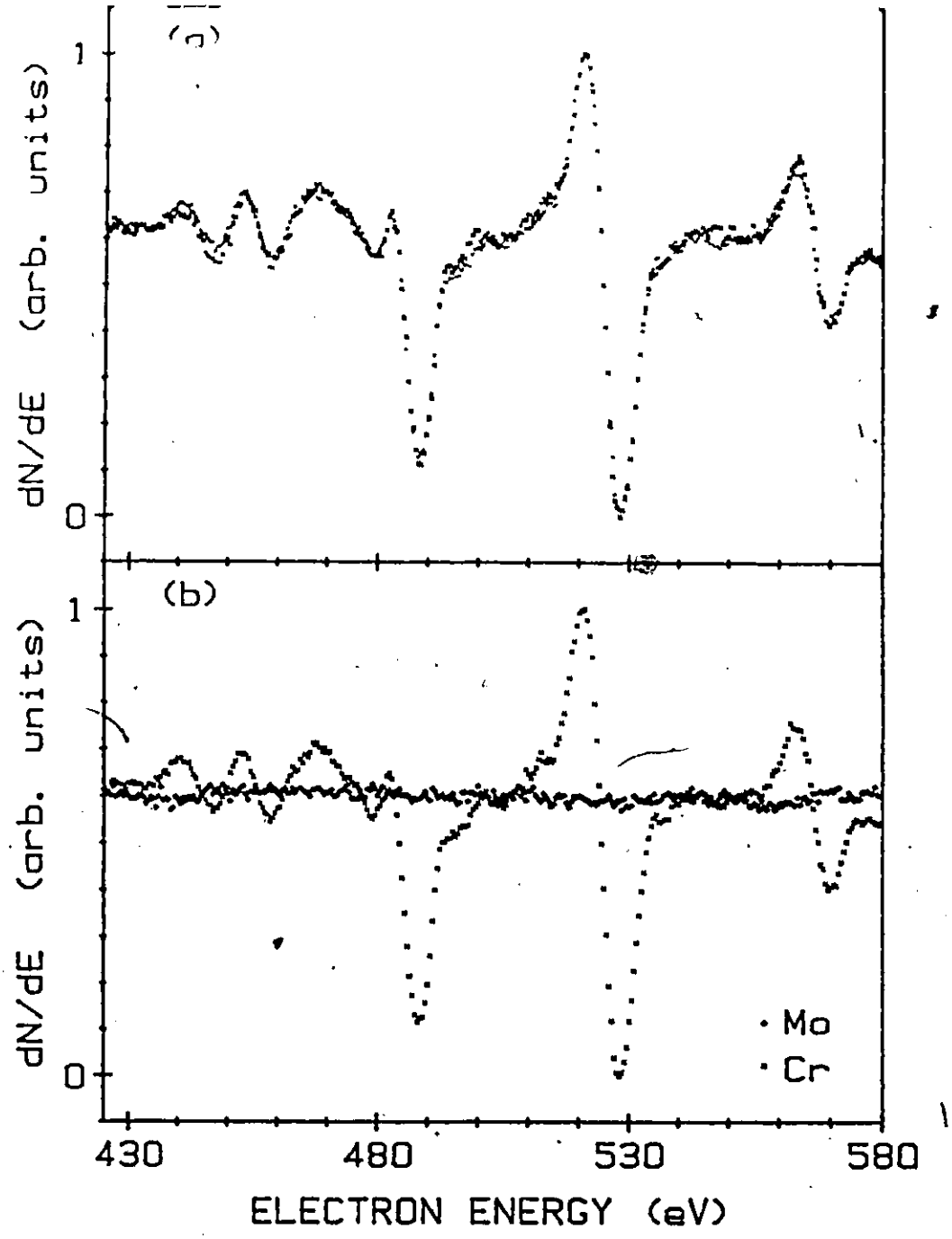

Figure 5.6: (a) Steady-state sputtered surface spectrum of the high energy region (425-580 eV). The best fit simulation obtained by the computer grid search technique is shown (dotted) and corresponds to fractions of the pure element spectra shown in (b) of f_{Cr} = 0.746 and f_{Mo} = 0.255.

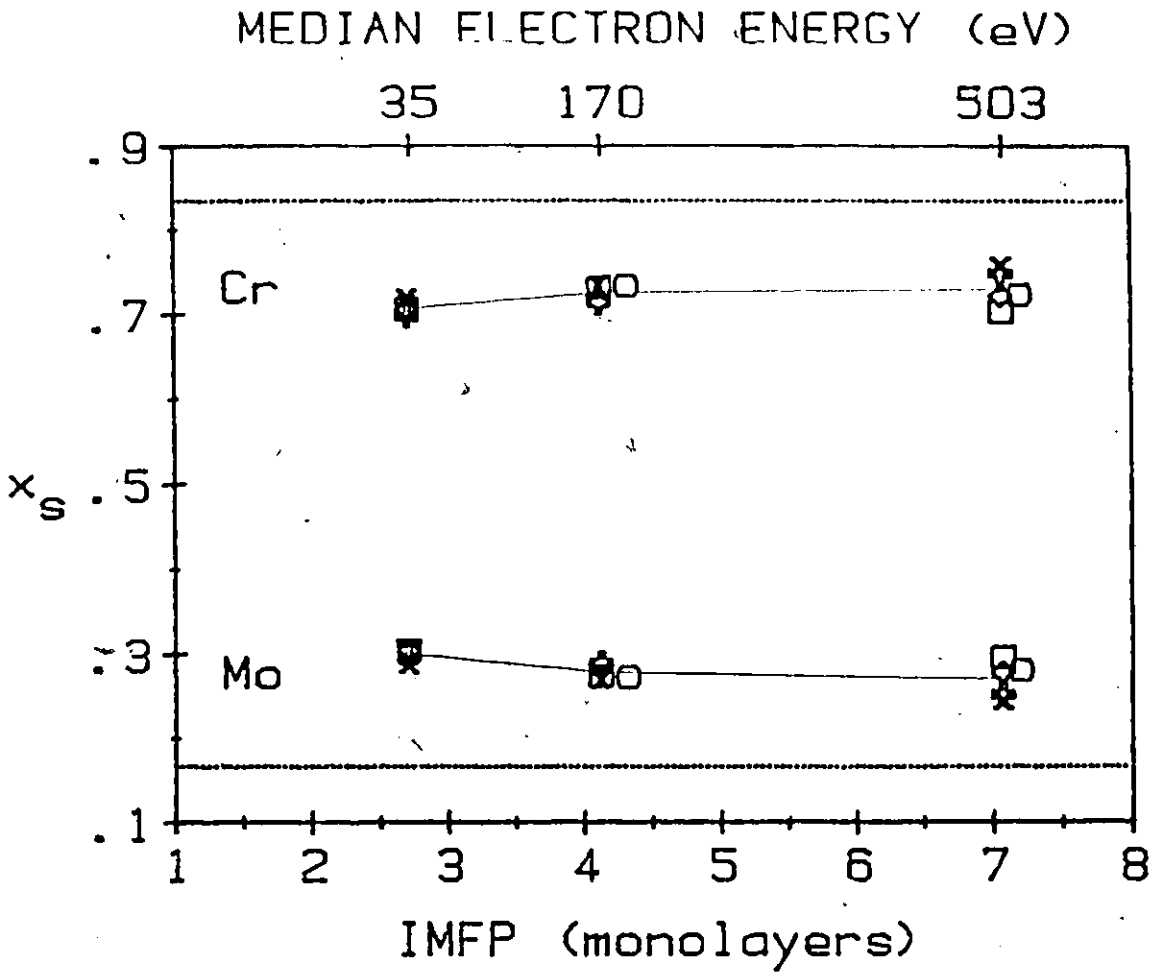

Figure 5.7: The average surface composition is plotted as a function of the IMFP, calculated according to eq. (3.31), and the median energy of the energy window used in the simulation procedure. The average surface composition was determined for each of five independent data sets consisting of a total of 210 best fit simulations per energy region. The alloy bulk composition is shown as dotted lines. The average at each median energy is joined solely to aid the eye. The results indicate that the compositional modifications due to preferential sputtering are much greater than the small gradient in composition suggested by the data.

Table 5.1: Steady-state sputtered surface composition of an 83.4 at.% Cr-Mo alloy determined by the simulation procedure.

Composition	Low Energy (20-50 eV)	Medium Energy (100-240 eV)	High Energy (425-580 eV)
x_s^{Cr}	0.707 ± 0.010	0.726 ± 0.013	0.730 ± 0.028
x_s^{Mo}	0.300 ± 0.009	0.278 ± 0.011	0.270 ± 0.027

Errors quoted : n = 5, 95% confidence limits from five independent data sets consisting of 210 independent simulations per energy region.

5.3.3 The Effect of Ion Flux

Six processes have been identified as potentially contributing to the radiation-induced compositional modifications of an alloy surface. An investigation was carried out to aquire an insight into the relative contribution to the steady-state sputtered surface composition from those processes which require the activated motion of defects, i.e., radiation induced segregation, radiation-enhanced diffusion and Gibbsian segregation. The contribution from such processes is expected to be a function of the defect concentration and hence the ion flux.

The nature of this investigation required short data collection time and for this reason the energy windows used for this series of experiments were reduced to 20-50, 170-200 and 500-540 eV. The steady-state composition of the 83.4 at.% Cr alloy was established at the standard ion flux of $\sim 4.1 \cdot 10^{14}$ ions/cm^{2}sec and then reduced to $\sim 1.9 \cdot 10^{13}$ and $\sim 8.9 \cdot 10^{12}$ ions/cm^{2}sec, respectively. The surface composition was monitored for as long as contamination was not detectable and further to study the effects of low contaminant levels. The results are shown in Fig. 5.8 for a reduction in ion flux of $\sim$ 20X ($1.9 \cdot 10^{13}$ ions/cm^{2}sec) as the best fit mole fractions obtained from the simulation procedure as a function of sputtering time. The data collected with no detectable contamination indicates that over a period of 8.0 hours, no detectable change in surface composition is observable in the three electron energy windows used. The data obtained under a 50 fold reduction in ion flux also indicated no variation; however, the sputtering time allowed before contaminants were detectable was reduced to $\sim$ 1.5 hours.

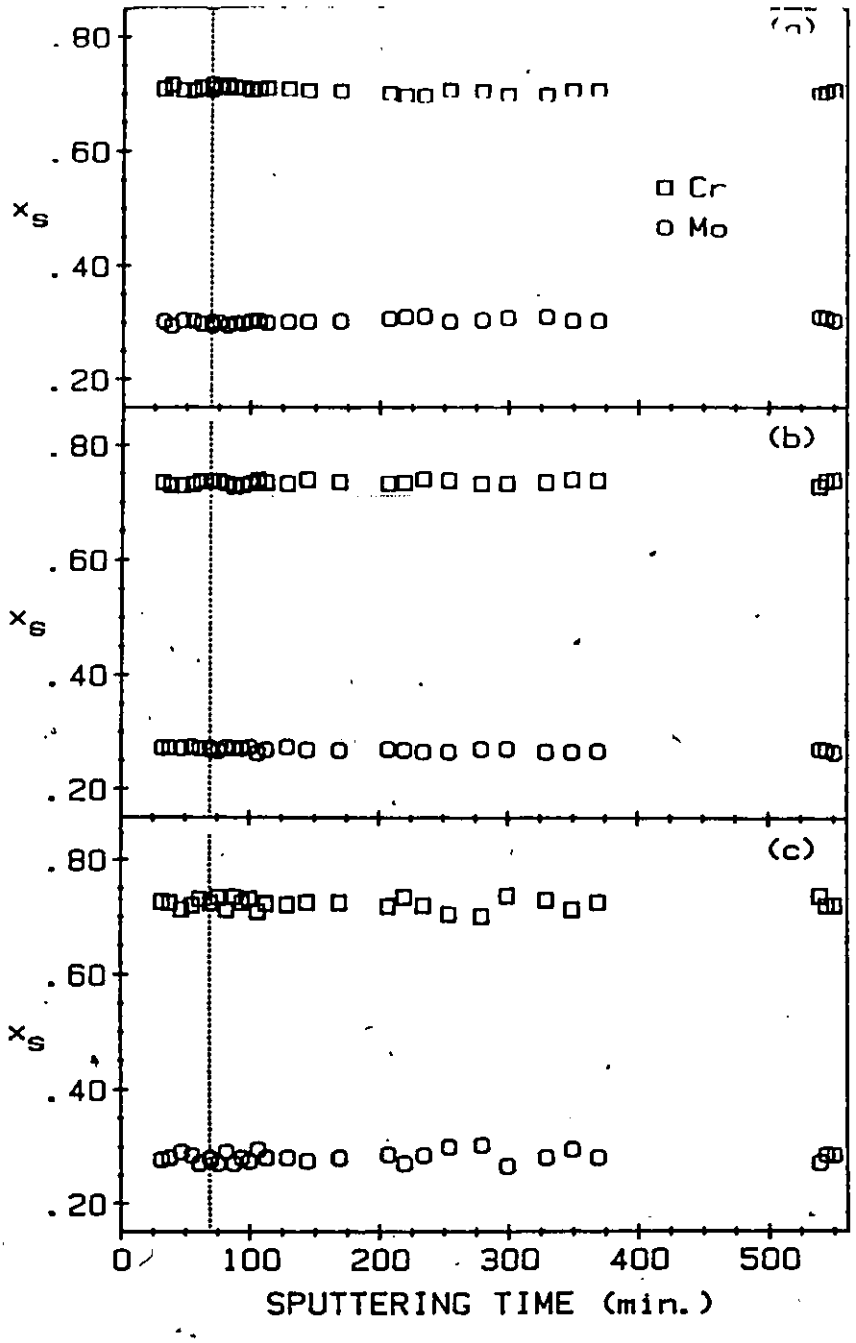

Figure 5.8: Surface composition as a function of ion flux for (a) low, (b) medium and (c) high energy regions. The vertical dotted line designates the time after which a steady-state sputtered condition was attained with the standard flux (~4.1 · 10^{14} ions/cm^2sec) and then reduced to ~1.9 · 10^{13} ions/cm^2sec.

5.3.4. Room Temperature 'Relaxation' of the Sputtered Surface

The study of the effect of ion flux on the steady-state sputtered composition was extended to the limit of zero flux. Upon establishing a steady-state surface composition under the standard ion flux, the ion bombardment was terminated and the surface allowed to 'relax'. The data was collected as in 5.3.3 and the results of the simulations plotted against 'relaxation' time shown in Fig. 5.9. The data indicate that over a period of 1.5 hours where contaminants were undetectable, no change in surface composition, i.e., relaxation, is observed.

For both this set of experiments and those of the previous section (5.3.3), monitoring of the surface composition was continued further than the experimental times indicated in order to establish the effect of low contaminant levels on the different transitions used. As the contaminant level increased to a detectable level, only the most surface sensitive transitions (20-50 eV) were affected; the higher energy peaks (> 100 eV) underwent no detectable changes.

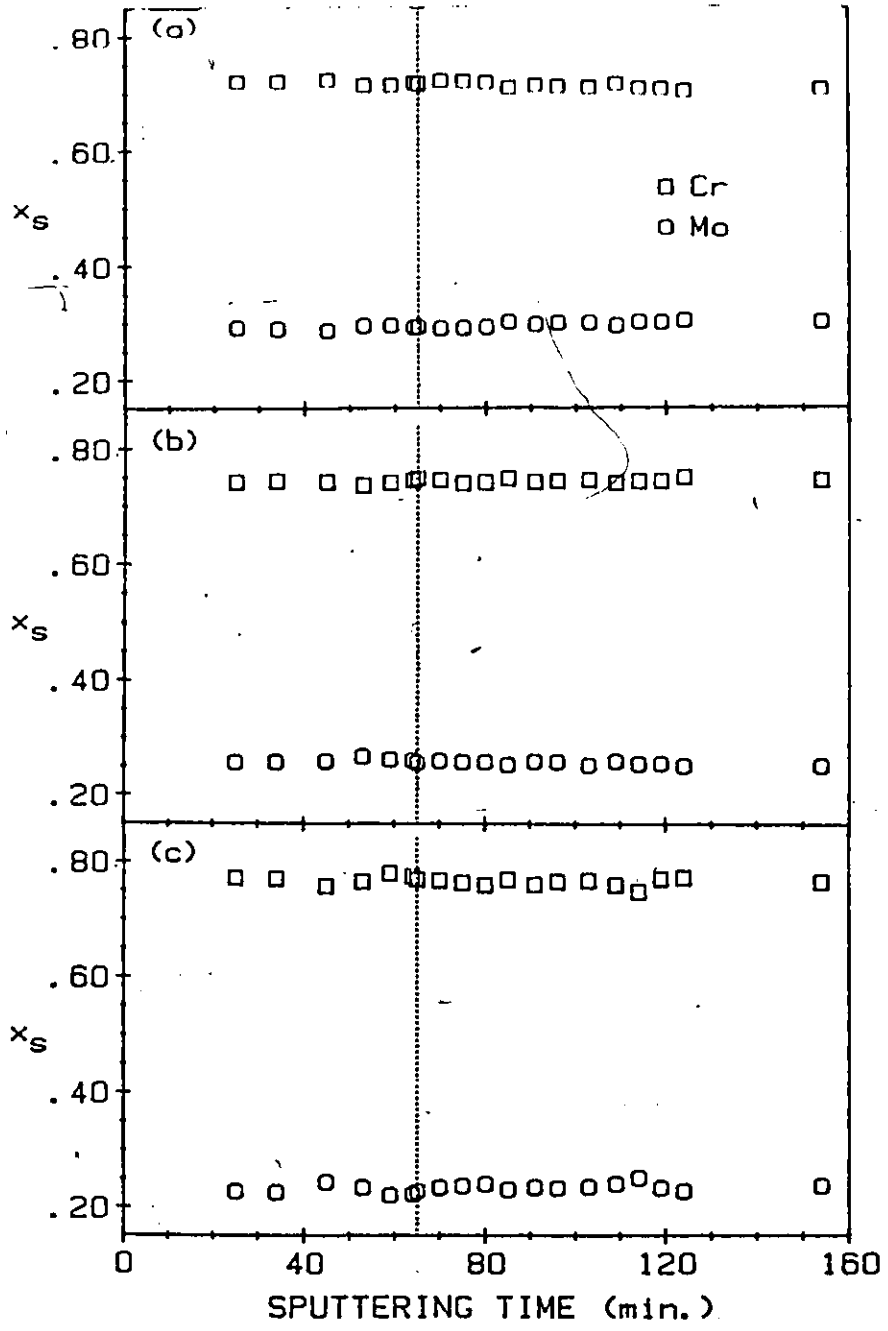

Figure 5.9: Surface composition as a function of relaxation time for (a) low, (b) medium and (c) high energy regions. The vertical dotted line designates the time after which a steady-state sputtered condition was attained with the standard flux (~4.1 × 10^{14} ions/cm^{2}sec) and then terminated.

5.4 DISCUSSION

5.4.1 A Phenomenological Model of the Sputtering Process

Compositional modifications of a binary alloy target arising from sputtering will ultimately attain a steady-state such that the target sputters stoichiometrically. Phenomenological models of this process have been developed from different types of analyses. For example, Shimuzu et al. [1973] used a conservation of mass argument while Dawson and Petrone [1981] used a kinetic analysis of the process. In the latter treatment, the argon ion sputter reactions are written as pseudo first order processes:

$$Cr(s) \xrightarrow{k_{Cr}} Cr(g)$$

$$Mo(s) \xrightarrow{k_{Mo}} Mo(g)$$

where the pseudo first order rate constants, k_{Cr} and k_{Mo}, are dependent on the energy of the ion and the ion beam current density. The sputter rate for Cr can be written as,

$$dN_g^{Cr}/dt = k_{Cr}\, x_s^{Cr},$$

where N_g^{Cr} is the number of Cr atoms which have entered into the gas phase.

The rate of change in the surface mole fraction of Cr will be given by the sputter rate for Cr, i.e. $k_{Cr}\, x_s^{Cr}$, multiplied by the probability that removing a Cr atom from the surface exposes a Mo atom and produces a detectable change, i.e., $(1 - x_b^{Cr})$:

$$dx_s^{Cr}/dt = k_{Cr}\, x_s^{Cr}\, (1 - x_b^{Cr}), \qquad (5.4)$$

Similarly for Mo,

$$dx_s^{Mo}/dt = k_{Mo}\, x_s^{Mo}\, (1 - x_b^{Mo}), \qquad (5.5)$$

and at steady-state the rate of change of x_s^{Cr} and x_s^{Mo} will be zero,

$$dx_s^{Cr}/dt = dx_s^{Mo}/dt = 0. \qquad (5.6)$$

Thus at steady-state the surface composition will be modified such that under the differential component sputter rates, the sputtered flux will have a composition equal to that of the bulk and no further change in composition will occur. Under this steady-state condition one can write from equations (5.4), (5.5), and (5.6),

$$\frac{x_s^{Cr}}{x_s^{Mo}} = \frac{k_{Mo}\,(1 - x_b^{Mo})}{k_{Cr}\,(1 - x_b^{Cr})} = \frac{k_{Mo}\, x_b^{Cr}}{k_{Cr}\, x_b^{Mo}} \qquad (5.7)$$

and,

$$x_s^{Cr} = \{\, 1 + K\, (x_b^{Mo}/x_b^{Cr})\}^{-1} \qquad (5.8)$$

where $K = (k_{Cr}/k_{Mo})$ is the ratio of the rate constants for sputtering Cr and Mo from the alloy.

It is expected that the sputtered atoms will originate mostly from the outer monolayer of the alloy [Sigmund et al. 1982, Dumke et al. 1983, Shapiro et al. 1985, Lam et al. 1985] and the above model for preferential sputtering assumes this simple picture where the first layer is sputter modified and the second and deeper layers all have the bulk composition. However, the ion beam will not only sputter atoms from the surface but will also induce homogenization of the surface region over a depth comparable with the penetration of the ion beam by collisional mixing and,

if the defects created are mobile, through RED. This will result in a surface region which is different in composition from that of the bulk over several layers. As fully discussed later, this is why the apparent surface composition determined by AES is identified with the actual sputtered surface composition since it can be adequately approximated as being uniform over the depth of the sample probed by the Auger electrons. This will only translate the interface between surface and bulk compositions deeper into the sample and is expected to have no effect on the above derivation.

According to eq. (5.8) a plot of $[(x_s^{Cr})^{-1} - 1]$ versus (x_b^{Mo}/x_b^{Cr}) should have a slope equal to K, and therefore will be linear if the sputter rate constant ratio, K, is independent of alloy composition. This is found to be the case, however this plot crowds most of the data near the origin and overemphasises the data points at high (x_b^{Mo}/x_b^{Cr}). For this reason a logarithmic plot of this function is preferred and is shown in Fig. 5.10. The linearity of this plot shows that the relative sputter rate constant K is insensitive to composition and has a value of 1.73 ± 0.04.

The theoretical dotted curve shown in Fig. 5.3 was calculated using eq. (5.8) with K = 1.73. These data for the sputtered alloy surfaces show that Cr is preferentially sputtered across the entire composition range. Additionally, because no systematic ordering is observed between the surface concentration determined from either the Mo(186) or Cr(529) transitions, the results suggest that the modified surface composition is uniform over the escape depth of the Auger electrons used. It is further observed, that in all cases, the sum of the sputtered composition determined

from the Mo and Cr data adds to 100 at.% to within 5 at.% and in most cases the deviation is less than 2 at.%. This result confirms the calculations in Section 3.4 which predicted that matrix effects in this alloy system are negligible for a sample homogeneous in depth over the analysed volume.

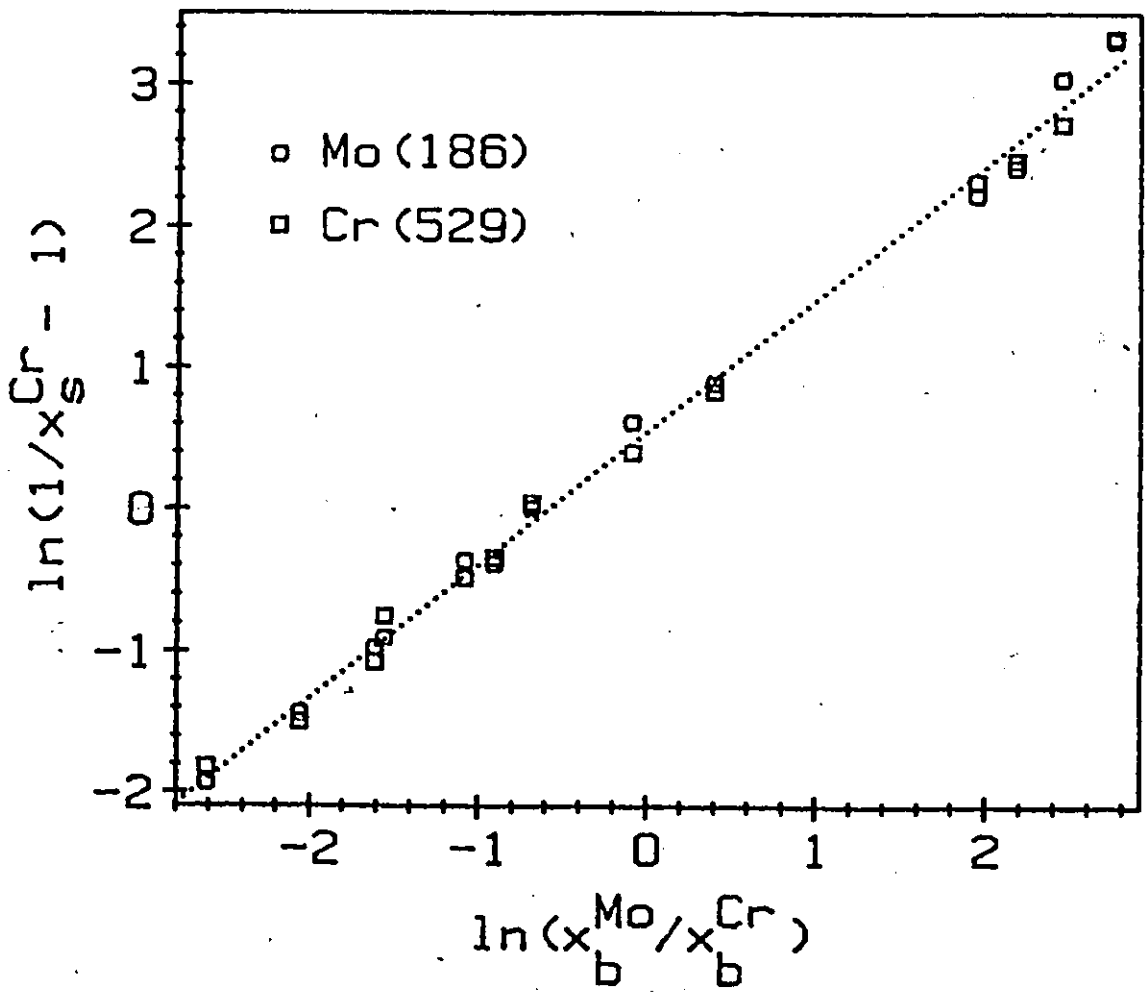

Figure 5.10: A logarithmic plot of eq. (5.8) for 13 Cr-Mo alloys.

5.4.2. Comparison With Sigmund Theory of Alloy Sputtering

Various models have been proposed to explain the surface enrichment in sputtered alloys. Based on an extension of collision-cascade theory to multicomponent targets by Andersen and Sigmund [1974] in the linear cascade regime, Sigmund [1981] has obtained the following expression for an enhancement ratio:

$$\frac{Y_A^C}{Y_B^C} = \frac{Y_A/x_A}{Y_B/x_B} = \left(\frac{M_B}{M_A}\right)^{2m} \left(\frac{E_{b,B}}{E_{b,A}}\right)^{1-2m} \qquad (5.9)$$

where Y_i^C is the component sputtering yield independent of concentration; Y_i is the partial sputtering yield; M_i is the atomic mass; $E_{b,i}$ is the surface binding energy in the alloy; and m is the power cross-section exponent (i = A,B). Since most collisions will occur at energies much lower than the primary ion energy, appropriate values of m will lie in the region $0 \leq m \leq 0.2$. Eq. (5.9) shows a weak dependence on the mass ratio and a much stronger dependence on the binding energy ratio.

A comparison between the experimentally determined value of K from Fig. 5.10 with the enhancement ratio Y_{Cr}^C/Y_{Mo}^C calculated from eq. (5.9) can be made. Approximating the surface binding energies $E_{b,i}$ to be independent of alloy composition and equal to the heats of sublimation of the pure elements [Hultgren et al. 1973a], yields $1.66 \leq Y_{Cr}^C/Y_{Mo}^C \leq 1.73$ for $0 \leq m \leq 0.2$. The agreement with the empirical result $K = 1.73 \pm 0.04$ is excellent. It is appropriate, however, to consider the major limitations associated with the application of eq. (5.9). Sigmund [1980, 1981] has made the distinction between primary and secondary sputtering effects. Primary effects comprising the physics of individual sputtering events define the

conditions under which eq. (5.9) is applicable, i.e., low fluence where the condition of a homogeneous target condition may be considered to be fulfilled. At higher fluences, numerous secondary effects which can give rise to compositional modifications in the surface region, e.g., thermally activated processes, may become a problem. Additionally, some uncertainty exists in using appropriate alloy component binding energies. The agreement suggests that indeed, in such refractory alloys under ion bombardment at room temperature, it is the 'primary' athermal 'ballistic' processes that play the dominant role in establishing the compositional modifications that arise.

5.4.3. Comparison With Elemental Sputter Yields

Another approach often used in comparing experimental results with theory has been to identify the component sputtering yield ratio in the alloy with the ratio of pure elemental sputtering yields. Sigmund [1969a] obtained the following expression for the elemental sputtering yield:

$$Y = 0.042\ F_D(0)/U_O \qquad (5.10)$$

where $F_D(0)$ is the recoil energy density at the surface, i.e., $x = 0$, and U_O the surface binding energy. Betz [1980] has reviewed the compositional modifications of numerous binary alloy systems under 1-2 KeV Ar^+ ion bombardment. He has found that if the pure elements have similar $F_D(0)$ values, then the observed preferential sputtering in alloys could be explained in terms of differences in surface binding energies of the alloy components which qualitatively agree with those of the pure elements. Generally, qualitative agreement is found between the component sputtering

yield ratios in the alloys and the corresponding measured and calculated pure elemental yield ratios. The analysis indicates:

1. the sputtering yields of the components are essentially preserved in the alloy;

2. enrichment of the low yield component is observed; and,

3. for most of the binary alloys analyzed, the component sputtering yield ratio is found to be insensitive to composition.

Ideally, the pure elements' slowing down density, $G_D(0)$, and its variation with composition should also be compared [Sigmund 1981]. Andersen and Sigmund [1974] have shown that for a binary alloy whose constituents' masses are similar, as for Cr-Mo, the slowing down densities of the components are very similar and the normalized densities vary approximately linearly with concentration.

Approximate values of $F_D(0)$ can be obtained by substitution of appropriate moments into a one-dimensional Edgeworth expansion normalized to unit dose which from eq. (5.1) can be written:

$$F_D(x) = [\nu(E)/(2\pi \langle x^2 \rangle)^{1/2}] \cdot \exp [-(x - \langle x \rangle)^2 / 2\langle \Delta x^2 \rangle] \cdot P(x) \qquad (5.11)$$

where the parameters are as defined earlier; and $P(x)$ is a polynomial weighting factor to the Gaussian distribution which by using Gibbons [1975] simplification is equal to unity for $x = 0$, i.e., at the surface. Using Winterbon's compilation [1975], yields $F_D^{Mo}/F_D^{Cr} = 1.08$, i.e., a difference in recoil energy density at the surface of less than 10%. Strictly speaking, the above calculation is valid for an amorphous target with bombardment at normal incidence and low fluence, i.e., in the limit of a zero sputter

rate. However, since only relative values are required the calculation is a reasonable approximation.

The similarities of the pure component Cr and Mo recoil energy and slowing down densities, suggests that the experimentally determined sputter rate constant ratio K for the Cr-Mo alloys should compare, at least, qualitatively with the sputter yield ratio of the pure elements, Y^o_{Cr}/Y^o_{Mo}. At present, Cr and Mo elemental sputtering yields under 2 KeV Ar^+ ion bombardment are not available from a common data source. A semi-empirical calculation according to Matsunami et al. [1983] yields Y^o_{Cr} = 2.77 ± 0.47 and Y^o_{Mo} = 1.25 ± 0.36 for a ratio Y^o_{Cr}/Y^o_{Mo} = 2.22 ± 0.74 in reasonable agreement with the empirical result K = 1.73 ± 0.04.

5.4.4. The Homogeneity Question

The question of the homogeneity of the sputtered surface can be addressed via an appropriate analysis of the experimental data. The energy range used (20-580 eV) should provide a sufficiently large variation in the analyzed depth, through the energy dependence of IMFP's on energy, to yield an insight into the concentration profile of the steady-state sputtered condition. If matrix effects are minimal and the surface region is homogeneous over the analyzed volume, then the steady-state composition should be independent of the electron energy used for the analysis.

It is expected that simulating a set of alloy data collected over the three energy regions with a set of elemental standards collected consecutively under the same conditions, should minimize most sources of instrumental errors. The average values of each energy region from five independent data sets, each consisting of numerous steady-state alloy and

elemental spectra collected consecutively, are plotted in Fig. 5.7 for the 83.4 at.% Cr-Mo alloy. This procedure yields excellent precision but problems with systematic errors, due mainly to the morphological changes of the three surfaces, lead to inaccuracies in the results. These latter errors can be minimized through a statistical average of the five independent data sets. The averages are shown in Table 5.1 with the corresponding 95% confidence intervals. The results clearly indicate that to within the experimental errors, the surface region is homogeneous over the analyzed depth. However, the average values suggest that a small inhomogeneity may exist in the expected directions. This result is expected in that the sputtered flux originates from the outermost few atomic layers, with the majority originating in the topmost monolayer, [Sigmund et al. 1982, Dumke et al. 1983, Shapiro et al. 1985, Lam et al. 1985] and hence compositional modifications will initiate in this region with a concentration gradient in a direction perpendicular to the surface.

The inhomogeneity in sample depth can be quantified by adopting an appropriate model for the composition profile and using a layer calculation to establish a calculated profile consistent with the experimentally determined compositions from the three energy regions. In the simplest model, one can assume that the inhomogeneity with depth is confined to the outermost layer x_1. The viability of such a profile can easily be tested using the monolayer calculation developed in Section 3.5. From Table 6.3, the experimentally determined fraction of the total signal that arises from x_1 for the Cr(529) transition is 0.109. Substituting the sputtered surface composition, x_S^{Cr} = 0.730 from Table 5.1 and the bulk alloy

composition, x_b^{Cr} = 0.834, into eq. (3.28b) yields a value for the outermost monolayer composition, x_1^{Cr} = -0.12. Clearly, the negative x_1 composition calculated is impossible and indicates that the sputter depletion of Cr is not limited to the outermost layer. This is due to the collisional mixing of the compositional modifications, due to preferential sputtering, over a depth comparable in magnitude to the ion penetration depth. Based on this picture of an 'altered layer' extending well beyond the source of the sputtered flux, two realistic models of the composition profiles which can lead to the observed inhomogeneity have been tested:

1. a linear variation in composition from x_1 to x_n, where x_i is the mole fraction in layer i; and,

2. a concentration spike at x_1 and a constant value for x_2 to x_n, i.e., a uniform sub-surface which may be different from the bulk.

In both cases, the bulk composition defines a limit for x_n. Using the experimentally determined IMFP's (Table 6.3), the equivalent inhomogeneity in terms of the above two profiles is shown in Table 5.2. The profiles shown in columns 5 and 6 yielded the best agreement between the experimentally determined (column 3) and calculated mole fractions (columns 4 and 6). For both profiles, the agreement is good: The observed differences in the mole fractions were $\leq$0.008 and $\leq$.001 in all three energy regions for profiles (1) and (2), respectively. The profiles for the Cr data are plotted in Fig. 5.11. The sampled depth appropriate to the Cr(529) transition is shown. The results indicate that the inhomogeneity in depth is small by either profile and that the surface region can be adequately approximated as being essentially uniform over the analyzed volume.

Table 5.2: Estimation of the inhomogeneity in the steady-state sputtered surface of an 83.4 at.% Cr-Mo alloy through layer calculations.

1	2	3	4	5	6	7
			Inhomogeneity Layer Calculations**			
	Energy Region	Expt'l* Results x_s	(1) Linear Variation Calc. x_s	Profile	(2) Spike at x_1 Calc. x_s	Profile
Mo	Low	0.300 ± 0.009	0.295	x_1 = 0.298	0.300	x_1 = 0.331
	Medium	0.278 ± 0.011	0.286	Δx/layer = -0.0038	0.278	x_n = 0.262
	High	0.270 ± 0.027	0.267		0.269	$(x_1 - x_n)$ = +0.069
Cr	Low	0.707 ± 0.010	0.712	x_1 = 0.709	0.707	x_1 = 0.683
	Medium	0.726 ± 0.013	0.719	Δx/layer = +0.0028	0.724	x_n = 0.737
	High	0.730 ± 0.028	0.733		0.731	$(x_1 - x_n)$ = -0.054

* From Table 5.1 and Fig. 5.7.

**Layer calculations performed using experimentally determined IMFP's (Table 6.3).

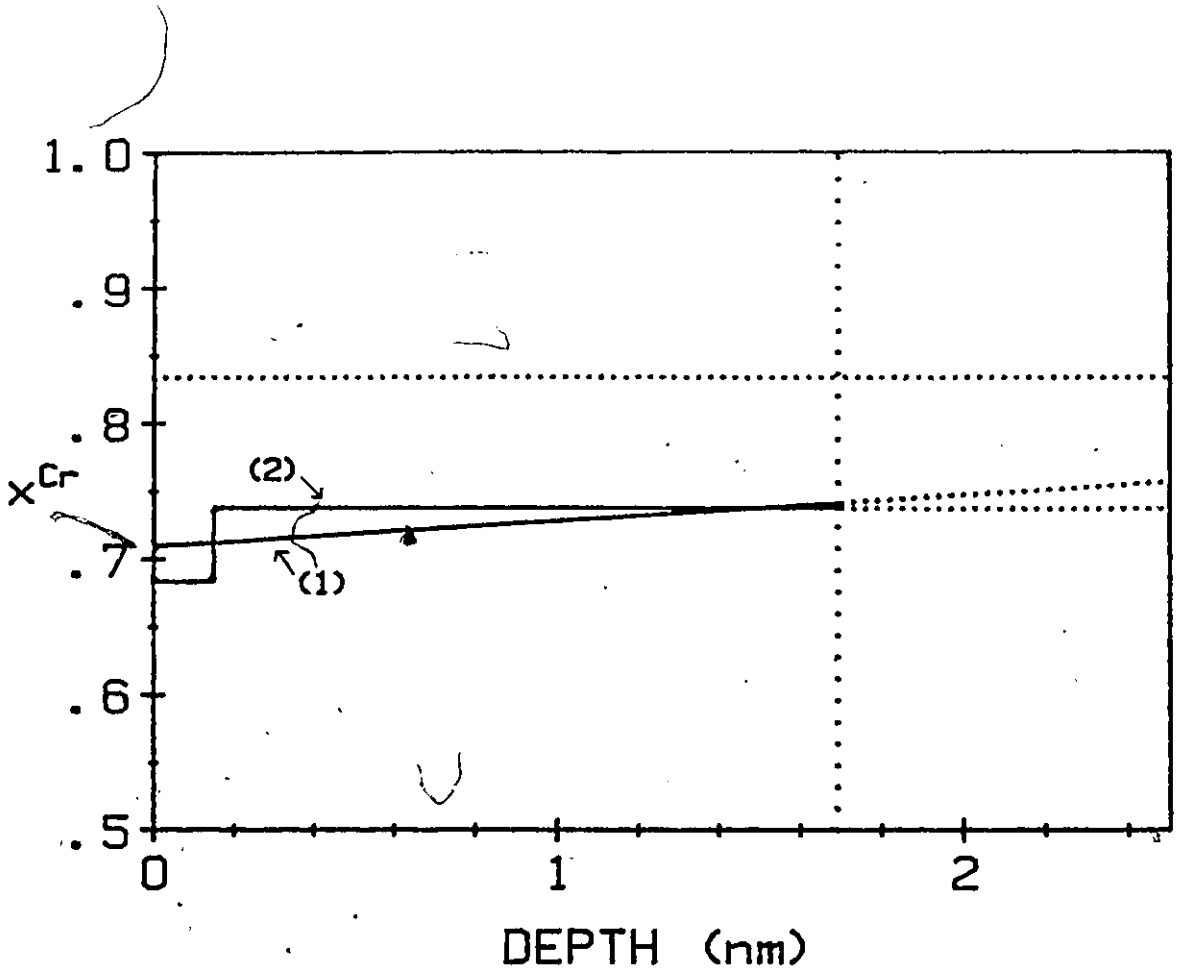

Figure 5.11: Calculated Cr composition profiles of a steady-state sputtered surface of the 83.4 at.% Cr alloy (from Table 5.2). These profiles represent an inhomogeneity in depth such that the calculated surface composition using layer calculations is consistent with the experimentally determined composition from the three energy regions: (1) a linear variation with depth; and (2) a concentration spike at x_1 and a sub-surface different from the bulk. The alloy bulk composition is shown as a dotted horizontal line. The depth scale was calculated using the $a_o/2$ estimation of the layer thickness. The dotted vertical line represents the sampled depth corresponding to the average IMFP of the high energy region.

5.4.5. The Effect of Ion Flux and the Room Temperature 'Relaxation' of the Surface

An insight into the processes responsible for the compositional modification of the alloy surface can be obtained from the experimental results relating the steady-state surface composition to the variation in ion flux. In crystalline solids, atomic transport occurs via defect migration, i.e., vacancy and/or interstitial type [Lazarus 1960, Shewmon 1963, Peterson 1968]. Any process dependent on defect concentration will be dependent on the rate of defect creation and annihilation, i.e. the ion flux.

The results indicate that even under a fifty fold reduction in ion flux, no detectable change in the steady-state composition is observable. Additionally, this observation extends to the limit of zero flux, i.e., no room temperature relaxation is observed on the experimental time scale.

An interpretation of these results requires a knowledge of the type and mobility of the equilibrium and non-equilibrium defects present in the surface region. A description of the types of defects created under the experimental bombardment conditions was given in Section 5.2. The incident ion energy is sufficient to generate Frenkel pairs and displacement cascades consisting of depleted zones, which can collapse into small clusters, and interstitials ejected into the surrounding lattice. The steady-state defect profile will be quite complex and will be determined by the mobility and interactions of the different defects formed with each other and existing sinks such as the surface, grain boundaries, immobile clusters, etc. Radiation damage recovery experiments indicate that for pure Mo and Cr, interstitials, and possibly some small interstitial clusters, are highly

mobile at room temperature. On the other hand, as in most refractory metals, the vacancy-type defect is not mobile at room temperature due to high vacancy migrational enthalpies. STAGE III recovery, i.e., mono-vacancy migration, is observed between 425-650 K in Mo depending on the experimental conditions, with clusters evaporating through emission at much higher temperatures. Because of the relatively short ion and damage range distributions, i.e., in Mo R_p = 1.7 and 1.5 nm from LSS and WSS theories, respectively, the surface will have a very large effect on the steady-state condition by supplying a very high sink density. Interstitials in the damaged zone can undergo annihilation through recombination with a vacancy or at a sink, predominantly, the surface; a fraction will survive and migrate into the bulk. This spatial inhomogeneity in defect production and annihilation will lead to substantial interstitial-type defect fluxes towards the surface and also into the bulk. Any preferential coupling between the defect flux and either alloying element will lead to a redistribution of atoms.

Of the three thermally activated processes indicated earlier, Gibbsian segregation and radiation enhanced diffusion are not expected to play a role below 0.3 T_m [Wiedersich 1983], where T_m is the alloy melting point. This has been confirmed experimentally in this alloy system: No room temperature 'relaxation' has been observed upon termination of ion bombardment and the segregation results presented in Chapter 6 indicate that temperatures of the order of 875 K are required to observe measurable changes in surface composition on the experimental time scale. Additionally, equilibrium (Gibbsian) segregation results show a cross-over in the

segregating element, as predicted by the Unified Segregation Model and observed experimentally (Chapters 6-8). This would then predict that if Gibbsian segregation played the dominant role in establishing the steady-state sputtered surface composition, a cross-over in the element enriched at the surface should occur from one end of the composition range to the other. An analysis of 13 alloys encompassing the entire composition range clearly indicates that such is not the case.

The question of the contribution from radiation-induced segregation (RIS) to the steady-state sputtered surface composition, can be addressed. Experimental and theoretical aspects of the RIS phenomenon have been well reviewed [Marwick 1983, Rehn and Okamoto 1983, Wiedersich and Lam 1983]. It has been established that the occurrence of RIS requires:

1. persistent defect fluxes into or out of certain spatial regions of a sample;
2. a preferential coupling of an alloying element with the defect flux to form an energetically favourable point-defect/atom complex; and,
3. the resulting complex to be mobile at the irradiating temperature.

Under the experimental conditions of this study, literature results can only establish that an interstitial-type defect flux towards the surface persists while irradiating. The experimental results from the ion flux investigation of this study (Sections 5.3.3 and 5.3.4), indicate that no dependence exists between the steady-state sputtered surface composition and the ion flux used. These results suggest that (2) and/or (3) do not occur to the extent of RIS playing the dominant role in establishing the steady-state sputtered

surface composition. However, the possible contribution of RIS in refractory alloys, even under room-temperature ion bombardment, cannot be ruled out.

The above analysis of ion bombardment at room temperature can be extended to other refractory alloy systems where similar results have been obtained: Mo-W [Dawson and Petrone 1981] and Cr-V [Dawson and Hu 1985]. However, for lower melting point alloys, both the thermally activated and athermal 'ballistic' processes may play a role in establishing the surface composition during or post irradiation, even at room-temperature. This is exemplified by the observation of surface segregation (relaxation) in a Ni-Ag alloy after room-temperature Ar^+ ion bombardment (1-4 KeV) was terminated [Fine et al. 1983]. Other surface compositional modifications attributed to thermally activated processes have also been observed at low temperatures (-120 ^{o}C to room temperature) in Au-Cu alloys [Li et al. 1982, Li and Koshikawa 1985].

5.4.6. A Unified Picture of the Sputtering Process

Clearly, understanding of ion bombardment-induced modifications of alloy surfaces will depend on recognizing the different effects that have been activated under a given set of experimental conditions. This understanding is simplified for room-temperature irradiation of refractory alloys by the fact that only the athermal 'ballistic' processes are expected to play a significant role. The experimental results obtained in this study are consistent with the athermal 'ballistic' processes playing the dominant role in establishing the steady-state composition: The value determined by preferential sputtering and the bulk composition. Collisional mixing, i.e., displacement mixing and possibly recoil implantation, maintain an

essentially uniform composition over the 'altered layer' depth. The composition profile corresponding to this approximation is shown schematically in Fig. 5.12. This is the profile of the surface region assumed once ion bombardment is terminated and the segregation studies at elevated temperatures, presented in the subsequent chapters, initiated.

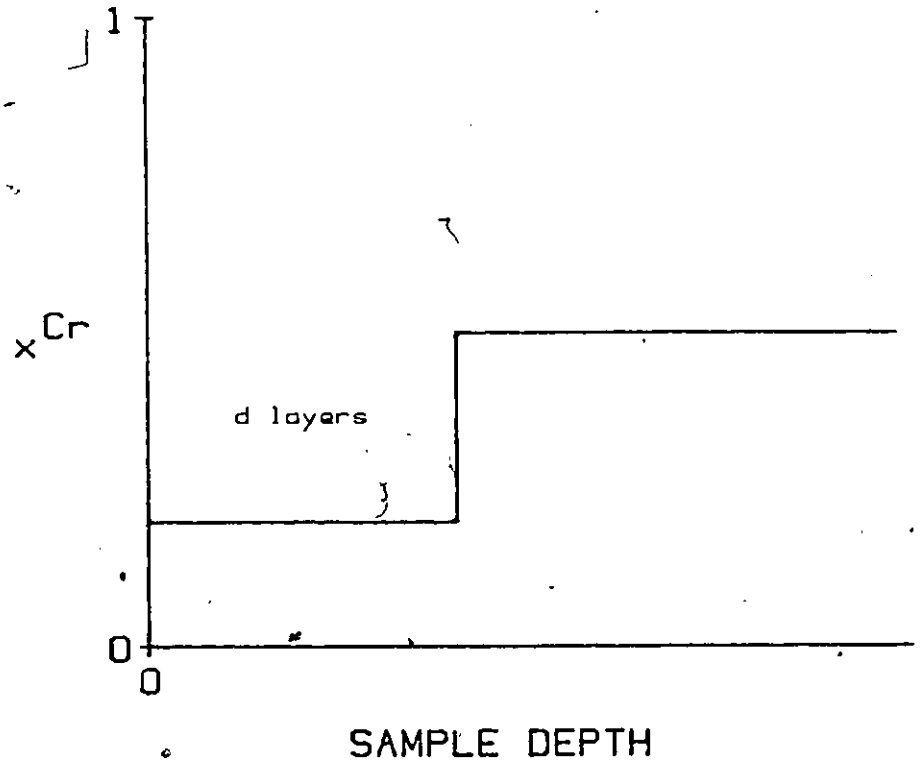

Figure 5.12: A schematic approximation of the composition profile in a refractory alloy where only athermal 'ballistic' processes are considered to play a significant role in establishing the steady-state surface composition.

CHAPTER SIX

SURFACE SEGREGATION IN Cr-Mo ALLOYS

This chapter reports on an investigation of the surface segregation phenomenon as it occurs in Cr-Mo binary alloys. The basis for the phenomenon is introduced and the theoretical model tested in this study against experimental results, is presented. Segregation results obtained from three Mo-rich Cr-Mo alloys are presented yielding an insight into the activated processes that occur upon annealing of a sample. In all cases, segregation studies were perfomed using a steady-state sputtered surface and, where necessary, the results interpreted in terms of the composition profile developed in Chapter 5 (Fig. 5.12).

6.1. INTRODUCTION

More than a century ago, Gibbs [collected works 1961], in a macroscopic thermodynamic formalism, predicted that the equilibrium composition of an alloy surface can be quite different from its bulk composition. The experimental inaccessability of important quantities for classical thermodynamic treatments has led more recent investigators to develop a number of other models which allow a simpler analysis of experimental results as summarized in two recent reviews [Kelley and Ponec 1981, Buck 1982]. Numerous investigators have used a microscopic statistical or a quasi-chemical approach [Guggenheim 1945, Defay et al.

1966, Swalin 1972, Williams and Nason 1974, Van Santern and Boersma 1974, Miedema 1978, Miedema et al. 1980] while others have correlated surface segregation with grain boundary segregation [McLean 1957, Hondros 1965, Seah and Hondros 1973, Seah and Lea 1975, Seah 1980], phase diagram data [Burton and Machlin 1976, Tsai et al. 1977] and diffusion data [Swartzfager and Kelley 1980]. Other models have been proposed based on computational approaches including Monte Carlo type [Sundaram and Wynblatt 1975, Abraham et al. 1976, 1978, 1979a, 1979b, Donnelly and King 1978, Abraham and Brundle 1981] and electron band energy methods [Gelatt and Ehrenreich 1974, Kerker et al. 1977, Balserio and Moran-Lopez [1980], Lambin and Gaspard 1980].

The two major driving forces for surface segregation in binary substitutional alloys, such as Cr-Mo, are differences in atomic interaction energy and size of the two elements. In a simple analysis [Kelley and Ponec 1981], if one considers the surface as being created by cleaving, for example, then those atoms in the surface experience a different environment from those in the bulk due to a difference in coordination: The surface atoms are missing bonds and hence, are in a higher energy state. Considering an atom's energy to be simply a sum of the energy of the bonds holding it in place, then the energy difference between the two environments can be expressed as a change in the atom's total bond energy. Generally, the bond energies of element A and element B will be different and hence, the energy to move from the bulk to the surface will be different for A and B. If we consider the two processes of interchanging A in the bulk with B in the surface, and vice-versa, one will release

energy so that it may occur spontaneously, while the other will not. If putting A on the surface releases energy, then this simple bond energy argument predicts that the surface becomes enriched in A and the bulk in B relative to the overall average composition. The enrichment of A at the surface does not occur without limitation. As the segregation proceeds, the randomness of the system is reduced and hence, the atoms will continue to move until the decrease in the energy state of the system is just balanced by the change in entropy. Therefore, it is the free energy which must be a minimum at equilibrium. Since in solids $\Delta E \simeq \Delta H$, the segregation process can be described in terms of minimizing the Gibbs free energy of segregation, ΔG_S given by:

$$\Delta G_S = \Delta H_S - T\Delta S_S \qquad (6.1)$$

where ΔH_S and ΔS_S are the changes in enthalpy and entropy associated with the segregation of the appropriate component.

The other major driving force for surface segregation arises from misfitting solute atoms in the lattice due to differences in atomic size. This elastic strain energy model, proposed initially by McLean [1957] to explain grain boundary segregation, predicts that if a significant size difference exists, the solute will segregate to relieve the lattice strain.

Experimental results contrary to the predictions of either of these driving forces have been observed and hence it has been suggested by Wynblatt and Ku [1977a, 1977b] that any complete treatment of equilibrium segregation must involve the minimization of the total free energy of the system and will include contributions from surface energies, alloy

interactions and elastic strain energy. As one can see, of the two major driving forces, minimization of the surface energy predicts segregation of the same component across the entire composition range, whereas minimization of the elastic strain energy always predicts segregation of the solute. In minimizing the total free energy of the system, the two driving forces will reinforce each other at one end of the composition range and oppose each other at the other end. Combining the bond-counting model of Defay et al. [1966] together with the elastic strain energy model of Mclean [1957] and Friedel [1954], Wynblatt and Ku [1977a, 1977b] have proposed the Unified Segregation Model (USM). This model has been qualitatively tested quite successfully against experimental results [Seah 1979, Blakely and Eizenberg 1981] but quantitative comparisons are few [for example, Mervyn et al. 1979, Lam et al. 1985] due to the problems associated with obtaining the appropriate experimental data.

As indicated in Chapter 1, because the Cr-Mo alloy system exhibits considerable difference in both atomic interaction energy and size, it provides adequate driving forces for both effects and hence is an ideal system for a segregation study. Additionally, the system has a tendency to cluster as manifested in a positive enthalpy of mixing [Hultgren et al. 1973b] and the possible existence of a miscibility gap at lower temperatures [Sully and Brandes 1967] and hence, the problems associated with an ordering alloy [Sundaram and Wynblatt 1975] are not encountered.

A THEORETICAL ANALYSIS OF THE SEGREGATION PHENOMENON: THE UNIFIED SEGREGATION MODEL

Combining the monolayer model where it is assumed that segregation alters only the outermost layer, together with the regular solution approximation for the alloy, it can be shown [Defay et al. 1966, Van Santen and Boersma 1974, Williams and Nason 1974] that the surface monolayer composition is given by:

$$\frac{x_s^A}{(1 - x_s^A)} = \frac{x_b^A}{(1 - x_b^A)} \exp(-\Delta H_s^A / RT) \qquad (6.2)$$

where component A is the solute; x_s^A and x_b^A are the equilibrium surface and bulk mole fractions, respectively; and ΔH_s^A is the enthalpy of segregation of the solute.

Using the formalism of Wynblatt and Ku [1977a, 1977b], the Unified Segregation Model gives the enthalpy of segregation of the solute A as:

$$\Delta H_s^A = (\gamma_A - \gamma_B)\,\sigma_B + \frac{2\,\Delta H_M}{Z\,x_b^A\,x_b^B}\left(Z_1\,(x_b^A - x_s^A) + Z_v\,(x_b^A - 1/2)\right) + \frac{24\,\pi\,K_A\,G_B\,r_A\,r_B\,(r_A - r_B)^2}{3\,K_A\,r_A + 4\,G_B\,r_B} \qquad (6.3)$$

The first term represents the surface energy contribution with γ_i being the surface energy of the pure component, at absolute zero, and σ_B the surface area per atom of the solvent. The second term arises from the regular solution approximation where the distribution of atoms is assumed to be random and hence an ideal entropy of mixing, but a non-zero enthalpy of mixing contribution, ΔH_M; Z is the bulk coordination number; Z_1 is the

number of lateral bonds made by an atom within its plane and Z_v is the number of vertical bonds made by an atom to an adjacent plane. The third term represents the elastic strain contribution where K_A is the bulk modulus of the solute, G_B is the shear modulus of the solvent and r_i is the appropriate atomic radius.

Since few surface energy measurements for pure metals have been made, an estimate of this quantity can be calculated from an empirical expression obtained by Overbury et al. [1975]. Using a more recent compilation of surface energies Wynblatt and Ku [1977b] have recalculated the correlation and obtained:

$$\gamma_i \sigma_i = 0.174\ \Delta H^i_{SUB} \qquad i = A,B \tag{6.4}$$

Using (6.4), the surface energy term becomes:

$$(\gamma_A - \gamma_B)\ \sigma_B = 0{,}174\ [\Delta H^A_{SUB}\ (\sigma_B/\sigma_A) - \Delta H^B_{SUB}] \tag{6.5}$$

where the surface area per atom, σ_i can be defined in terms of the Seitz radius:

$$r_i = (3\Omega_i / 4\pi)^{1/3} \tag{6.6}$$

yielding,

$$\sigma_i = \pi r_i^2 = \pi (3\Omega_i / 4\pi)^{2/3} \qquad i = A,B \tag{6.7}$$

where Ω_i is the atomic volume.

It has been suggested [Tsai et al. 1977] that the elastic strain energy contribution should only be added in eq. (6.3) when the solute radius is greater than that of the solvent. This is based on atomic calculations indicating no significant relaxation of atomic positions around a vacancy

and that an undersized solute atom may be considered as a vacancy within this context. The effect of this contribution is discussed later for each end of the composition range. It has been further suggested that eq. (6.3) may overestimate the elastic strain energy contribution as it is already partially included in the enthalpy of mixing term [Kumar 1979]. In general, the predictions of the above model, together with the refinements of Tsai et al. [1977] are reasonably consistent with experimental results obtained from numerous investigations as indicated in a review by Seah [1979].

4.3. THE IMPURITIES PROBLEM: ATTAINING A BINARY SYSTEM

Studies of the surface segregation phenomenon in binary alloys are often complicated by the presence on non-metallic bulk impurities present at trace levels which strongly segregate to a free surface upon annealing. The Cr-Mo system has been no exception and indeed, the problems have been compounded by the fact that one of the components (Cr) has a much higher vapour pressure than the other (Mo). This then, has limited the temperature range which can be used to remove, or reduce, the impurities' level and has thus imposed a severe restriction to the techniques that can be used which do not induce irreversible perturbations to the bulk alloy composition.

Depending on the purity of starting materials used in the alloy preparation, the preparation procedure and the annealing temperature, the following contaminants have all been observed to segregate: C, N, O, P, Si, Cl and S. The ultimate use of the high-purity material grades indicated in Chapter 2, reduced all but the first three to sufficiently low bulk concentrations that a relatively small number of sequential anneal-sputter cycles was effective at removing these contaminants over a very large sample depth. However, severe problems were encountered at removing, or reducing, the C, N and O levels so as to study the segregation behaviour of the binary Cr-Mo system. Through a combination of a number of techniques, procedures were established so that the impurities were sufficiently depleted over some sample depth such that an experimental time scale existed where the segregation behaviour of the 'pure' binary

system could be studied. As will be presented, this annealing time constraint can lead to some interpretation problems. The exact 'recipe' that was found successful depended on the alloy composition and the associated impurities and is indicated in the subsequent sections for the appropriate alloys.

Although a quantitative study of surface segregation is difficult at the binary alloy level, the presence of additional components, albeit trace impurities, renders any analysis to a qualitative description at best. This problem is attributable to kinetic, equilibrium, and radiation-induced effects, depth resolution of AES, unavailability of appropriate standards, etc. Despite the obvious limitations, in arriving at the 'cleaning' procedures mentioned above, an insight into the segregation behaviour of some impurites has been attained and will be published [Dawson and Petrone, in preparation].

6.4. SURFACE SEGREGATION IN Mo-RICH Cr-Mo ALLOYS

6.4.1. Theoretical Prediction

The theoretical prediction of the equilibrium surface concentration of Mo-rich alloys was determined according to equations (6.2) and (6.3). Using literature lattice parameter measurements [Pearson 1958, 1967, Rudy 1969], Seitz radii were calculated according to eq. (6.6) yielding r_{Mo} = 0.1550 nm and r_{Cr} = 0.1423 nm [King 1966]. The corresponding surface area per atom values of σ_{Mo} = 0.7548 nm^2 and σ_{Cr} = 0.6363 nm^2 were obtained from eq. (6.7). Hultgren et al. [1973a] give ΔH^{Mo}_{SUB} = 157.3 kcal/mole and ΔH^{Cr}_{SUB} = 95.0 kcal/mole. Substitution of these data into eq. (6.5) yields for the surface energy term (Term 1), -7758 kcal/mole.

The second term estimating the alloy interaction energy contribution is both surface coverage, through the x^{Cr}_S parameter, and crystal orientation dependent. Values for the enthalpy of mixing, ΔH_M, were obtained from Hultgren et al. [1973b].

The elastic strain energy contribution (Term 3) was calculated using elastic moduli of K_{Cr} = 1.940 · 10^6 kg/cm^2 and G_{Mo} = 1.18 · 10^6 kg/cm^2 obtained from Gschneidner [1964] along with the above Seitz radii to yield a value of -5557 kcal/mole.

As an example, for a 90 at.% Mo-Cr alloy, ΔH_M = 0.495 kcal/mole; for bcc alloys Z = 8 and for the (110) orientation, Z_y = 4, Z_v = 2. Substitution of these data into equations (6.2) and (6.3) yields:

$$(x^{Cr}_S / x^{Mo}_S) = (0.1111) \exp \{ [(7758) + (5500\, x^{Cr}_S + 550) + (5557)] / RT \} \quad (6.8)$$

similarly, for the (100) or (111) orientations where $Z_1 = 0$ and $Z_v = 4$,

$$(x_s^{Cr} / x_s^{Mo}) = (0.1111) \exp ([(7758) + (2200) + (5557)] / RT) \qquad (6.8a)$$

Clearly, for Mo-rich alloys all three contributions reinforce each other and predict strong solute (Cr) segregation. The surface energy of Cr is lower than that of Mo therefore this effect will drive Cr to the surface; the enthalphy of mixing favours segregation of the solute (Cr) in clustering alloys ($\Delta H_M > 0$); and the elastic strain energy term always favours solute (Cr) segregation. The theoretical predictions of this model yield, for the three low index orientations over the experimental temperature range of 875-1075 K, $x_1^{Cr} \geq 0.98$ for $x_b^{Cr} \geq 0.03$. Therefore, for the three Mo-rich alloys used in this study, $x_b^{Cr} = 0.402$, 0.125 and 0.102, essentially a pure monolayer of the solute Cr is predicted at the surface.

The question of whether or not the elastic strain energy contribution (term 3 in eq. (6.8)) should be included is applicable to this end of the composition range. That is, although Cr is the solute, its atomic radius is smaller than that of the solvent Mo and hence according to Tsai et al. [1977] no lattice strain is reduced by the segregation of Cr. Theoretical calculations according to eq.(6.2) indicate that in the experimental temperature range, a bulk composition of $x_b^{Cr} < 0.02$ is required before the theoretical prediction neglecting this contribution deviates significantly from an essentially pure monolayer of Cr at the surface, i.e., $x_1^{Cr} < 0.8$. Given the Mo-rich alloys used in this investigation and the resolution of the technique, this question cannot be addressed in the present study.

6.4.2 Experimental Results

The non-metallic impurities which posed a problem in segregation studies of Mo-rich alloys were C and O. The combination of C oxidation, in low pressures of O_2 ($P = 2\text{-}5 \cdot 10^{-9}$ torr, T = 1000-1075 K) and sequential anneal to cause segregation, followed by sputtering to remove the segregant, has been successfully applied to the Mo-rich alloys of bulk composition 59.8, 87.5 and 89.8 at.% Mo. The three alloys have been sufficiently depleted of the impurities with no detectable perturbation in composition so as to allow a segregation study of the binary system on an experimental time scale of minutes (< 1 hour). The 89.8 at.% Mo alloy was further subjected to a more extensive 'cleaning' procedure so as to allow long-term annealing experiments over the experimental temperature range. In general, once the alloys were 'cleaned' surface contamination at temperatures > 970 K was not a problem. At lower temperatures, slow C and/or O contamination defined the maximum annealing time over which data collected was acceptable. Once measurable levels above noise were detected, further data were not used.

Surface segregation in Mo-rich Cr-Mo alloys has been observed on annealing the sputtered alloys at various temperatures in the range 875-1075 K. Typical results for the Mo(186) and Cr(529) APPH variations with time are shown in Figs. 6.1a and 6.1b for the 59.8 at.% Mo alloy annealed at 920 and 1075 K, respectively. Actual Auger spectra of the appropriate energy regions for the sputtered (t=0) and annealed surfaces are shown in Fig. 6.2. Clearly both sets of data show that the surface becomes enriched in Cr on annealing, viz. Cr segregates to the surface. While the

rate of segregation is higher at the higher temperature as expected, the extent of Cr enrichment at the surface is surprisingly greater at the higher temperature. The asymptotic Cr to Mo peak height ratios are 0.75 at 920 K and 1.2 at 1075 K. This result is unexpected since the free energy of segregation becomes less negative with increasing temperature (eq. 6.1). This surprising result was observed in all three alloys.

The lower limit of the temperature range used for the study (875 K) was established by the contamination problem described above and additionally due to diffusion being too slow to allow measurable compositional changes over the experimental time scale; the upper limit (1075 K) by the evaporation of Cr becoming a problem with extended annealing time (Chapter 7). The asymptotic apparent surface compositions $\bar{x}_s$, for all three alloys calculated from the normalized APPH's (eq. 3.25b) after an 'equilibrium' condition was attained at the surfaces are shown in Table 6.1. The errors indicated reflect the scatter obtained from numerous experiments. The experimental temperatures that were accessible for each of the alloys are also indicated.

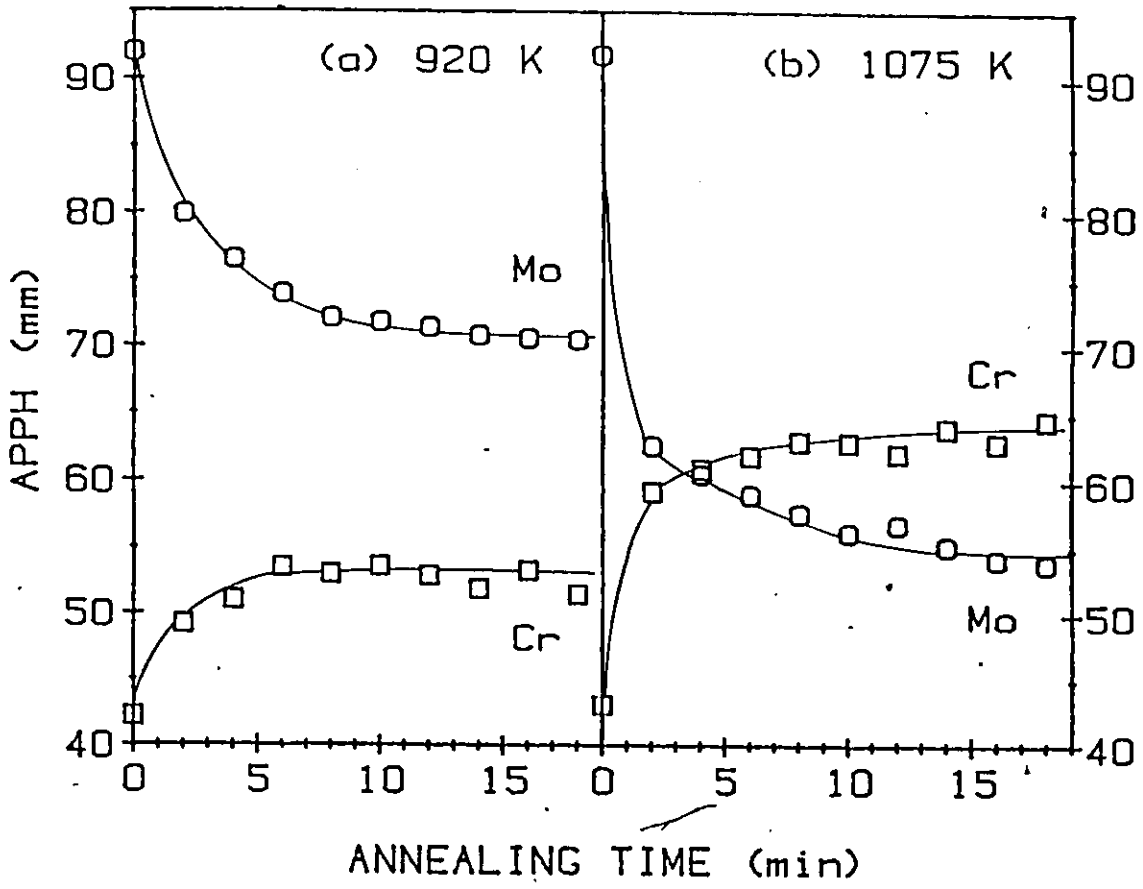

Figure 6.1: The variation in Cr and Mo APPH's for a sputtered 59.8 at.% Mo alloy with annealing time. Panel (a) shows the results for an annealing temperature of 920 ± 5 K whereas (b) is for a temperature of 1075 ± 5K. The Cr APPH's have been multiplied 2.5X.

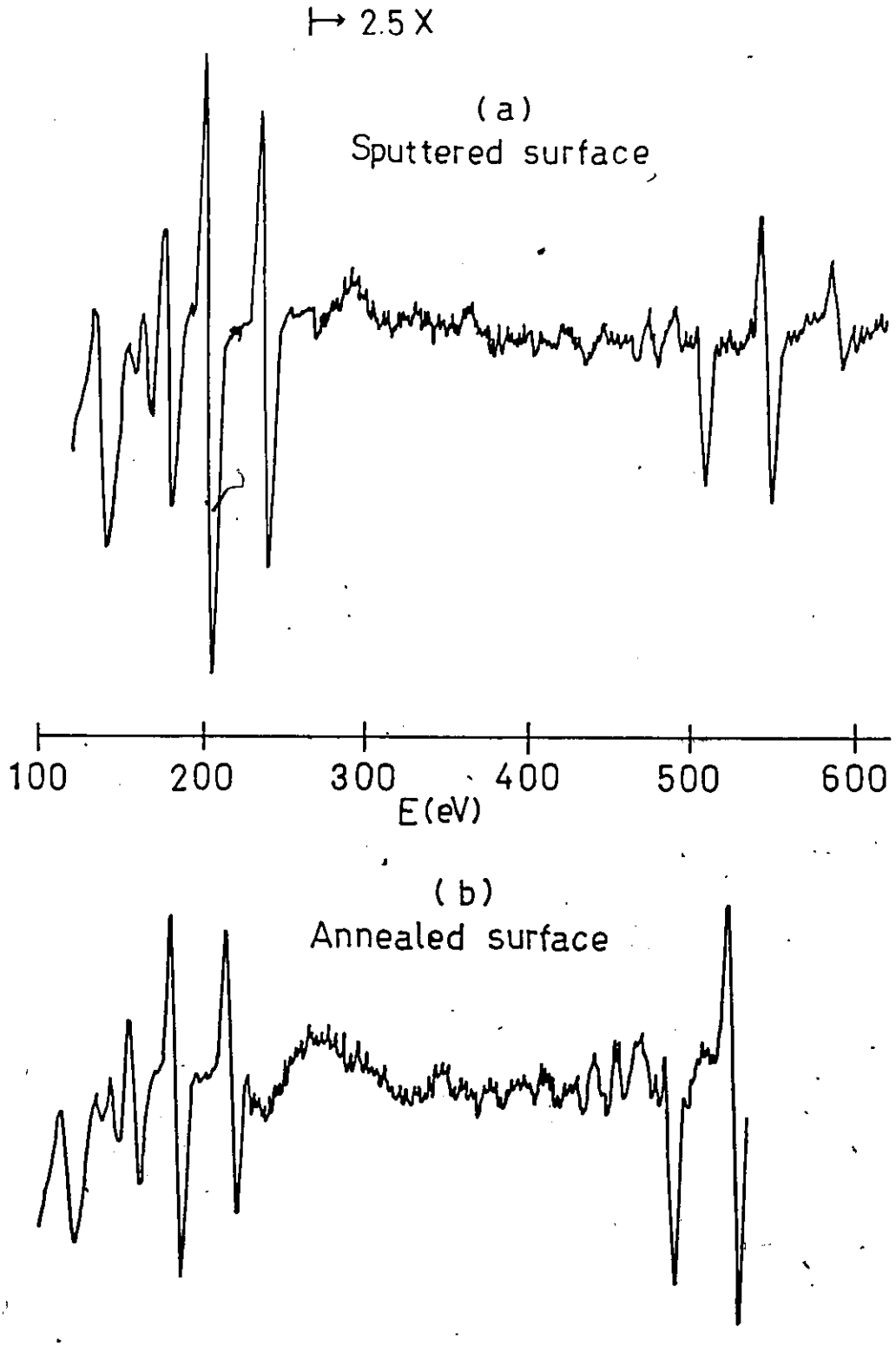

Figure 6.2: Auger spectra of (a) a sputtered 59.8 at.% Mo alloy surface and (b) an equilibrated surface at 1075 K.

Table 6.1 : Normalized Auger data for three Mo-rich Cr-Mo alloys.

1	2	3	4	5	6
Elem.	x_b	Peak	Normalised Auger Peak Heights (%)		
			Sputtered $100 \cdot x_s$	Annealed at Low T $100 \cdot \bar{x}_s$	Annealed at High T $100 \cdot \bar{x}_s$
				($T \leq 920$ K)	($T \geq 1025$ K)
Cr	0.402	Cr(529)	30.4 ± 0.7	38.0 ± 1.5	46.0 ± 2.0
Mo	0.598	Mo(186)	70.8 ± 0.6	54.0 ± 1.5	43.0 ± 1.5
Sum	1.000		101.2 ± 0.9	92.0 ± 2.1	89.5 ± 2.5
				($T \leq 920$ K)	($T \geq 1025$ K)
Cr	0.125	Cr(529)	9.0 ± 0.4	15.5 ± 1.5	22.0 ± 2.0
Mo	0.875	Mo(186)	90.2 ± 0.8	76.0 ± 1.5	67.0 ± 1.5
Sum	1.000		99.2 ± 0.9	91.5 ± 2.1	89.0 ± 2.5
				($T \leq 920$ K)	($T \geq 950$ K)
Cr	0.102	Cr(529)	7.9 ± 0.2	14.5 ± 1.5	20.5 ± 1.5
Mo	0.898	Mo(186)	91.8 ± 0.5	77.5 ± 2.0	69.5 ± 1.5
Sum	1.000		99.7 ± 0.6	92.0 ± 2.5	90.0 ± 2.1

The accessible temperature range used for all annealing experiments is 875-1075 K. For each alloy, the temperatures at which the annealing results indicated in columns 5 and 6 were obtained are shown in brackets.

6.4.3. Discussion

The segregation results obtained from the Mo-rich alloys are qualitatively in agreement with the theoretical prediction of a surface enrichment in the solute Cr upon annealing. However, the thermodynamic predictions of eq. (6.8) indicate, not only a negligible temperature dependence in the experimental temperature range, but equally important, that the extent of any enrichment decreases with increasing temperature. Because the experimental results are inconsistent with these thermodynamic predictions, a non-equilibrium interpretation of the increase in Cr segregation with increasing temperature is adopted.

Consider a solid whose sub-surface region, d layers in thickness, has been modified by ion-bombardment and whose composition profile can be approximated as shown in Fig. 5.12. This damaged sub-surface with a radiation-induced enhanced defect concentration can give rise to compositional modifications through diffusion at temperatures lower than expected for normal thermal diffusion, i.e., radiation-enhanced diffusion (RED). It has been proposed [Dawson and Petrone 1985] that at the lower temperatures ($\leq$ 920 K), homogenization between the bulk and sub-surface cannot occur on the experimental time scale. This kinetic limitation then effectively defines a 'new alloy' surface region which can be described as having a 'bulk' composition equal to the sputtered surface composition, i.e., only local equilibrium can be attained. At the higher temperatures, the bulk diffusion rates are increased sufficiently that the sub-surface equilibrates with the bulk and attains the true bulk composition on the time scale of the experiment. This model has been tested in two ways:

first, by calculating the diffusion times appropriate to the two temperature extremes and second, by calculating the outer monolayer compositions predicted at each temperature and showing them to be consistent with thermodynamic predictions only if the sub-surface compositions are those required by the model.

For the first test, the feasibility of the model can be illustrated via an order of magnitude calculation of the times required to equilibrate the sub-surface with the bulk. As an example, consider the segregation results at 920 K and 1075 K obtained from the 59.8 at.% Mo alloy shown in Fig. 6.1. Assume that the sputter modified surface is uniform over the 'altered layer' depth z, estimated to be about 8.5 nm for the ion energy and geometry used [McCargo et al. 1963]. An underestimate of the time required to homogenize the sub-surface and bulk compositions can be obtained from the diffusion time for atomic diffusion over this distance, i.e., $z^2/2D$. The diffusion coefficient for Cr in a 17 at.% Cr-Mo alloy has been measured over the temperature range 1200-1350 ^{o}C as [Kalinovich et al. 1961],

$$D = 4.3 \exp(-72{,}700/RT) \quad cm^2\ s^{-1}.$$

This calculation gives a diffusion time of 4.3 hours at 920 K and 51 sec at 1075 K, showing that it is reasonable to expect homogenization on the time scale of the experiment at the higher temperature but not at the lower. Annealing at 920 K would presumably lead to a slow approach to the higher temperature result, but this requires a much higher level of sample 'cleanliness' to prevent contaminant interference.

A second test of the model is through the determination of the outer monolayer composition x_1 using the monolayer calculation developed in Section 3.5. Let us initially consider the high temperature results where equilibrium conditions are expected to prevail. Using the apparent annealed surface composition, $\bar{x}_s$, of Table 6.1 and the true bulk [B] values for x_b yields, for the monolayer Cr mole fraction x_1^{cr}[B], the values shown in column (4) of Table 6.2. The results using the Mo(186) data are in excellent agreement with theoretical prediction. For all three alloys, the value of x_1^{cr} determined from experimental results agrees with the prediction of the USM to within experimental error. The results using the higher energy, Cr(529) transition, yield a lower enrichment of Cr at the surface than theoretically predicted. Weighted averages of the these two independent data sets indicate an acceptable agreement with theory. The discrepancy between the two data sets is attributed mainly to the inaccuracy of the IMFP literature values used and will be discussed in Section 6.5.

Extending the calculation to the low temperature results ($\lesssim$ 920 K), one finds poor agreement with theory (column 5). If the sputter modified compositions, column 4 of Table 6.1, are used to represent the sub-surface sputtered bulk [SB] composition at the low temperatures, and the monolayer calculation is repeated, the values of x_1^{cr} [SB] shown in column (6) of Table 6.2 are obtained. Initially limiting the discussion to the results from the 59.8 at.% Mo alloy (x_b^{cr} = 0.402), good agreement is found with the USM prediction. This confirms the hypothesis that sub-surface homogenization with the bulk does not occur on the time scale of the experiments at temperatures $\lesssim$ 920 K.

Table 6.2 · Monolayer compositions of annealed Mo-rich alloys.

1	2	3	4	5	6	7	8
Alloy	Peak	Theor. Pred.	Monolayer Compositions				
x_b^{cr}		x_1^{cr}	High T x_1^{cr}[B]	Low T x_1^{cr}[B]	Low T x_1^{cr}[SB]	% solute depleted	mobile layers
0.402	Cr(529)	$\geq$ 0.98	0.75 ± 0.20	0.27 ± 0.17	0.76 ± 0.15	-	-
	Mo(186)		1.05 ± 0.10	0.62 ± 0.10	0.94 ± 0.08	-	-
Weighted Average			0.99	0.53	0.89		
0.125	Cr(529)	$\geq$ 0.98	0.70 ± 0.20	0.31 ± 0.17	0.49 ± 0.15	48	22
	Mo(186)		0.92 ± 0.10	0.57 ± 0.10	0.65 ± 0.08		(3.4 nm)
Weighted Average			0.87	0.50	0.59		
0.102	Cr(529)	$\geq$ 0.98	0.73 ± 0.17	0.36 ± 0.17	0.49 ± 0.15	62	20
	Mo(186)		0.89 ± 0.10	0.58 ± 0.12	0.63 ± 0.10		(3.1 nm)
Weighted Average			0.84	0.50	0.57		

[B] ≡ using X-ray determined bulk composition in monolayer calculation.

[SB] ≡ using sputtered bulk composition in monolayer calculation.

Theoretical prediction using Unified Segregation Model for 875-1075 K; (100), (110), (111) orientations; $x_b^{cr} \geq 0.03$; including strain energy term.

It appears that the above model is reasonable and explains the observed non-equilibrium effect quite well. However, extension of this calculation procedure to the other two more Cr dilute alloys, column 6 of Table 6.2, reveals that although an improvement is observed, the agreement with theory is still poor. This is an expected result in that if an alloy is sufficiently dilute in the segregating component, then the damaged depth over which enhanced diffusion can occur will dictate the perturbation over this depth required to satisfy the driving force for segregation. In other words, because of kinetic constraints, the semi-infinite pool in the bulk cannot be tapped and further depletion of the sub-surface will occur until a local equilibrium condition is attained.

This process can be modelled by considering an effective number of mobile layers m, that can attain 'local equilibrium', of the d layers damaged due to ion bombardment such that $d \geq m$. By a conservation of mass argument, it can be shown (Appendix 1) that by using the homogeneous approximation for the sputtered surface, i.e., $x^{Cr}_{i(S)} = x^{Cr}_{(S)}$ for $i \leq m$, where the subscript in brackets indicates a sputtered (S) or annealed (A) surface, and assuming a composition profile for the annealed surface that has attained 'local equilibrium' to consist of a pure Cr monolayer, i.e., $x^{Cr}_{1(A)} = 1$ and for the underlying layers ($2 \leq i \leq m$), $x^{Cr}_{i(A)} = x^{Cr}_{(A)}$, one obtains,

$$m\, x^{Cr}_{(S)} = 1 + (m-1)\, x^{Cr}_{(A)} \qquad (6.9)$$

isolating for $x^{Cr}_{(A)}$ yields,

$$x^{Cr}_{(A)} = (m\, x^{Cr}_{(S)} - 1) / (m-1) \qquad \text{for } 2 \leq i \leq m \qquad (6.9a)$$

As an example, if $x^{cr}_{(S)} = 0.10$ and only ten layers (m=10) are sufficiently mobile to homogenize then $x^{cr}_{(A)} = 0$ for $2 \leq i \leq 10$, i.e., all nine layers would be totally depleted of component A to satisfy $x^{cr}_{1(A)} = 1$. However, if m = 50, then a value of $x^{cr}_{(A)} = 0.082$ for $2 \leq i \leq 50$ is obtained, i.e., a homogeneous depletion of $x^{cr}_{(S)} = 0.018$.

Eq. (6.9) can be used to estimate the number of mobile layers in a sputter-modified surface if an appropriate value for the bulk composition $x^{cr}_{(A)}$ ($2 \leq i \leq m$) can be determined when local equilibrium is established. Using the monolayer calculation one can obtain the required bulk compositions that will yield $x^{cr}_{1(A)}$ values consistent with the equilibrium prediction, as exemplified by the high-temperature results of the segregant (Cr) and observed for the 59.8 at.% Mo alloy where this problem is not observed. Isolating m in eq. (6.9) yields,

$$m = (1 - x^{cr}_{(A)}) / (x^{cr}_{(S)} - x^{cr}_{(A)}) \qquad (6.9b)$$

The homogeneous depletion of the sputtered bulk, equal to $x^{cr}_{(S)} - x^{cr}_{(A)}$, necessary to satisfy the above requirement is shown in column (7) of Table 6.2 as a percentage of the sputtered bulk solute mole fraction for the appropriate alloys. Corresponding values of m calculated using eq. (6.9b) are shown in column (9). Using the $a_0/2$ approximation for the monolayer thickness of bcc metals yields an average mobile depth of $\sim$3.3 nm. A comparison with other experimentally estimated 'altered layer' depths of 1 - 10 nm [Betz and Wehner 1983], obtained under similar irradiating conditions for numerous alloy systems, yields satisfactory agreement. This result can also be compared with the ion penetration and damage range predictions of LSS and WSS theories, respectively. As calculated in

Section 5.2.3 for the experimental conditions used, the effective ion and damage ranges in pure Mo are 4.3 and 3.5 nm, respectively. Within the context of the limitations of the theoretical predictions (Section 5.2.3), the agreement with the estimated mobile depth of ~ 3.3 nm is acceptable.

6.4.4. Summary

In this investigation, the segregation behaviour of three Mo-rich Cr-Mo alloys has been established in the accessible temperature range of 875-1075 K. It has been observed that annealing of a sputter-modified surface leads to Cr enrichment of the surface, in agreement with the theoretical predictions of the USM. While the rate of segregation is observed to increase with increasing temperature, the extent of enrichment is higher at the higher temperatures, inconsistent with thermodynamic predictions. For this reason, a non-equilibrium interpretation has been adopted. It has been proposed that at the lower temperatures, homogenization between the sputter-modified sub-surface and the unperturbed bulk cannot occur on the experimental annealing time scale of < 1 hour. An order of magnitude calculation to estimate the time required for the homogenization, using literature diffusion parameters and 'altered layer' depth, confirms this picture. The model was further tested by using the monolayer calculation to deconvolute the outer monolayer composition from that averaged over the finite escape depth of the Auger electrons. The results indicate that if the appropriate sub-surface composition is used, the calculated monolayer composition is in agreement with theoretical predictions. A question arises as to the actual composition of the sub-surface at different annealing temperatures. At sufficiently high

temperatures, homogenization between the bulk and sub-surface occurs very rapidly and the sub-surface is of bulk composition. However, at lower temperatures, the homogenization is too slow and only the sputter-modified sub-surface with a radiation-induced enhanced defect concentration can attain 'local equilibrium' due to RED. If the alloy is sufficiently rich in the segregating component, then the sub-surface can be adequately represented as having the sputtered composition. However, if the alloy is too dilute in the segregating component, then the sputtered composition is no longer appropriate: A severe depletion of the segregating component occurs over the mobile depth so as to satisfy the driving force for segregation. This depletion, assumed homogeneous over some depth of m mobile layers, has been quantified and found to be in good agreement with literature 'altered layer' depths and theoretical ion and damage range calculations.

6.5. LIMITATIONS OF THE MONOLAYER CALCULATION AND AN EXPERIMENTAL DETERMINATION OF IMFP VALUES

The monolayer calculation has been used to determine the outer monolayer composition in annealed alloys. It has been shown to be quite effective in allowing a comparison between experimental results and theoretical predictions, and in the understanding of non-equilibrium and equilibrium effects that occur in segregation studies. The results shown in Table 6.2 indicate that the x_1 composition determined, varies with the energy of the transition used for the analysis: As the energy increases, the value of x_1^{cr} calculated decreases. In order to gain some insight into the potential problems and limitations of the calculation, it is appropriate to review the basic assumptions made in its development and the accuracy of the input parameters. It was assumed that (Section 3.5):

1. the Auger intensity arising from a solid surface can be separated into contributions from distinct layers;
2. compositional modifications arising from surface segregation are limited to the outer monolayer only; and,
3. negligible matrix effects.

The first two assumptions are presently considered reasonable. However, the assumption of negligible matrix effects has been shown to be valid in this alloy system, only for sample surfaces homogeneous over the analyzed volume (Section 3.4). For the annealed samples in this study, the assumption may break down: Its validity is expected to be a function of the energy of the transition used and the extent of inhomogeneity with

depth. The overall effect of the inhomogeneity, possibly leading to non-negligible matrix effects, is difficult to quantify.

The second aspect of the layer calculation that needs to be addressed is in the accuracy of the input parameters:

1. the bulk or sub-surface composition, x_b;
2. the appropriately weighted average surface composition, $\bar{x}_s$, and,
3. the IMFP of the Auger electrons for the transition used.

The accuracies of the compositions, i.e., the first two parameters, are limited by the accuracy of the technique used for their determination. These have been quantified and are considered acceptable. It is then the value of the IMFP that represents the largest uncertainty in the accuracy of the input parameters. Therefore, the accuracy of the final quantitative result depends directly on the accuracy with which the IMFP is known.

The major limitations of the monolayer calculation have been identified as due to the uncertainty in the IMFP value used and the validity of the negligible matrix effects assumption. As a first order approximation, it is suggested, that the IMFP uncertainty is the major source of the problem leading to the dependence of the x_i values calculated on the Auger transition used. Since the driving force for Cr segregation is so strong in Mo-rich alloys, it has been calculated with confidence, that the outer monolayer of the equilibrated surfaces is essentially pure Cr (Section 6.4.1). It is then possible to obtain an experimental estimation of IMFP values in monolayers using the apparent surface compositions $\bar{x}_s$, of the three Mo-rich alloys equilibrated at high temperature, and the layer model

described in Section 3.5. According to eq. (3.28b) a plot of $|(\bar{x}_s - x_b)|$ versus $|\Delta x_1|$ should yield a straight line with slope equal to $I_1 / \sum_{i=1}^{\infty} I_i$. The data for the two major transitions, Mo(186) and Cr(529), are plotted in Fig. 6.3. The low-temperature results of the 59.8 at.% Mo alloy have been included due to the certainty of the sub-surface composition; however the effect on the calculated slopes is negligible. A weighted least-squares analysis forced through the origin, as demanded by the layer model, yields the slopes in column (2) of Table 6.3. From eq. (3.29), the corresponding experimentally determined λ_m^e values obtained by iteration are shown in column (3). A comparison with corresponding values calculated according to Seah and Dench [1979] using eq. (3.30a) shown in column (4) indicates the gross underestimation of λ_m values obtained by their procedure. Much better agreement is found when comparing to modified Seah and Dench values (λ_m') calculated according to eq. (3.31) using a more accurate layer spacing and shown in column (5). However, even these values indicate that for both electron energies, λ_m' is too small, i.e., too surface sensitive.

If the experimentally determined λ_m^e values were used in the monolayer calculation, the x_1^{cr} values calculated using either the Mo(186) or Cr(529) transition, shown in column 4 of Table 6.2, would be essentially equal to unity. It is of interest to calculate the dependence of the IMFP on energy suggested by the λ_m^e values determined from the experimental data. This dependence has been expressed empirically by some authors in the form:

$$\lambda_m(E) = k\, E^n \qquad (6.10)$$

where for example, according to Seah and Dench [1979] for electron energies > 150 eV, $k = 0.41\, a^{1/2}$ and $n = 0.5$; Wagner et al. [1980] obtained for

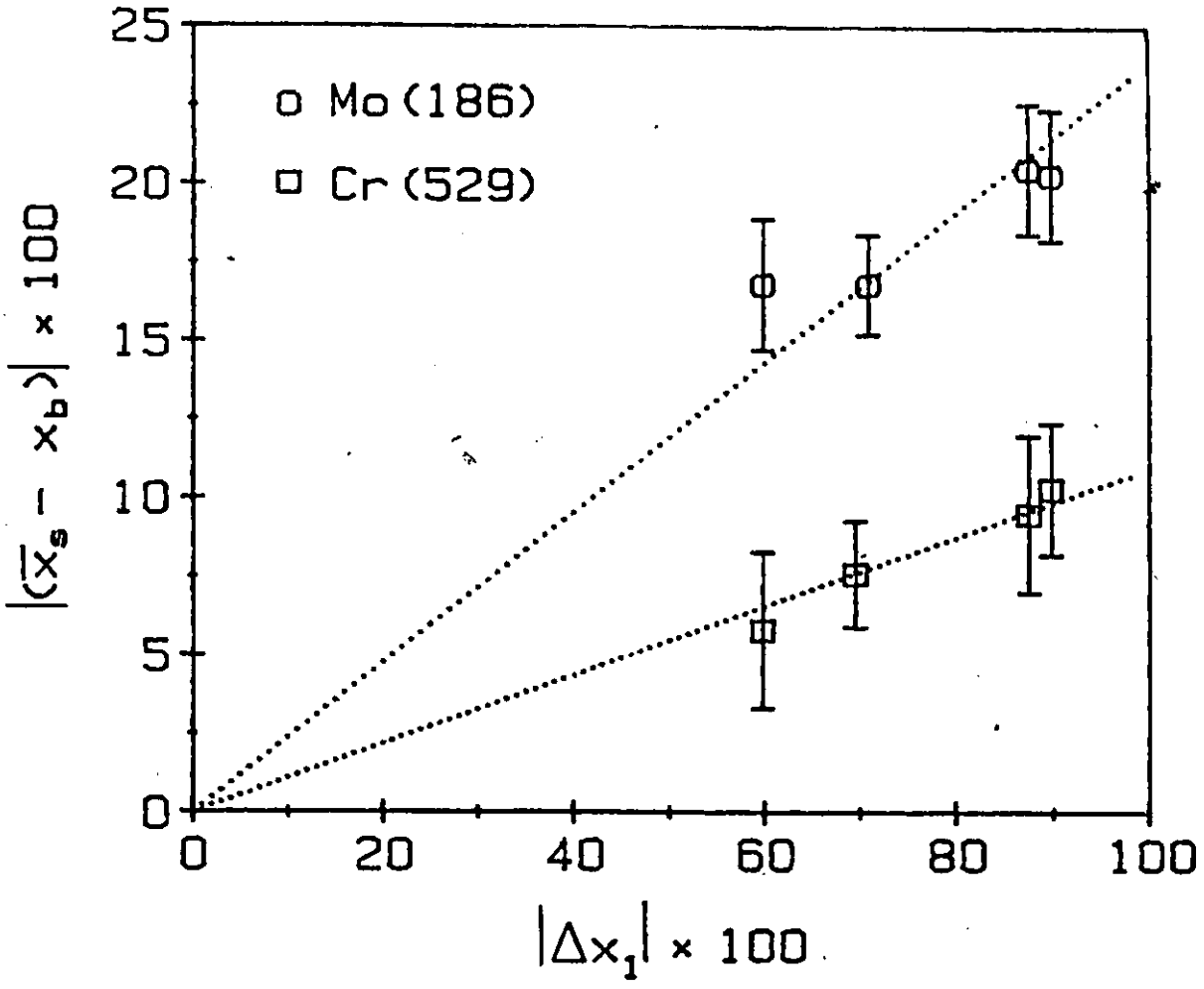

Figure 6.3: An experimental estimation of IMFP's according to eq. (3.28b) using the appropriately weighted Auger surface composition, $\bar{x}_s$ and assuming a pure monolayer of Cr at the surface as calculated with confidence from the USM for the Mo-rich alloys used in this study.

E > 300 eV a materially dependent k and a value of n ranging from 0.54 to 0.81. An analytical expression by Szajman et al. [1981] suggests an energy dependence of n = 0.75 for E > 300 eV in a variety of solids. Powell [1985a, 1985b, 1985c] has suggested similar values of n, also material dependent.

For two transitions in the same matrix, one obtains from (6.10):

$$[\lambda_m^e(E_1) \,/\, \lambda_m^e(E_2)] \;=\; (E_1/E_2)^n$$

Using the λ_m^e values in Table 6.3 yields a value of n = 0.82 ± 0.15 in good agreement with the current literature values expected for the energy dependence.

Table 6.3 : IMFP's in monolayers (λ_m) calculated from experimental results and literature data.

1	2	3	4	5
Transition	Experimental Results		Seah & Dench	Modified Seah & Dench
	$I_1 / \sum_{i=1}^{\infty} I_i$	λ_m^e	λ_m	λ_m'
Mo(186)	0.239 ± 0.013	4.9 ± 0.3	2.7 - 2.8	4.3 - 4.5
Cr(529)	0.109 ± 0.014	$11.5^{+1.8}_{-1.4}$	4.5 - 4.7	7.2 - 7.5

Seah and Dench λ_m calculated according to eq. (3.30a).

Modified Seah and Dench λ_m' calculated according to eq. (3.31).

In both cases the data shown correspond to the variation in IMFP from a pure Cr to a pure Mo matrix.

In summary, the major limitations of the monolayer calculation have been identified. It has been suggested that the major problem is due to the uncertainty in the IMFP value used. Under the assumption of essentially pure Cr in the outer monolayer, as calculated with confidence using the USM, experimental estimates of the appropriate IMFP values were determined. These values indicate that the major problem with the Seah and Dench [1979] IMFP's used is due to their $E^{1/2}$ dependence. This leads to IMFP values that are too low and hence, the corresponding transitions, too surface sensitive. A review of more current literature indicates that indeed, the dependence on energy is stronger and that a value of $E^{3/4}$ is more appropriate. This is in good agreement with the experimentally determined prediction of E^n, $n = 0.82 \pm 0.15$.

6.6. SUMMARY

The results that have been presented in this chapter have established the segregation behaviour of Mo-rich Cr-Mo alloys. The Unified Segregation Model was adopted predicting that because the driving forces considered for segregation all reinforce each other, an essentially pure Cr monolayer is predicted at the surface over the accessible temperature range. This prediction has allowed: (1) a test of the monolayer calculation used to deconvolute the outer monolayer composition, in a monolayer approximation, from that obtained by AES averaged over the electron escape depth; and (2) an investigation into non-equilibrium effects present at lower annealing temperatures where homogenization between the sputtered 'altered layer' and the unperturbed bulk is too slow on short experimental time scales (< 1 hour).

The experimental results were found to be in qualitative agreement with theoretical predictions. For a quantitative comparison, the outer monolayer compositions were determined using the monolayer calculation. Using literature IMFP values and sub-surface compositions appropriate to the annealing termperatures, acceptable agreement was found between theoretically predicted and calculated outer monolayer compositions. A major limitation of the monolayer calculation is identified as being due to the uncertainty in the literature IMFP values used. The experimental results suggest that the dependence of the IMFP on energy is greater than that of the literature data set used. This result is in good agreement with more current literature values of the energy dependence.

The investigation of non-equilibrium effects has only been possible because of the strong driving force for segregation: If a temperature dependence had been predicted over the experimental temperature range, it would have been difficult, if not impossible, to deconvolute the contributions from equilibrium and non-equilibrium effects which both predict a varying surface composition with temperature. The model proposed to explain the non-equilibrium effects is reasonable and shown to be consistent with experimental and literature data and theoretical predictions. Its ultimate test lies in obtaining experimental data over much longer annealing times, i.e., hours. This feat has been successfully accomplished with the extensive 'cleaning' of the 89.8 at.% Mo alloy and the results are presented in the subsequent chapter (7).

CHAPTER SEVEN

A KINETIC ANALYSIS OF THE SURFACE SEGREGATION PHENOMENON IN A SPUTTER-MODIFIED, Mo-RICH Cr-Mo ALLOY

In this chapter, the segregation results of a Mo-rich alloy that underwent a very extensive 'cleaning' treatment, are presented. With the annealing time extended to hours before impurity interference, the results obtained from this alloy provide an experimental test of the model proposed in Chapter 6 to explain the apparent non-equilibrium effects observed. Additionally, the results are used for a kinetic analysis of the segregation phenomenon.

7.1. INTRODUCTION

In the segregation study of Mo-rich alloys presented in Chapter 6, the level of non-metallic bulk trace impurities was sufficiently reduced so as to allow a study of the 'pure' binary sytsem on an experimental annealing time scale of < 1 hour. Because of this annealing time constraint, apparent non-equilibrium effects were observed. A model was proposed and tested to explain this unexpected result through characteristic diffusion times and monolayer composition calculations. It was concluded that the experimental results are both qualitatively and quantitatively in agreement with theoretical predictions if the sub-surface composition is that appropriate to the annealing temeperature used. The

asymptotic approach to a non varying surface composition at low temperatures (< 920 K) does not represent an equilibrium condition. At these temperatures, the sputter modified sub-surface cannot homogenize with the unperturbed bulk on the experimental time scale due to bulk diffusion being too slow. The segregation data obtained at these temperatures must then be interpreted relative to the appropriate sub-surface composition.

The model proposed was reasonable and self-consistent, however, its ultimate test lies in obtaining experimental data over longer annealing times, i.e., hours. This has been accomplished through a very extensive 'cleaning' of the 89.8 at.% Mo alloy. The segregation data collected thus provides a test of the model and an appropriate kinetic analysis of the data yields an insight into the activated processes that occur upon annealing a sputter modified binary alloy.

7.2. EXPERIMENTAL RESULTS

The combination of the two 'cleaning' techniques described in Chapter 6 sufficiently depleted the non-metallic impurities in an 89.8 at.% Mo alloy so as to allow long term annealing experiments, i.e., hours, and a kinetic analysis of the segregation phenomenon over the temperature range 875-1075 K. After a steady-state sputtered condition was established, surface compositional changes were measured in appropriate annealing time intervals. A total of 20 experiments were performed over the entire temperature range with a minimum step of 25 K; typical results are shown in Fig. 7.1 as the APPH as a function of annealing time at 920 and 1025 K. For the kinetic analysis of the data, the APPH ratio Cr(529) / Mo(186), was plotted against the annealing time. The ratios of the APPH's from the alloy have been multiplied by an average value of the ratio of the corresponding pure elemental APPH's Mo^{o}/Cr^{o} obtained over a period of 4 years, (= 2.51 ± 0.04, n = 80, 95% confidence limit). This procedure normalizes the data as per eq. (3.25b) but does not yield a surface composition and is used solely to compensate for differences in elemental sensitivity.

The results shown in Figs. 7.1 and 7.2 indicate that on an experimental time scale of minutes the surface enrichment appears to be greater at the higher temperatures. This non-equilibrium result is caused by the annealing time being too slow at the low temperature for the slow homogenization of the sputter-modified sub-surface and the unperturbed bulk (Chapter 6). If the alloy is sufficiently depleted of impurities so as to allow longer term annealing experiments, i.e., hours, in the intermediate

temperature range, the results shown in Fig. 7.3 indicate that the low temperature plateaus do not define a true equilibrium condition. The high temperature, or equilibrium, surface composition can be attained at the lower temperatures if the sample can be annealed for a sufficiently long time.

The results shown in Fig. 7.2 also indicate that although the asymptotic surface composition is approached at the upper limit of the experimental temperature range of 1075 K, prolonged annealing at this temperature leads to a decrease in the surface concentration of Cr. This effect has been modelled [Lea and Seah 1977, Wynblatt and Ku 1977b] and is attributed to Cr losses from the near surface via evaporation faster than it can be replenished by diffusion from the semi-infinite bulk. An analysis of literature vapour pressure data for the two pure elements, yields, $P_{Cr} = 6.8 \cdot 10^{-11}$ and $P_{Mo} = 9.9 \cdot 10^{-25}$ torr at 1000 K [Hultgren et al. 1973a]: A difference greater than 13 orders of magnitude. In light of these literature data, the experimentally observed preferential loss of Cr at 1075 K is reasonable. The upper limit of the accessible temperature range used in this study was established based on this observation.

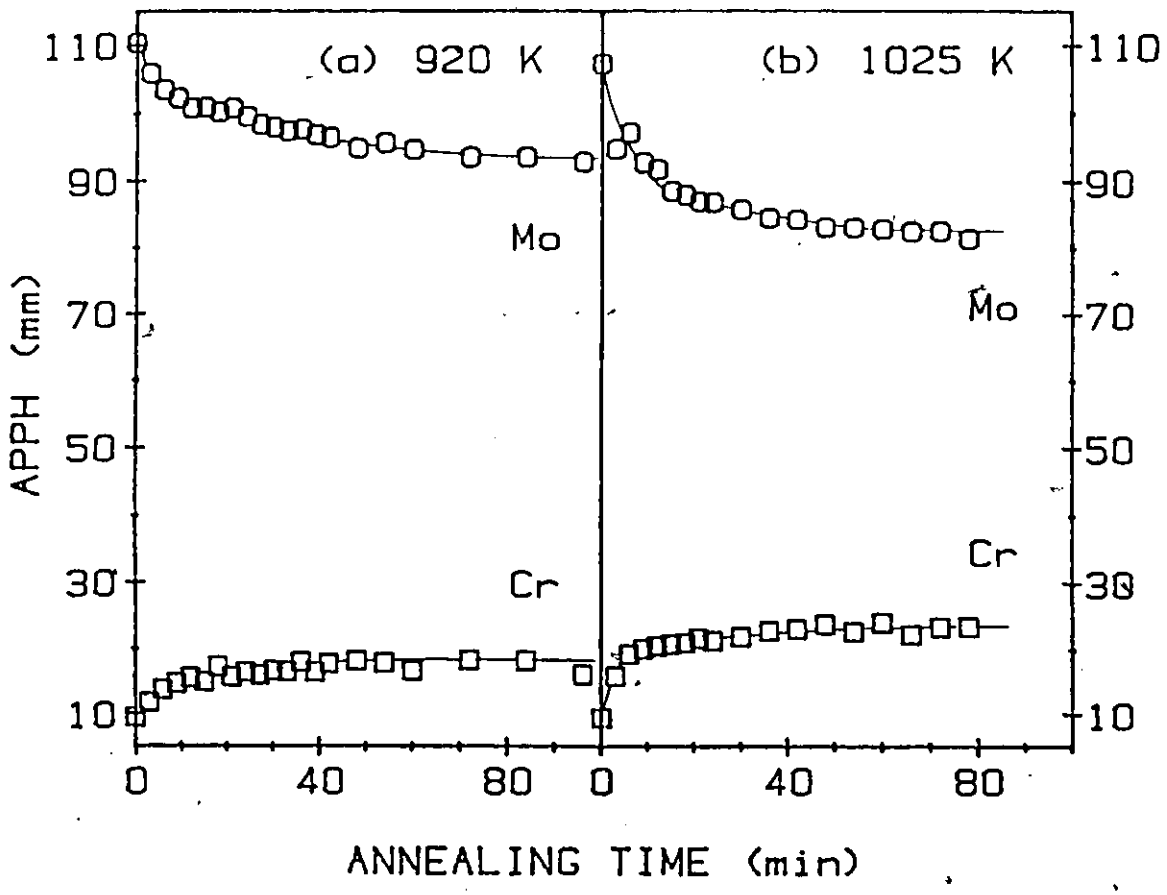

Figure 7.1: The variation in Cr and Mo APPH's for a sputtered 89.8 at.% Mo alloy with annealing time. Panel (a) shows the results for an annealing temperature of 920 ± 5 K whereas (b) is for a temperature of 1025 ± 5K. The experimental annealing time allowed before impurity interference is much longer in this alloy due to an extensive 'cleaning' treatment. The Cr APPH's have been multiplied 2.5X.

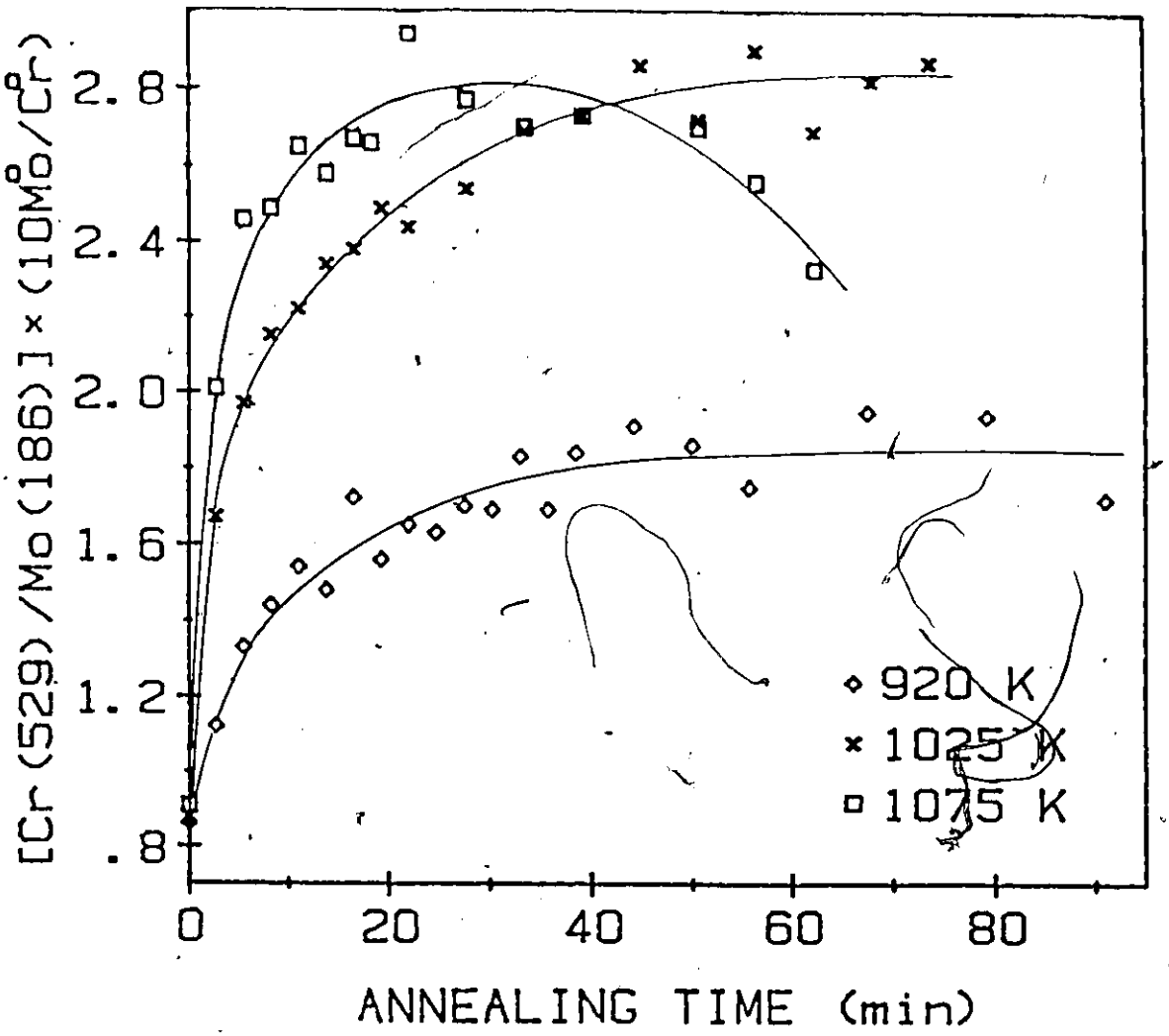

Figure 7.2: Kinetic data obtained from the 89.8 at.% Mo alloy plotted as a ratio of the two elements' major peaks as a function of annealing time. The alloy ratios are multiplied by a ratio of the corresponding pure elemental peaks (as per eq. 3.25b) so as to correct for differences in elemental sensitivity. The annealing time does not include the 15 sec required to attain target temperature. The data indicate two asymptotic plateaus at low (920 K) and high T (1025 and 1075 K). Continued annealing at 1075 K leads to evaporation losses becoming detectable.

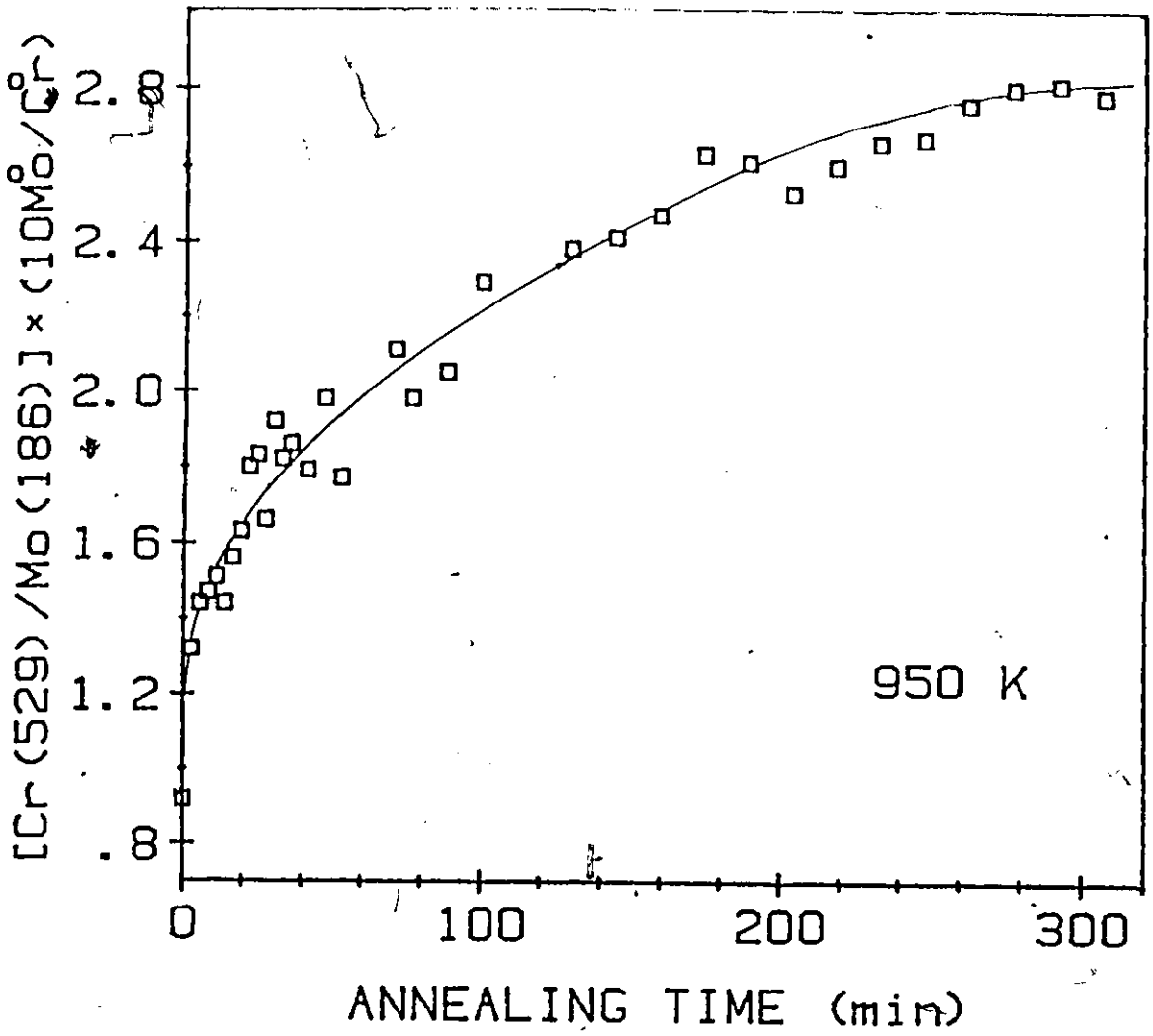

Figure 7.3: Kinetic data from the same 89.8 at.% Mo alloy obtained at an intermediate temperature of 950 K over a period of 5 hours. The results indicate that the low temperature plateau in Fig. 7.2 does not represent an equilibrium condition.

7.3 A KINETIC ANALYSIS OF THE SURFACE SEGREGATION PHENOMENON

Most investigators have analyzed the kinetics of segregation to a free surface according to a solution of the diffusion equation by Lea and Seah [1977] based on McLean's [1957] solution of solute segregation to grain boundaries. Using the formalism of Hennesen et al. [1984] the appropriate equation is:

$$\frac{C_S^{\ast}(t) - C_S^{\ast}(t=0)}{C_S^{\ast}(t=\infty) - C_S^{\ast}(t=0)} = 1 - \exp\left(Dt / \alpha^2 d^2\right) \operatorname{erfc}\left(Dt / \alpha^2 d^2\right)^{1/2} \qquad (7.1)$$

where $C_S^{\ast}(t)$ is the surface concentration of the segregating solute within a surface monolayer of thickness 'd'; D is the diffusion coefficient for bulk diffusion which is assumed to be the rate determining step; t is the time; and α is the surface enrichment factor such that at equilibrium $C_S^{\ast}(t=\infty) = \alpha\, C_B(t=\infty)$ where $C_B(t=\infty)$ is the bulk solute concentration. At all other times, local equilibrium is assumed between the surface monolayer and the underlying sub-surface. Eq. (7.1) is an approximation valid for $\alpha \gg 1$ and constant. For short times $Dt/\alpha^2 d^2 \ll 1$ and eq. (7.1) approximates to:

$$\frac{C_S^{\ast}(t) - C_S^{\ast}(t=0)}{C_S^{\ast}(t=\infty) - C_S^{\ast}(t=0)} = 1 - \exp\left(Dt / \alpha^2 d^2\right) \qquad (7.2)$$

A power series expansion in $P = Dt/\alpha^2 d^2$ yields for small P and neglecting higher order terms:

$$\frac{C_S^{\ast}(t) - C_S^{\ast}(t=0)}{C_S^{\ast}(t=\infty) - C_S^{\ast}(t=0)} = (2/\pi)\left(Dt / \alpha^2 d^2\right) \qquad (7.3)$$

For the case where the initial surface concentration $C_S^{\blacksquare}(t=0) \sim 0$, using the relation $C_S^{\blacksquare}(t=\infty) = \alpha\, C_B(t=\infty)$ and replacing $C_S^{\blacksquare}$ by an areal concentration $C_S = C_S^{\blacksquare} \cdot d$ yields:

$$C_S(t) = 2\, C_B\, (Dt/\pi)^{1/2} \qquad (7.4)$$

which is the infinite solid solution for Fick's second law [Crank 1956].

Clearly such an analysis has two major requirements: (1) the change in concentration at the surface monolayer has to be accurately determined; and (2) bulk diffusion must be the rate determining step. When surface analysis is performed via AES, both of the above conditions are met only for very dilute alloys. In such systems, the observed changes in composition can be attributed solely to the outer monolayer, i.e., a negligible contribution from the underlying layers. Secondly, with $\alpha \gg 1$, any enhancement in diffusion from the sputter-modified sub-surface due to the pre-cleaning treatment by inert ion sputtering will be negligible due to the relatively short damage depth. For an alloy such as the one used in this study, neither of the above conditions is met and a different approach is required.

The kinetic data of this study can be interpreted in terms of a phenomenological model. In all cases the initial condition (t=0) is a steady-state sputtered surface with an enhanced defect concentration. Clearly, a steady-state surface composition as determined by AES can only be attained if the defect distribution attains a steady-state, or at least, a pseudo-steady-state condition. The equilibrium condition dictates essentially a monolayer of Cr at the surface and a sub-surface of bulk composition, i.e., $x_1^{Cr} = 1$, $x_i^{Cr} = x_b^{Cr}$ for $i \geq 2$ as $t \longrightarrow \infty$. It is assumed

that in a temperature range where a given atomic transport mechanism is operating, the concentration profile in the surface region yields a characteristic surface composition as determined by AES; i.e., a given Cr/Mo ratio will correspond to the same concentration profile at all temperatures within that range because the same process is occuring, only at different rates. In other words, the Cr/Mo ratio provides a measurable physical property which is directly related to the activated process of surface segregation. The isothermal annealing curves obtained can then be appropriately analysed by the method of 'cross-cut' [Parkins et al. 1951, Damask and Dienes 1963].

The difference in Cr/Mo ratio between the initial and final state was partitioned in terms of percent completion of the total process with a resolution of 10%. The characterisitic time t_x, with x denoting the percent completion, is identified with the diffusion time t where,

$$t = z^2 / 2D \qquad (7.5)$$

where z^2 is the mean square distance travelled and D the diffusion coefficient given by,

$$D = A_o \exp(-Q/RT) \qquad (7.6)$$

yielding,

$$\mathrm{Ln}(t) = C + Q/RT \qquad (7.7)$$

where C is a constant. Thus, a plot of Ln(t) versus 1/T should yield a straight line with slope Q/R. Characteristic times for < 30% completion could not be determined accurately because even at lower temperatures, i.e., < 970 K, these values were obtained very quickly: Times were

comparable to annealing intervals. Values for < 60% completion at the high temperatures, i.e., > 970 K, could also not be determined accurately for the same reason. The results are shown in Figs. 7.4 and 7.5 for high and low percent completion, respectively. The same scale expansion was used thereby allowing a direct comparison of the slopes. The 1075 K data is not included as it consistently yields characteristic times longer than expected, consistent with evaporation being a problem. The corresponding activation energies calculated from the slopes are shown in Table 7.1.

The results clearly indicate that the complete segregation process occurs with two very different activation energies. Atom transport in the regime associated with a high percent completion, i.e., 60-90%, occurs with an apparent high activation energy, Q^H. However, in the low percent completion regime, i.e., 30-50%, a much lower apparent activation energy Q^L is observed.

There will be some systematic errors with the type of analysis used, attributable to end corrections and residual defects; these will be addressed in the discussion (Section 7.4). In order to minimize most sources of errors, a plot of Q^H versus percent completion is expected to yield the most accurate value of the activation energy in the high percent completion regime when extrapolated to 100% completion. These data are shown in Fig. 7.6 yielding an apparent activation energy $Q^H = 53 \pm 5$ kcal/mole in the temperature range 950-1025 K. For the low percent completion regime an average value of $Q^L = 20$ kcal/mole is obtained in the temperature range 875-970 K.

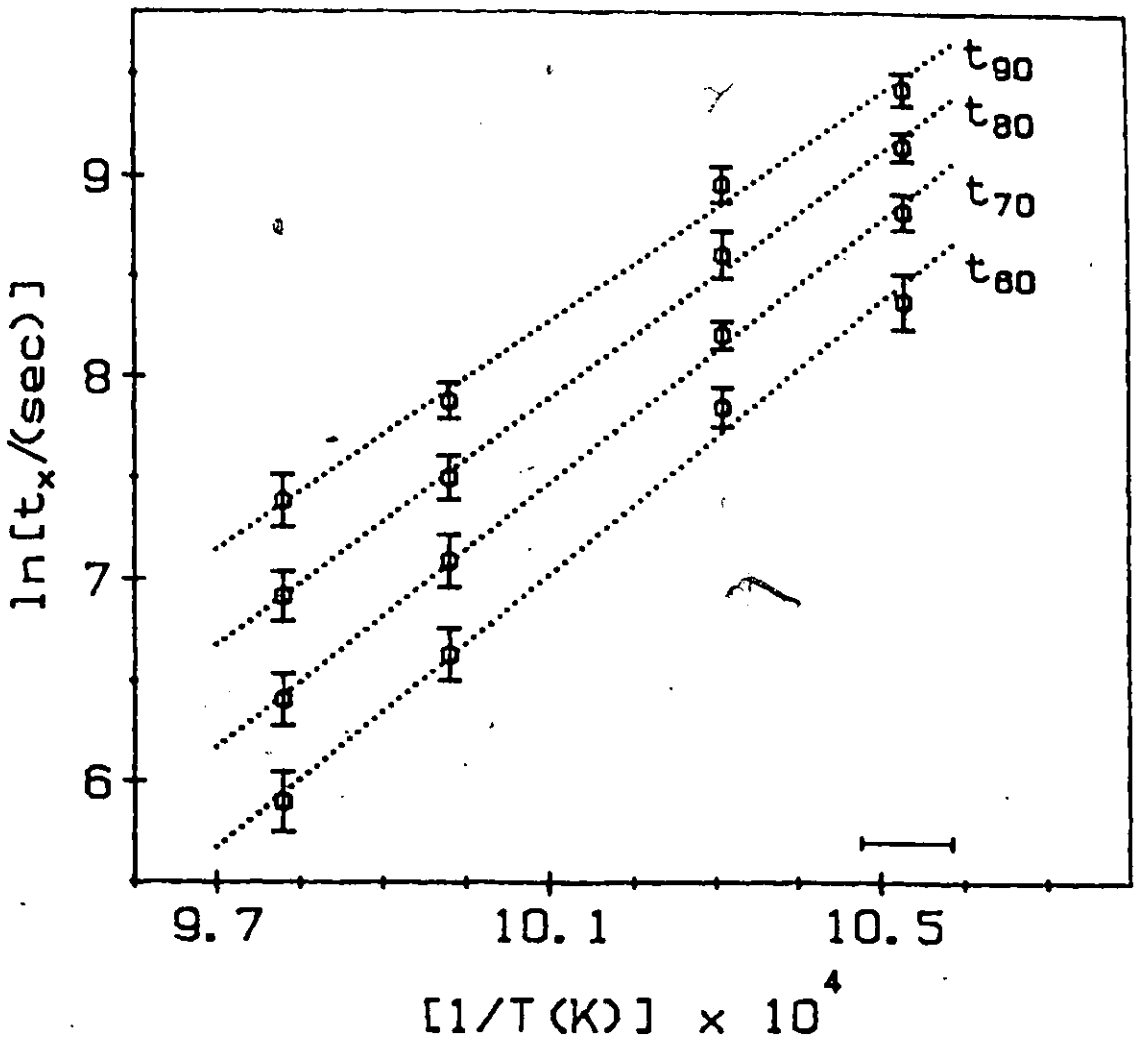

Figure 7.4: A logarithmic plot according to eq. (7.7) of the characteristic times for diffusion (t_x) in the temperature range 950-1025 K where greater than 50% completion was attained. The error in abscissa is shown for the lowest temperature data in the bottom right-hand corner.

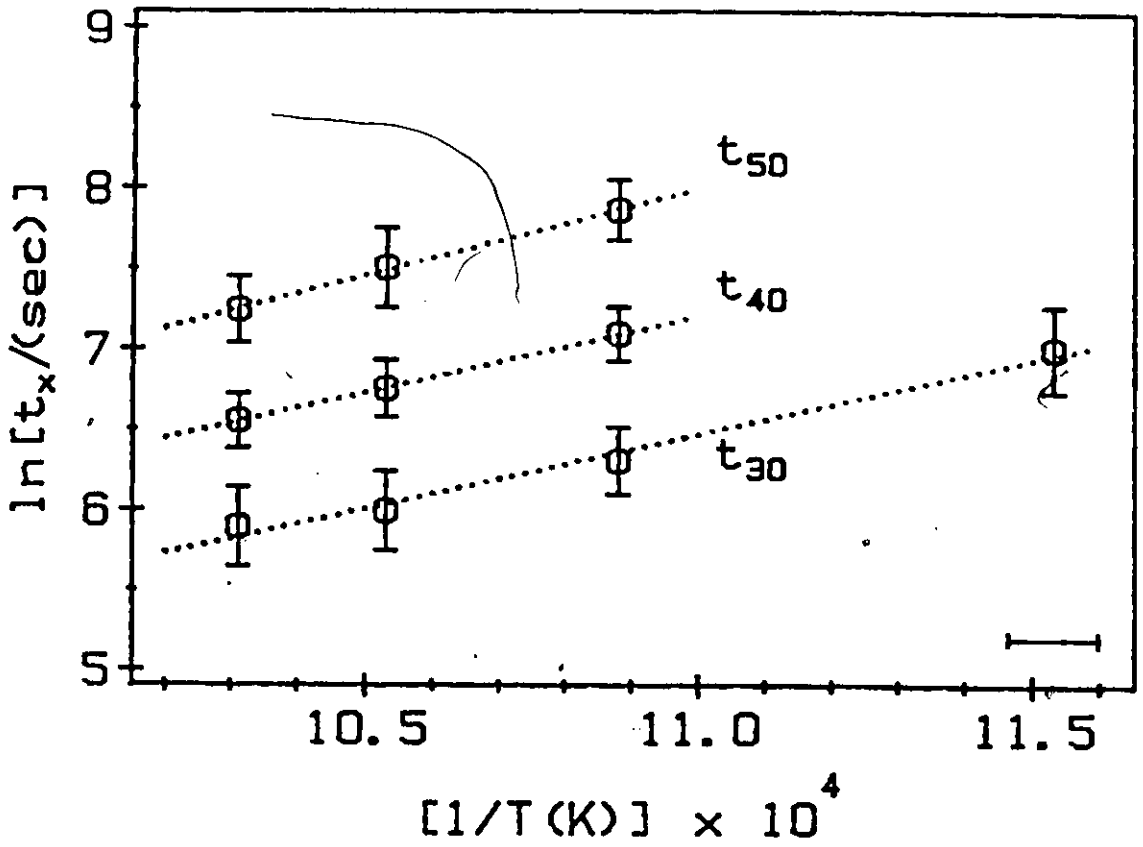

Figure 7.5: A logarithmic plot according to eq. (7.7) of the characteristic times for diffusion (t_x) in the temperature range 875-970 K where ≤ 50% completion was attained or, for intermediate temperatures, the time could be determined accurately. The same scale expansion in both directions has been used for a direct comparison with slopes in Fig. 7.4. The error in the abscissa is shown for the lowest temperature data in the bottom right-hand corner.

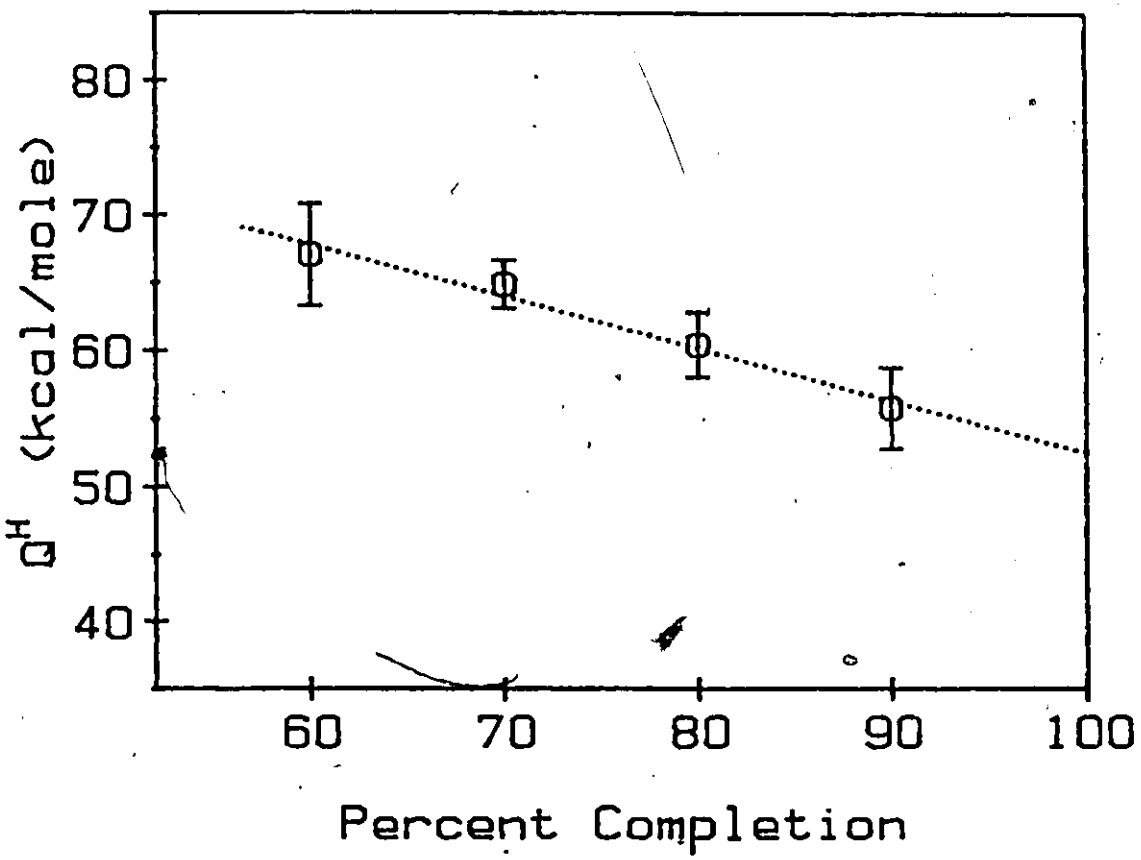

Figure 7.6: A plot of the apparent activation energy in the higher percent completion regime, Q^H, as a function of percent completion. If there were no systematic errors associated with the experimental results, the slope of this plot is expected to be zero.

Table 7.1: Experimentally determined activation energies of diffusion.

	Temperature Range (K)	Data Set	Activation Energy (kcal/mole)
1	950-1025	t_{60}	67.0 ± 3.8
		t_{70}	64.8 ± 1.8
		t_{80}	60.4 ± 2.4
		t_{90}	55.8 ± 3.0
		$(t_{100})^*$	53 ± 5
2	875-970	t_{30}	18.5 ± 1.6
		t_{40}	18.9 ± 0.4
		t_{50}	21.5 ± 0.8
		Average	19.6

$(t_{100})^*$ activation energy value obtained by extrapolation of data in row 1 (from Fig. 7.6).

Average of data in row 2 is an unweighted average.

7.4 DISCUSSION

A model describing the apparent 'non-equilibrium' effect of surface enrichment has been proposed and shown to be consistent with the theoretical prediction if the appropriate sub-surface composition is used in the monolayer calculation (Chapter 6). Ion-bombardment creates a sputter-modified sub-surface 'd' layers in thickness depleted of Cr due to preferential sputtering. The profile can be adequately approximated as shown in Fig. 5.12 due to collisional mixing. Once ion bombardment is terminated two regions can be distinguished in the alloy: A sub-surface depleted of Cr with an excess concentration of radiation-induced defects, vacancy and interstitial-type, and a bulk which has not been perturbed by ion-bombardment. In the absence of irradiation, diffusion in such substitutional alloys is considered to occur via the thermally activated motion of equilibrium lattice vacancies, i.e. the mono-vacancy mechanism [ASM 1965] with the contribution from interstitials being negligible. Radiation-enhanced diffusion (RED) can occur by increasing the concentration of vacancies and/or interstitials, accelerating their motion, or creating totally different diffusion mechanisms [Lam and Rothman 1975]. The temperature range over which this enhancement in diffusion is observable will be limited by the requirements that the excess defect is mobile and that the defect concentration is much larger than the equilibrium concentration.

Upon annealing three processes will occur:

1. the segregation of Cr to essentially a pure monolayer at the surface;

2. the homogenization of the sub-surface with the bulk; and,

3. the annihilation of excess defects through mutual recombination or migration to sinks such as the surface, grain boundaries, immobile defect clusters, etc.

The results shown in Figs. 7.2 and 7.3 provide experimental evidence of the model proposed in Chapter 6 to explain the non-equilibrium effects observed: If the alloy is sufficiently depleted of impurities so as to allow long term annealing experiments, the surface composition attained at higher temperatures, where equilibrium conditions prevail, can also be attained at the lower temperatures where homogenization between the bulk and sub-surface occurs very slowly.

A kinetic analysis of the data reveals that the complete segregation process, from a sputter-modified to an equilibrated surface, occurs by atomic transport with two very different activation energies. The observed difference in the apparent activation energies greater than a factor of two, as shown in Figs. 7.4 and 7.5 and summarized in Table 7.1, can be understood as follows. Monolayer calculations indicate that the plateau observed at low temperatures is consistent with an essentially pure Cr monolayer at the surface over a sub-surface that has attained local equilibrium. That is, because of RED the sputter-modified sub-surface has increased 'mobility' over 'd' layers due to a lower activation energy for diffusion. The calculations indicate that by approximately t_{50} both the segregation of Cr to a pure monolayer and local sub-surface equilibration is complete. Between t_{50} and t_{100} homogenization with the bulk will occur under normal thermal diffusion conditions with an appropriate activation

energy, i.e., RED no longer plays a significant role. In order to understand this enhanced mobility, one must consider the state of the sputter-modified sub-surface when ion-bombardment is terminated and an annealing experiment about to commence.

Based on the present literature, a qualitative description of the defect distribution in the surface region under the experimental irradiating conditions, is possible (Section 5.2.2). It is well documented that, for pure Mo and Cr, interstitials and possibly some small interstitial clusters are mobile at room temperature but vacancies are immobile. Because of the relatively short ion and damage range distributions (R_p = 1.7 and 1.5 nm from LSS and WSS theories in pure Mo, respectively), the surface will have a very large effect on the steady-state condition by supplying a very high sink density. Interstitials in the surface region can undergo annihilation through recombination with a vacancy or at a sink, predominantly, the surface. However, a fraction will survive and migrate into the bulk. The latter has been observed as very large interstitial agglomerates well beyond the ion range in Cu and Nb under 5 KeV Ar^+ ion bombardment [Hertel et al. 1974]. The net effect will lead to a surface region, comparable to the ion range, with an excess vacancy concentration present mostly as uncollapsed depleted zones or small clusters. The interstitial concentration in this region will be negligible: If any do exist it will be most likely as immobile clusters. At greater depths into the bulk, beyond the ion range, a high interstitial concentration is expected. The presence of these defects above equilibrium concentrations will lead to RED at the experimental annealing temperatures where both types of

defects are mobile; the vacancy-type expected to have the greatest effect under AES surface analysis. The annealing temperature required to observe RED, arising from the thermal evaporation of vacancies from the clusters, is expected to be ~ 875 K. With the large sink density supplied by the surface, further cluster growth is not expected. This temperature is consistent with the experimentally established lower temperature limit of 875 K below which diffusion is too slow to allow measurable surface compositional changes.

The two apparent activation energies can be compared with appropriate literature diffusion parameters. Q^M, representing the activation energy associated with the homogenization of the sub-surface with the bulk, should correlate with normal thermal diffusion in an alloy matrix since the rate determining step in this atomic transport mechanism is diffusion from the unperturbed bulk. B.c.c refractory elements which exhibit 'normal' diffusional behaviour, as is the case for Cr and Mo [Askill 1965], undergo self-diffusion with an activation energy $Q^{SD} = E^F + E^M$, where E^F and E^M are the vacancy formation and migration energies, respectively. Generally, alloying of such metals changes both diffusion parameters D_o and Q^{SD}. In numerous refractory alloy systems, an enhancement in D is observed through a lower Q^{SD} and/or a higher D_o [Askill 1970, Mrowec 1980, Fedorov and Smirnov 1984, Agarwala 1984]. The limited data available for the Cr-Mo system indicates that such is the case in this system. The most recent study by Borisov et al. [1968] has obtained for ^{51}Cr tracer in Mo and ^{99}Mo tracer in Cr, Q values of 54.0 (T=1000-1500 ^oC) and 58.0 (T=1100-1420 ^oC) kcal/mole, respectively. Additionally, an earlier study

[Kalinovich et al. 1961] of ^{51}Cr tracer in a 17 at.% Cr-Mo alloy has found a Q value of 72.7 kcal/mole (T=1200-1350 ^{o}C). The agreement with the experimentally determined Q^{M} = 53 ± 5 kcal/mole is acceptable.

The apparent activation energy Q^{L} associated with atom transport in a defect enriched zone may represent a combination of activated processes. In the simplest interpretation, the surface compositional changes observed in the low percent completion regime are attributed to the migration of mono-vacancies emitted from vacancy clusters. Therefore, the activation energy should be lower than Q^{SD} by an amount E^{F}, i.e., equal to E^{M}. In other words, the vacancies have already been created by ion bombardment: The only energy required for atomic transport, by the vacancy mechanism, is that corresponding to the vacancy migration energy E^{M}. Values of E^{M} for a Cr-Mo alloy matrix are not available; however, the corresponding best E^{M} value in pure Mo is 1.3 eV (30 kcal/mole) [Nihoul 1970, Baluffi 1978]. The value of E^{M} in the Cr-Mo alloy matrix is expected to be lower as a lower Q^{SD} in the alloy can only be obtained with a lower E^{F} or a lower E^{M} or both. In light of these limitations, the agreement with the experimentally determined Q^{L} = 20 kcal/mole, is acceptable.

The kinetic analysis of the segregation data has clearly established that atomic transport, upon annealing a sputter-modified alloy, occurs with two very different activation energies, namely Q^{M} and Q^{L}. It is appropriate to address the separability of these two processes. Recall that the defect distribution after ion bombardment is terminated, and a segregation experiment about to commence, is expected to be similar for all experiments.

At any given temperature, contributions to the measured surface compositional changes from both processes, will occur. The key is in identifying which percent completion regime and temperature range best represents the two activated processes.

In the low percent completion regime (30-50%), established in the temperature range of 875-970 K, the bulk and sub-surface homogenization occuring with an activation energy Q^H, makes a negligible contribution to the surface compositional changes observed. Therefore, Q^L represents the activation energy for atomic transport in the defect-enriched sub-surface. It represents the process yielding an essentially pure Cr monolayer at the surface over a sub-surface that has attained local equilibrium due to RED.

The high percent completion regime (60-90%), established in the temperature range of 950-1025 K, represents the bulk and sub-surface homogenization that occurs once the very rapid segregation process is essentially complete. The question then, is of the relative contribution of Q^L at different temperatures and percent completion, in this regime. As the temperature is increased, the number of excess defects above the equilibrium value, decreases. Additionally, the annihilation of any excess defects becomes much more efficient. At sufficiently high temperatures, the contribution of excess defects will become negligible, i.e., RED no longer plays a significant role. The surface compositional changes observed will be due to atomic transport with an activation energy Q^H. At intermediate temperatures, contributions from both of these processes is expected: The contribution from excess defects (Q^L) decreasing with annealing time due

to their continual annihilation.

Therefore, the separability of these two processes, by the kinetic analysis adopted, leads to some systematic errors. The Q^L value is best determined at lower temperatures and lower percent completion where Q^H contributions are negligible. The Q^H value is best determined at higher temperatures and higher percent completion where the relative contribution from Q^L is small. This is best accomplished with the extrapolation of the Q^H data to 100% completion.

A second source of systematic errors exists due to end corrections. The data as plotted in Figs. 7.4 and 7.5 reflects characteristic times obtained with the time required to attain experimental temperature subtracted from each annealing interval, i.e., 15 sec. Therefore, no end corrections have been made. The error associated with this procedure yields t_x values too low by a relative amount which is not constant, thereby yielding a systematic error. For the accuracy of the analysis appropriate to this study, neglect of this error is considered acceptable.

Despite the sources of error that have been identified with the procedure used for the kinetic analysis, a reasonable understanding of the activated processes that occur upon annealing a sputter-modified surface, has evolved. Acceptable agreement is observed between the experimentally determined activation energies and appropriate literature data.

7.5. SUMMARY

Experimental techniques have been developed to deplete non-metallic impurities in Mo-rich Cr-Mo alloys over very large sample depths. These techniques have been successfully applied to an 89.8 at.% Mo alloy. The segregation results obtained have provided experimental evidence of the model proposed in Chapter 6 to explain apparent non-equilibrium effects that are observed when an annealing time constraint of < 1 hour exists.

A kinetic analysis of the segregation results has yielded an insight into the activated processes that occur upon annealing a sputter-modified binary alloy. The equilibrated surface requires segregation of the solute Cr to an essentially pure Cr outer monolayer and the homogenization of the bulk and the sputter-modified sub-surface. At temperatures where the radiation-induced excess defect concentration is appreciable, RED plays a significant role. This leads to the sputter-modified sub-surface attaining 'local equilibrium' at temperatures lower than expected under normal thermal diffusion. In a simple interpretation, the activation energy associated with this process is expected to be less than that for bulk diffusion by an amount equal to the vacancy formation energy. This is expected since the vacancies whose motion lead to the observed compositional changes, have already been created by ion bombardment. This translates into an expected activation energy equal to the vacancy migration energy. Acceptable agreement is found between the experimentally determined activation energy for this process, Q^L, and appropriate literature data.

Accompanying the segregation process, is the homogenization of the bulk and sub-surface. Its contribution to the measured compositional changes will depend on the annealing temperature: It will be negligible at lower temperatures and short annealing times, and rate-determining once the rapid segregation process is complete. This process is expected to occur with an activation energy appropriate to bulk diffusion in the alloy matrix. Acceptable agreement is found between the experimentally determined activation energy for this homogenization, Q^H, and appropriate literature values.

The existence of these two processes occurring with very different activation energies, leads to the pseudo-equilibrium results that have been observed when a reasonable annealing time constraint of < 1 hour exists. The study of the segregation behaviour of Mo-rich alloys that has been presented, indicates the great care that is needed in the interpretation of segregation results when using a sputtered surface. An asymptotic approach to a non-varying surface composition does not necessarily indicate an equilibrium condition: The composition of the sub-surface may not be that of the bulk. In the alloys studied, the significant surface compositional changes that have been observed at temperatures $\leq$ 920 K are attributed mainly to RED.

CHAPTER EIGHT

EQUILIBRIUM SEGREGATION IN Cr-RICH Cr—Mo ALLOYS

In this chapter, the investigation of the segregation phenomenon in Cr-Mo alloys is extended to Cr-rich alloys. In the accessible temperature range attained, the experimental data establishes the equilibrium segregation behaviour of a Cr-rich alloy and provides a qualitative and a quantitative test of the Unified Segregation Model.

8.1 INTRODUCTION

The investigation of the segregation phenomenon in Mo-rich alloys, presented in Chapters 6 and 7, has led to a good understanding of equilibrium and non-equilibrium effects that are present when annealing a sputter-modified alloy and a successful test of the the monolayer calculation. This has been possible because the driving forces for segregation all reinforce each other predicting an essentially pure Cr monolayer at the surface. The investigation is now extended to Cr-rich alloys where a competition between the driving forces for segregation occurs. The experimental data establishes the equilibrium segregation behaviour for such an alloy and through the monolayer calculation, allows both a qualitative and a quantitative test of the USM.

8.2. THEORETICAL PREDICTION

The Unified Segregation Model (USM) predictions for Cr-rich alloys were calculated as in Chapter 6. The elastic strain energy contribution was calculated using elastic moduli of $K_{Mo} = 2.779 \cdot 10^6$ kg/cm^2 and $G_{Cr} = 1.19 \cdot 10^6$ kg/cm^2 obtained from Gschneidner [1964]. All other parameters are as defined in Section 6.4.1. For an 83.4 at.% Cr alloy, substitution of the appropriate data into eqs. (6.2) and (6.3) for the solute Mo, yields for the surface composition of a (110) surface:

$$(x_s^{Mo} / x_s^{Cr}) = (0.1990) \exp \{ [(-6539) + (8113\ x_s^{Mo} + 8) + (6357)] / RT \} \quad (8.1)$$

similarly, for the (100) or (111) orientations,

$$(x_s^{Mo} / x_s^{Cr}) = (0.1990) \exp \{ [(-6539) + (2710) + (6357)] / RT \} \quad (8.2)$$

Of the three contributions to ΔH_s^{Mo} considered, only the surface energy term, i.e., the first term, favours Cr segregation due to its lower surface energy. Both the enthalpy of mixing and elastic strain energy terms, i.e., the second and third terms, respectively, favour segregation of the solute Mo. The overall prediction of this model will depend on the absolute magnitudes of the three contributions which in turn depend on the model chosen to calculate the input parameters.

In some studies, hard sphere radii, rather than Seitz radii, are used to calculate the elastic strain energy contribution. For bcc metals these can be calculated according to the expression:

$$r = \sqrt{3}\, a_o / 4 \quad (8.3)$$

Using this approach reduces the elastic strain energy contribution in equations (8.1) and (8.2) from 6357 to 4465 kcal/mole. This procedure should ideally be used for alloy systems where experimental values of the surface energies are available since the empirical expression used to estimate surface energies (eq. 6.4) is based on the Seitz definition of atomic radius.

A second approach involving the enthalpy of mixing term is to consider both first and second nearest neighbours. Williams and Nason [1974] defined an effective number of nearest neighbours equal to the number of first plus half the number of second nearest neighbours. The changes in the enthalpy of mixing contribution, term 2 in eqs. (8.1) and (8.2), that result by taking this approach for the low index orientations are:

$$(100) \quad : \quad (2950\ x_S^{MO} + 1727)$$

$$(110) \quad : \quad (7375\ x_S^{MO} + 254)$$

$$(111) \quad : \quad (2709)$$

Regardless of which of the above procedures is chosen, the USM predicts a competition between the driving forces for segregation and hence experimental data should provide both a qualitative and a quantitative test of the model and of the methods available for calculating the input parameters.

8.3. EXPERIMENTAL RESULTS

In addition to the major non-metallic impurities observed to segregate in Mo-rich alloys, annealing of Cr-rich alloys leads to the strong segregation of nitrogen (Fig. 2.5). Through the 'cleaning' techniques described in Chapter 6, all impurities could be removed except for N. The surface becomes saturated with N, independent of annealing time, in the accessible temperature range. Numerous techniques have been tried to reduce the bulk N concentration such that a segregation study of the binary system was possible. These have included:

1. annealing in a low pressure of H_2, since it has been suggested in the literature, that for some Cr containing alloys, N, present as either a solid solution or as a nitride could be removed as NH_3 under appropriate experimental conditions [White et al. 1970, Kretschmeru and Koch 1977];
2. addition of cerium to the melt during preparation to 'fix' the trace N in the bulk and prevent it from segregating upon annealing; and,
3. hot-sputtering to remove the contaminant as it continually segregates.

Each method successfully reduced the level of N that segregated to the surface upon annealing, however, all were accompanied by a new series of problems. In some cases, the new problems that developed were more difficult to solve than the original. For example, the third method was found to be quite effective at reducing the nitrogen bulk concentration, however, this was accompanied by a severe Cr depletion of the surface region due to the co-segregation of Cr with N during processing.

A great accomplishment of this study has been in the solution of the N problem. The procedure adopted involved the sequential annealing of the sample to cause segregation of the contaminant followed by its sputter removal at room-temperature. The process was optimized by establishing the kinetics of the segregation at numerous temperatures and the sputter-removal rates so as to maximize the contaminant removal but minimizing the sample erosion. The upper limit of the temperature used was established by Cr evaporation becoming a problem after prolonged annealing at 1075 K (Section 7.2). The procedure needed to be automated because 530 sequential anneal-sputter cycles were required for 'cleaning' the 83.4 at.% Cr alloy. This was accomplished using the IBACON code described in Section 2.2.2. Perturbations to the sample composition were monitored at different stages of the cleaning operation with no changes detected to within the resolution of the X-ray and Auger techniques.

The Cr-rich alloy was sufficiently depleted of non-metallic impurities by this procedure so as to allow a segregation study of the binary system in the temperature range 1000-1054 K. The lower limit established by contamination being a problem due to a decrease in the impurities' solubility. Additionally, serious interpretation problems would be encountered with the non-equilibrium effects (Chapters 6 and 7) present at lower temperatures where kinetic limitations prevent the homogenization between the sputter-modified sub-surface and the bulk on the experimental time scale. For these reasons, the temperature range used establishes only the equilibrium segregation behaviour of this alloy. For all annealing data, once any contaminant level reached a measurable level above noise, no

further results were accepted for this part of the study

The results obtained from the Mo(186) and Cr(529) transitions are shown in Table 8.1 as the asymptotic normalized peak-peak heights consistent with 6 independent experiments in the experimental temperature range. Unlike the steady-state sputtered surface, the inhomogeneity over the analyzed depth in the annealed alloy is such that the digitally collected data cannot be adequately simulated over the full width of each of the three energy windows used for data collection (20-50, 100-240, 425-580 eV). This is attributable to the variation in sampling depth with electron energy. As described in the discussion, an appropriate analysis of the digitally collected data yields an insight into the inhomogeneity with depth as determined with varying sampling depth.

The results shown in Table 8.1, clearly indicate a surface enrichment in Cr over the analyzed depth, relative to the Cr-depleted sputter modified surface. However, this does not necessarily imply Cr segregation at equilibrium because two processes accompany high-temperature annealing: 1) Gibbsian segregation; and 2) homogenization of the sub-surface with the unperturbed bulk. The net effect of these two processes, expected to be in opposite direction, will yield an apparent Auger composition which can only be deconvoluted via the monolayer calculation. The composition of the outer monolayer determined using the monolayer calculation is shown in columns 4 and 6 of Table 8.1. The results indicate that the outer monolayer is enriched in the solute Mo relative to the bulk composition, i.e., a cross-over in the segregating element, relative to Mo-rich alloys, has occured.

Table 8.1: Normalized Auger data, monolayer calculations and enthalpy of segregation results for an 83.4 at.% Cr-Mo alloy.

1	2	3	4	5	6	7
Peak	Sputtered $100 \cdot x_s$	Annealed $100 \cdot \bar{x}_s$	Calculated Values from Experimental Results			
			Using Lit. λ_m'		Using Expt'l λ_m^e	
			x_1^{MO}	ΔH_s^{MO} (kcal/mole)	x_1^{MO}	ΔH_s^{MO} (kcal/mole)
Mo(186)	27.3 ± 0.1	19.5 ± 1.5	0.28 ± 0.08	-1.4 ± 0.9	0.29 ± 0.09	-1.5 ± 1.0
Cr(529)	74.7 ± 0.4	79.5 ± 1.5	0.40 ± 0.14	-2.5 ± 1.2	0.52 ± 0.22	-3.6 ± 1.8
Weighted Average			0.31	-1.8	0.33	-1.9

Annealed data collected over the temperature range 1000-1054 K (six experiments).

Table 8.2: Theoretical predictions of the Unified Segregation Model using Seitz radii for an 83.4 at.% Cr-Mo alloy at 1054 K.

1	2	3	4	5
Crystal Plane	Nearest Neighbours Only		1st & 2nd Nearest Neighbours	
	x_1^{MO}	ΔH_s^{MO} (kcal/mole)	x_1^{MO}	ΔH_s^{MO} (kcal/mole)
(100)	0.40	-2.5	0.43	-2.8
(110)	0.81	-6.4	0.73	-5.4
(111)	0.40	-2.5	0.40	-2.5
Average	0.54	-3.8	0.52	-3.6

8.4. DISCUSSION

The Unified Segregation Model, using either Seitz or hard-sphere radii, predicts that for a sufficiently Cr-rich alloy, Mo segregation will occur, i.e., a cross-over in the segregating element from that predicted and observed in Mo-rich alloys. The surface energy and elastic strain energy terms are of comparable magnitude but in opposite direction; the surface concentration dependent enthalpy of mixing term reinforces solute segregation. The effect of considering nearest neighbours only or both first and second nearest neighbours is minimal. However, using hard-sphere radii predicts very little Mo segregation above the bulk value.

The relevant theoretical predictions for 1054 K are summarized in Table 8.2 using Seitz radii only. A negligible temperature dependence is predicted over the experimental temperature range of 1000-1054 K. The variation in the average predicted x_1^{Mo} is less than 0.03. The errors in the theoretical values are those corresponding to the uncertainty in the bulk alloy composition; no attempt was made to estimate the errors in any of the parameters of eq. (6.3). For x_b^{Mo} = 0.166, an unweighted average of the three low-index planes yields a predicted x_1^{Mo} = 0.54 with a corresponding ΔH_S^{Mo} = -3.8 kcal/mole; slightly smaller values are obtained if one considers second nearest neighbours as well. Using hard-sphere radii, one obtains predicted values of x_1^{Mo} = 0.17 with an essentially zero enthalpy of segregation.

The major test of the USM lies in its ability to correctly predict the segregating component. The outer monolayer composition calculated from the experimental data, column 4 of Table 8.1, is qualitatively in agreement

with the theoretical prediction, i.e., Mo segregation. The agreement confirms that any complete treatment of equilibrium segregation must involve minimization of the total free energy of the system. This must include contributions from surface energies, alloy interactions and elastic strain energy.

A second test of the USM lies in a quantitative comparison between the extent of enrichment predicted at the surface and that determined from experimental data. The outer monolayer composition x_1^{Mo}, as determined using either the Mo(186) or Cr(529) data, agree to within experimental error. The theoretical predictions, as calculated by the two methods of estimating the atomic radii, straddle the experimentally determined weighted average values of $x_1^{Mo} = 0.31$ and $\Delta H_S^{Mo} = -1.8$ kcal/mole. However, as indicated earlier, the theoretical predictions calculated using Seitz radii are self-consistent with the method used in determining the surface energies and hence should be the more appropriate. In this case, the USM predictions overestimate the elastic strain energy contribution which reinforces segregation of the solute Mo. A small improvement is observed by using experimentally determined IMFP's (Section 6.5) in the monolayer calculation yielding weighted average values of $x_1^{Mo} = 0.33$ and $\Delta H_S^{Mo} = -1.9$ kcal/mole.

An appropriate analysis of the digitally collected data can provide a test of the calculated inhomogeneities with depth. The medium energy region of 100-240 eV consists almost entirely of Mo transitions. The entire region cannot be simulated as per eq. (5.3) with one set of pure element fractions, i.e., the variation in the IMFP over this energy window is sufficient to detect the existing inhomogeneity with depth. However,

excellent simulations can be obtained over a smaller energy region, i.e., a smaller variation in IMFP. Using a 30 eV window with a step of 10 eV, the composition as a function of the energy window's median energy is plotted in Fig. 8.1. The results indicate a small gradient in the expected direction, i.e., a decrease in $\bar{x}_S^{MO}$ with increasing energy or increasing sampling depth. The theoretical dotted line was calculated according to eq. (3.28a) using the experimentally determined monolayer composition from that element's transition (Table 8.1, column 6) and the experimentally determined IMFP's. The agreement is good and reflects a change in $\bar{x}_S^{MO}$ of $\sim$ 2 at.% with a variation in the IMFP (λ_m^e) of 3.0-6.0 monolayers over the energy region 100-240 eV, i.e., $\sim$ 100% variation in sampling depth. The corresponding contribution of the first layer varies from 36 to 20 percent of the total signal.

The total high energy region of 425-580 eV, consisting entirely of Cr transitions, can be simulated with only one set of pure elemental fractions. This suggests that the variation in sampling depth over this energy range is too small to detect the inhomogeneity present. Applying the procedure used for the medium energy region of using 30 eV windows yields a scatter, rather than a distinct gradient, as can be seen in Fig. 8.2. The theoretical dotted line calculated as above, is consistent with the results and predicts a change in $\bar{x}_S^{Cr}$ of $<$ 1 at.% with a variation in the IMFP of 9.7-12.4 monolayers over the energy region 430-580 eV, i.e., a variation in analyzed depth of $\sim$ 30%. The corresponding contribution of the first layer over this energy region varies from 13 to 10 percent of the total signal.

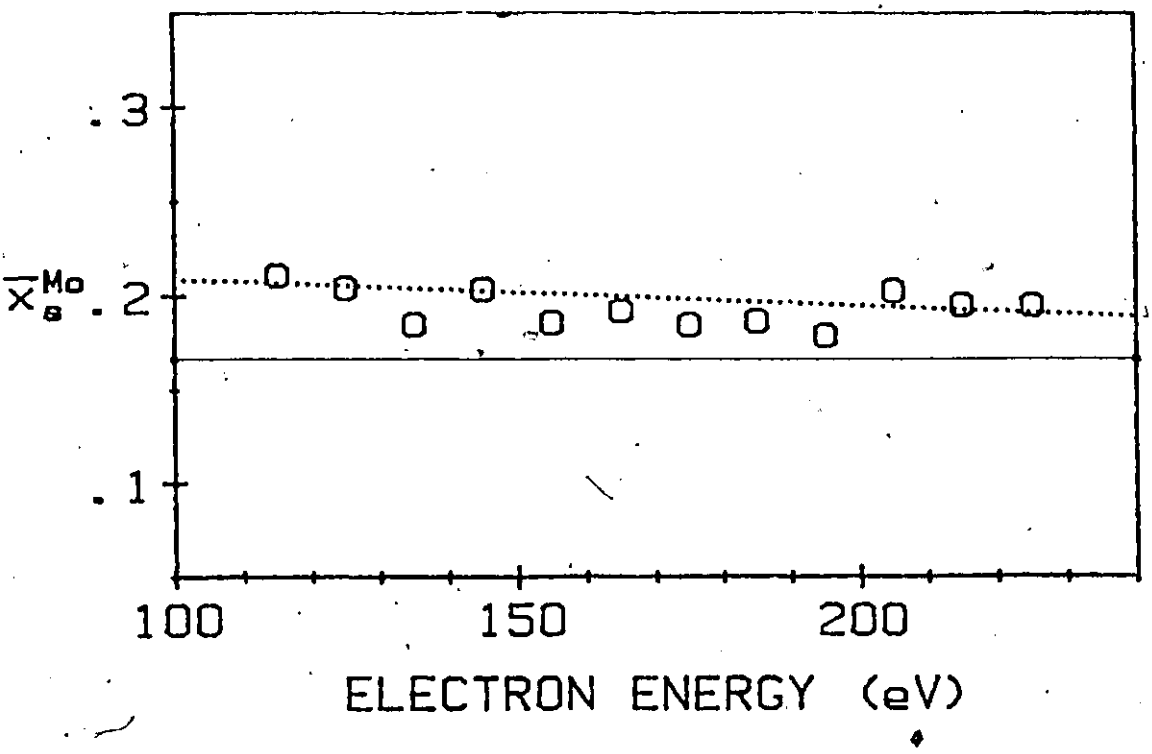

Figure 8.1: The appropriately weighted surface composition, $\overline{x}_s^{Mo}$, in the medium energy region (100-240 eV) determined by the simulation procedure as a function of the electron energy using a 30 eV window and plotting the median energy. The data reveal a concentration gradient within the energy range consistent with a surface enrichment of Mo. The bulk composition is indicated as a solid line. The theoretical dotted line was calculated according to eq. (3.28a) using the experimentally determined monolayer composition and IMFP's.

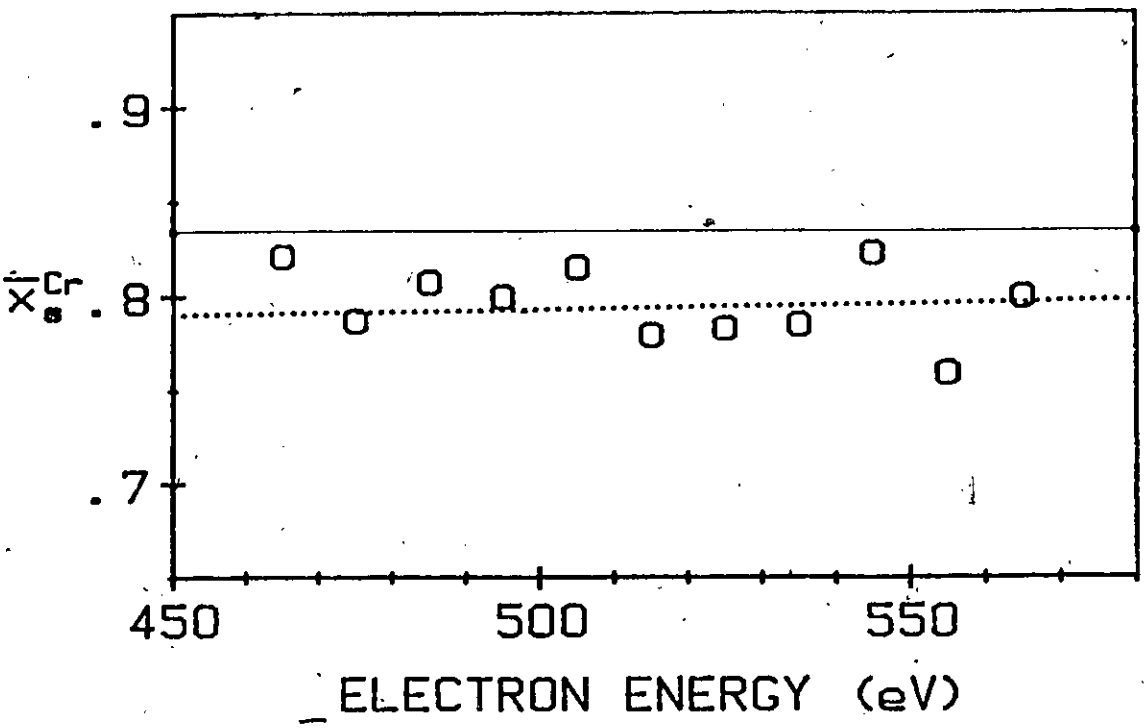

Figure 8.2: The appropriately weighted surface composition, $\bar{x}_s^{Cr}$, in the high energy region (425-580 eV) determined by the simulation procedure as a function of the electron energy using a 30 eV window and plotting the median energy. Unlike the medium energy region, the data reveal a scatter within this energy range due to a much smaller variation in the contribution from the first layer as a function of energy. These data are also consistent with a surface enrichment of Mo. The bulk composition is indicated as a solid line. The theoretical dotted line was calculated according to eq. (3.28a) using the experimentally determined monolayer composition and IMFP's.

The results presented in Figs. 8.1 and 8.2 indicate that the precision of the data corresponding to the Mo transitions (100-240 eV) is much better than that from the Cr transitions (425-580 eV). This is attributable to the elemental sensitivity of Mo being approximately 2.5 times that of Cr for the Auger electron energy analyzer used.

The low energy region of 20-50 eV should potentially provide the greatest test of the calculated inhomogeneities due to its extremely high surface sensitivity. However, a number of problems have been encountered with simulations of this energy region in the annealed alloy. It has been observed that annealing pure Cr or a Cr-Mo alloy such that a monolayer of nitrogen segregates to the surface leads to a second feature, or peak, at a slightly lower energy than the Cr(36) transition. A similar feature has been observed by introducing a monolayer of oxygen from the gas phase. The shifted Cr transition adds intensity to the Mo feature and can lead to large errors in simulations using only pure elemental spectra. This phenomenon is due to the Cr(36) transition involving two valence band electrons and is thus susceptible to matrix effects. These include peak shape and energy variations of the initial peak and possibly the existence of new features involving, for example, cross-transitions. This phenomenonen has been observed and well documented for the Ti-N system [Dawson and Tzatzov 1986]. A similar effect is expected from carbon and extendable to the Mo(28) transition.

In addition to the experimental evidence of the effect of high contaminant levels, evidence of the effect of low levels has also been obtained. In Section 5.3.4 the sputtered surface composition was followed

from a very 'clean' state under ion bombardment, with contaminants below detection level, to a state where the contamination level was barely detectable. It was observed that the effect of very low contaminant levels is negligible on Auger transitions > 100 eV. However, their effect on the highly surface sensitive low energy peaks is considerable in terms of both intensity and peak shape. Therefore, the level of surface 'cleanliness' that is required before the low energy transitions may be used for quantitative analysis is much more demanding and is very difficult to attain in annealing experiments. The experimental evidence suggests that the same high sensitivity of low energy transitions that makes them potentially very useful for quantitative AES, also leads to a large dependence on the chemical environment. This dependence translates into appreciable matrix effects which must be considered in any quantification procedure. Great care must be taken in using two pure element spectra to simulate an annealed alloy spectrum in this energy region.

8.5. SUMMARY

An 83.4 at.% Cr-Mo alloy has been sufficiently depleted of the nitrogen impurity through 530 sequential anneal-sputter cycles. The extent of sample 'cleanliness' attained has allowed an investigation of the equilibrium segregation behaviour of this alloy. The results indicate that relative to the sputtered surface, Cr enrichment is observed in the equilibrated alloy surface as determined by AES. However, upon applying the monolayer calculation, it is found that the outer surface monolayer is enriched in the solute Mo. This represents a cross-over in the segregating element from that observed with Mo-rich alloys, The results provide a qualitative and quantitative test of the USM and the procedures available for calculating the appropriate contributions of the driving force for segregation.

Qualitatively, the Unified Segregation Model, in minimizing the total free energy of the system, does correctly predict the segregating element. This has been achieved by considering contributions from surface energies, alloy interactions and elastic strain energy.

Quantitatively, the extent of surface enrichment in the solute Mo has been determined using the monolayer calculation. A corresponding enthalpy of segregation has also been calculated. In a quantitative comparison with the USM predictions, the procedures for calculating the alloy interaction and elastic strain energy contributions have been tested. The theoretical prediction, calculated as an average of the three low-index orientations, reveals a negligible difference in considering only first or first and second nearest neighbour interactions. For the elastic strain

energy contribution, using either Seitz or hard-sphere radii correctly predicts the segregating element. The theoretical prediction for surface enrichment using Seitz radii is greater than the experimentally determined enrichment, while that using hard-sphere radii is lower. That is, the theoretical predictions straddle the experimental result. However, use of Seitz radii is considered more appropriate in the USM for maximum self-consistency. In this case, the USM overestimates the elastic strain energy contribution which reinforces segregation of the solute Mo. This is consistent with Kumar's [1979] suggestion that the USM overcompensates for the elastic strain energy contribution as it is already partially included in the enthalpy of mixing term.

It was possible to exploit the variation in depth sensitiviy of Auger electrons with energy to probe the concentration profile in the segregated alloy. Surface impurity effects prevented use of the low energy region for this purpose, however, the medium (100-240 eV) and high (425-580 eV) energy regions of the spectrum could be used for quantitative analysis of annealed alloys. The results obtained from these data are consistent with the composition profiles calculated by the monolayer calculation.

CHAPTER NINE

SUMMARY AND CONCLUSIONS

Detailed observations and conclusions have been summarized in individual chapters. In this chapter, only the highlights of the thesis are summarized with suggestions for future work.

9.1. QUANTITATIVE AES

A major limitation to quantitative AES has been identified as due to differences in surface roughness between the alloy and elemental standards, or indeed temporal variations for a single sample. An experimental investigation was carried out to establish a correlation between sputtering, crystal-orientation and surface roughness. The resulting effect of the surface roughness that evolved on the detected Auger current was quantified. A pure polycrystalline Mo sample was prepared with two large grains of different crystallographic orientation, one high index (1,4,11) and the other low index (100). An appropriate polishing technique produced a uniform featureless surface which yielded a constant detected Auger current across both grains. On ion bombardment, the Auger current from the two grains changed and ultimately attained a steady-state yielding a difference of ~ 18% between the two grains. The origin of this effect was revealed by an SEM analysis of the final sputtered-state, which established a surface morphology quite different

from the initial state. It was concluded that, with increasing ion fluence, as the polishing damage was removed, a surface morphology evolved highly dependent on the crystallographic orientation. Relative to the polished surface, the low-index grain became smoother, whereas, the high-index grain developed considerable texture consisting mainly of 'hills and valleys' with a 'furrowed' fine structure in the direction of the ion beam. The differences in texture were attributed to differences in the sputter rates which depend on the crystallographic orientation and effects such as re-deposition, or re-capture, of a dislodged surface atom and the relative stability of the crystal faces. The changes in Auger current, consistent with literature results and Monte Carlo calculations, were attributed to an increase in the extent of shadowing of the emitted electrons with increasing surface roughness.

It was concluded that an analytical standard exhibiting differences in Auger current of ~ 18% with position on sample analyzed, or crystal orientation, is totally unacceptable for a quantitative study. Procedures have been recommended and adopted to minimize this effect: (1) an initial well polished sample with uniform morphology over the entire sample must be used; (2) total ion fluence must be maintained to a minimum; (3) the analyzed area must be such that the detected Auger current is averaged over numerous grains; and (4) since annealing the roughened Mo sample at temperatures up to half of the sample's melting point was ineffective in smoothing the sample, once a sample has been subjected to significant ion bombardment cleaning it must be repolished.

The quantification of AES results obtained from sample surfaces inhomogeneous in depth has been discussed. When, as for surface segregation it is reasonable to assume that the inhomogeneity is limited to the outer surface monolayer, it is possible to deconvolute x_{i1} from the apparent Auger composition appropriately weighted over the escape depth of the Auger electrons, $\bar{x}_{is}$.

A measure of the accuracy of the AES technique, given the procedures adopted for its quantification, can be obtained from the experimental results of sputtered and equilibrated alloy surfaces. In the analysis of the steady-state sputtered surface of 13 Cr-Mo alloys, the sample was essentially uniform over the analyzed volume. The surface composition, determined using the major Auger transition for each component, added to 100 at.% in all cases to within 5 at.%; in most cases the difference approached 2 at.%. This is consistent with calculations indicating negligible matrix effects in a sample surface homogeneous in depth. For an inhomogeneous surface, where the extent of enrichment at the equilibrated surface can be calculated with confidence as a pure monolayer, application of the monolayer calculation yielded an accuracy of $\sim$ 10-30 at.% in the composition of the outer monolayer.

9.2. ION BOMBARDMENT MODIFICATIONS OF ALLOY SURFACES

The steady-state sputtered composition of 13 homogeneous Cr-Mo alloys, irradiated at room temperature with 2 KeV Ar^+ ions, has been established. The results indicated a surface depletion of Cr relative to the bulk composition, across the entire composition range. A phenomenological model of preferential sputtering has been presented and the experimental data analysed accordingly. The results yielded a sputter rate ratio $K = (k_{Cr}/k_{Mo}) = 1.73 \pm 0.04$ insensitive to composition. This value was compared with a theoretical prediction according to Sigmund [1981] of the component sputter yield ratio, $1.66 \leq Y^o_{Cr}/Y^o_{Mo} \leq 1.73$ for the irradiating conditions, in good agreement with the empirical result. The empirically determined value of K, being insensitive to composition, was also identified with the sputter yield ratio of the pure elements calculated from a semi-empirical expression [Matsunami et al. 1983] of $Y^o_{Cr}/Y^o_{Mo} = 2.22 \pm 0.74$, also in reasonable agreement.

The homogeneity of the 'altered layer' has been investigated by exploiting the variation in depth sensitivity of Auger electrons with energy. No systematic ordering was observed between the surface composition determined by either the Mo(186) or Cr(529) transitions. This led to the conclusion that the surfaces were homogeneous over the escape depth of the Auger electrons used in the analysis. Additionally, a comprehensive study of an 83.4 at.% Cr alloy using digitally collected data over the energy range 20-600 eV, probed a greater variation in sampled depth. The analysis indicated that the surface was homogeneous over the

analyzed depth, although average values of a large data set suggested that a small inhomogeneity may exist with a compositional gradient in the expected direction. The inhomogeneity was quantified using layer calculations and adopting appropriate models for the composition profile. The inhomogeneity in depth was small relative to the gross compositional perturbation of the surface due to preferential sputtering.

The dependence of the steady-state sputtered composition on the ion flux was investigated. No change in composition was detected under a 20 or 50 fold reduction in ion flux. The results indicated that any process dependent on the mobile defect flux towards the surface, such as radiation-induced segregation, does not play the dominant role in establishing the surface composition. It was further observed that after termination of ion bombardment, no 'relaxation' of the sputtered surface occurred. This result, consistent with radiation damage recovery literature, indicates that once the defect production ceases, i.e., zero ion flux, the surface region is essentially quenched since the remaining defects consisting of vacancies, vacancy-type clusters and interstial-type clusters are immobile. The contribution of Gibbsian segregation and radiation-enhanced diffusion (RED) is considered negligible at the irradiating temperature, again due to the immobility of the vacancy-type defect. Indeed, Gibbsian segregation predicts, and experimentally established, a cross-over in the segregating element from one end of the composition range to the other and yet, ion bombardment was observed to deplete the surface of Cr across the entire composition range.

A unified picture of the sputtering process has evolved for the refractory alloys used in this study, recognizing the different processes that are activated under a given set of experimental conditions. The experimental results obtained are consistent with the athermal 'ballistic' processes playing the dominant role in establishing the steady-state surface composition: The value is determined by preferential sputtering and the bulk composition. Collisional mixing, consisting of displacement mixing and recoil implantation, maintains an essentially uniform composition over the 'altered layer' depth. The detailed picture that evolved was essential in the interpretation of segregation results obtained after ion bombardment was terminated and the sample was annealed at temperatures where non-equilibrium effects play a significant role in establishing the alloy surface composition.

9.3. SURFACE SEGREGATION IN Cr-Mo ALLOYS

9.3.1. Surface Segregation in Mo-Rich Cr-Mo Alloys

A theoretical analysis of the segregation phenomenon was performed by adopting the Unified Segregation Model (USM). Calculations for the Cr-Mo system revealed that for the Mo-rich alloys studied, the driving forces for segregation all reinforce each other predicting with confidence, an essentially pure Cr monolayer at the surface in the experimental temperature range.

Three Mo-rich alloys of bulk composition, 59.8, 87.5 and 89.8 at.% Mo have been sufficiently depleted of non-metallic impurities allowing a segregation study of the binary system in the temperature range 875-1075 K. Annealing of a sputter-modified surface led to Cr enrichment of the surface for all three alloys. While the rate of segregation was observed to increase with increasing temperature, the extent of enrichment was surprisingly higher at the higher temperatures, inconsistent with thermodynamic predictions. For this reason, a non-equilibrium interpretation was adopted. Upon annealing a sputter-modified surface, three processes occur: (1) surface segregation to lower the total free energy of the system; (2) annihilation of radiation-induced excess defects (vacancy and interstitial type); and (3) homogenization of the sputter-modified surface region with the unperturbed bulk. It was proposed that at lower temperatures, only (1) and (2) can occur, i.e., homogenization between the sub-surface and the bulk (3) cannot occur on the experimental time scale of < 1 hour. An order of magnitude calculation to estimate the time required for the homogenization, using literature diffusion parameters and 'altered layer'

depth, confirmed this picture. The model was further tested by using the monolayer calculation to deconvolute the outer monolayer composition from that averaged over the finite escape depth of the Auger electrons. The results indicated that if the appropriate sub-surface composition was used, the calculated monolayer composition agreed with theoretical predictions. A question arose as to the actual composition of the sub-surface at different annealing temperatures. At sufficiently high temperatures, homogenization between the bulk and sub-surface occurs very rapidly and the sub-surface is of bulk composition. However, at lower temperatures, the homogenization is too slow and only the sputter-modified sub-surface with a radiation-induced enhanced defect concentration can attain 'local equilibrium' due to RED. If the alloy is sufficiently rich in the segregating component, then the sub-surface can be adequately represented as having the sputtered composition. However, if the alloy is too dilute in the segregating component, then the sputtered composition is no longer appropriate: A severe depletion of the segregating component occurs over the mobile depth so as to satisfy the driving force for segregation. This process has been modelled using a conservation of mass argument to estimate the mobile depth that can attain 'local equilibrium' to be $\sim$ 3.3 nm. This result is in good agreement with experimental literature estimates of the 'altered layer' depth ranging from 1-10 nm and effective ion penetration and damage range predictions of 4.3 and 3.5 nm for a Mo target, calculated from LSS and WSS theories, respectively.

The annealing time constraint of $<$ 1 hour, was overcome through an extensive 'cleaning' treatment of an 89.8 at.% Mo alloy. The segregation

results obtained, clearly indicated that the asymptotic approach to a non varying surface composition observed at lower temperatures does not reflect an equilibrium condition. The high temperature, or equilibrium, surface composition could be attained by annealing sufficiently long at the lower temperatures, for example, 5 hours at 950 K.

A kinetic analysis of the segregation has been performed using the data obtained from the 89.8 at.% Mo alloy yielding an insight into the activated processes that occur upon annealing a sputter-modified binary alloy. Two processes have been identified as occuring with very different activation energies. At temperatures where the radiation-induced excess defect concentration is appreciable, RED plays a significant role. This leads to the sputter-modified sub-surface attaining 'local equilibrium' with a measured activation energy for atom transport of Q^L = 20 kcal/mole. In addition to the rapid segregation process there is a slow homogenization of the bulk and sub-surface. This process is expected to occur with an activation energy appropriate to bulk diffusion in the alloy matrix. The experimentally determined activation energy Q^H = 53 ± 5 kcal/mole is in good agreement with literature activation energies for interdiffusion of 54.0 and 58.0 kcal/mole for ^{51}Cr in Mo and ^{99}Mo in Cr, respectively [Borisov 1968].

It has been concluded that the existence of these two processes occuring with very different activation energies, leads to the pseudo-equilibrium results that have been observed when a reasonable annealing time constraint of < 1 hour exists. The study of the segregation behaviour of Mo-rich alloys presented, indicates the great care that is needed in

the interpretation of segregation results when using a sputtered surface. An asymptotic approach to a non-varying surface composition does not necessarily indicate an equilibrium condition: The composition and defect distribution of the sub-surface may not be that of the bulk. This is a problem in any low temperature studies, particularly when studying alloys containing volatile metals, such as Cr, thereby limiting the temperature range over which experiments may be performed.

9.3.2. Experimental Determination of IMFP Values

The segregation study of Mo-rich alloys has provided a test of the accuracy of the monolayer calculation since the equilibrated surface can be calculated with confidence to consist of a pure Cr monolayer. A major limitation to the ultimate accuracy attained has been identified as due to the uncertainty in the literature IMFP values used. The results of this study, indicate that acceptable agreement is found with theoretical predictions when using Seah and Dench [1979] values of the IMFP but that the dependence of the IMFP on energy is stronger than the $E^{1/2}$ value assumed in their statistical analysis of experimental measurements. Experimental estimates of the IMFP have been determined in this study which would make the experimental results identical with the theoretical prediction. For the Mo(186) and Cr(529), the calculated IMFP values in monolayers are 4.9 ± 0.3 and $11.5^{+1.8}_{-1.4}$, respectively. These data indicate that the Seah and Dench [1979] values are too low, i.e., too surface sensitive. The energy dependence of the IMFP suggested by the experimental IMFP's was calculated to be E^n, n= 0.82 ± 0.15, consistent with more recent literature suggesting that an $E^{3/4}$ dependence is more appropriate.

7.3.3 Surface Segregation in Cr-Rich Cr-Mo Alloys

The study of the surface segregation phenomenon has been extended to Cr-rich alloys where the driving forces for segregation act in opposite direction. The experimental data have provided a qualitative and quantitative test of the USM. An 83.4 at.% Cr-Mo alloy has been sufficiently depleted of the nitrogen impurity through 530 sequential anneal-sputter cycles. The extent of sample 'cleanliness' attained has allowed an investigation of the equilibrium segregation behaviour in the temperature range 1000-1054 K. The results indicated that relative to the sputtered surface, Cr enrichment is observed in the equilibrated alloy surface as determined by AES. However, the contributions from Gibbsian segregation and homogenization of the sub-surface with the unperturbed bulk, had to be deconvoluted via the monolayer calculation.

Applying the monolayer calculation, the weighted average monolayer composition was determined as $x_1^{Mo} \simeq 0.31$ with a corresponding enthalpy of segregation of $\Delta H_s^{Mo} = -1.8$ kcal/mole. Relative to the bulk composition $x_b^{Mo} = 0.166$, this represents a cross-over in the segregating element from that observed in Mo-rich alloys.

A major test of the USM has been possible in a qualitative comparison with the experimental results. The USM, in minimizing the total free energy of the system, correctly predicts the observed cross-over in the segregating element.

In a quantitative comparison, the procedures for calculating the alloy interaction and elastic strain energy contribution have been tested. The theoretical prediction, calculated as an average of the three low-index

orientations, revealed a negligible difference in considering only first or first and second nearest neighbour interactions. For the elastic strain energy contribution, using either Seitz or hard-sphere radii to estimate the atomic radii, correctly predicts the segregating element. The theoretical prediction for surface enrichment using Seitz radii, $x_1^{Mo} = 0.54$, is greater than the experimentally determined enrichment, while that using hard-sphere radii, $x_1^{Mo} = 0.17$, is lower: That is, the theoretical predictions straddle the experimental result of $x_1^{Mo} = 0.31$. The corresponding enthalpies of segregation show the same behaviour. However, use of Seitz radii is considered more appropriate in the USM for maximum self-consistency. In this case, the USM overestimates the elastic strain energy contribution which reinforces segregation of the solute Mo. This is consistent with Kumar's [1979] suggestion that the USM overcompensates for the elastic strain energy contribution as it is already partially included in the enthalpy of mixing term.

Finally, it has been possible to exploit the variation in depth sensitivity of Auger electrons with energy to probe the concentration profile in the segregated alloy. The results obtained are consistent with the composition profiles calculated by the monolayer calculation.

9.4. SUGGESTIONS FOR FUTURE WORK

9.4.1 The Effect of Surface Roughness on Quantitative AES

A major aspect of surface roughness that requires further investigation is in establishing the importance of the ion bombardment geometry on the morphology that develops. This can be accomplished through the variation of the ion incidence angle and extending the study to other crystal orientations.

A second aspect involves developing experimental procedures for minimizing the differences in morphology that develop. These could include: (1) the use of two ion sources or rotation of the sample while irradiating to minimize geometry effects; and (2) the introduction of O_2 in the sputter gas so that one is continually sputtering the oxidized surface, thereby minimizing crystal orientation effects.

Finally, the effect of surface roughness on Auger spectra acquired in the N(E) mode should be investigated. Since surface roughness is expected to affect the entire secondary electron distribution, quantification through the procedure of peak to background ratio [Langeron et al. 1984] should be less sensitive to morphological variations of the surface. However, any increase in accuracy will be offset by a decrease in the precision of the measurement.

9.4.2. Compositional Modifications of Alloy Surfaces

The results of this study have established a good understanding of compositional modifications of Cr-Mo alloy surfaces under various ion bombardment and annealing conditions. Composition profiles have been

determined by exploiting the variation in sampling depth with Auger electron energy and through layer calculations. The outer monolayer composition corresponding to these profiles should be confirmed by other, more surface sensitive techniques. This can be accomplished by using Ion Scattering Spectroscopy (ISS), Secondary Ion Mass Spectrometry (SIMS) or Secondary Neutral Mass Spectrometry (SNMS).

The interpretation of the steady-state sputtered surface composition via the phenomenological preferential sputtering model could be extended to other refractory alloy systems and to lower melting point alloys where activated processes may no longer be negligible, thereby, giving rise to greater inhomogeneities with depth.

The simulation procedure used with digitally collected data was shown to successfully exploit the variation in sampled depth with Auger electron energy. To-date this has been limited to sputtered surfaces and one equilibrated Cr-rich alloy where the inhomogeneity in depth was relatively small, yet detectable. The procedure should be extended to alloy surfaces where the inhomogeneity is much greater, i.e., equilibrated Mo-rich alloys where an essentially pure Cr monolayer surface has been calculated with confidence.

The study of the segregation phenomenon should be extended to more dilute Cr-Mo alloys which could not be done in this study due to the limited elemental sensitivity of the analyzer used. In the case of very Mo-rich alloys, one could address the question of whether or not the elastic strain energy contribution should be included with an undersized solute (Cr). However, it is the Cr-rich alloys that provide a competition for the

driving forces considered for segregation, and hence a quantitative test of the theoretical model. It appears imperative that alloys on either side of the cross-over composition should be studied. However, given the time required to attain a 'clean alloy' requiring a minimum of 250-300 machine hours, this is an unrealistic expectation. Although the starting impurity levels are low (ppm levels), the effort should be directed towards preparing purer samples rather that improving the procedure for removing existing impurities. Additionally, the temperature range where equilibrium segregation can be studied in such alloys is limited to approximately 50 K, i.e., 1000-1050 K. This temperature range is too narrow to study the temperature dependence of segregation, given the magnitudes of the segregation driving forces in this system. With the present understanding of the Cr-Mo system, it is strongly suggested that the competing effect of the driving forces for segregation should be studied in a different alloy system. Such a system should be chosen so as to allow a large accessible temperature range and preferably have less impurity interference problems, e.g., Ta-Mo and Nb-Mo alloys.

With the present knowledge of segregation in polycrystalline Cr-Mo alloys, the investigation should be extended to the orientation dependence of segregation as a further test of the USM. This would require better spatial resolution of the primary electron beam than that available for this study.

This investigation has provided a test of the USM where both considerable differences in atomic interaction energy and size exists. A model system where a difference in interaction energy dominates, i.e., Mo-

W, has already been studied [Dawson and Petrone 1981, Dawson and Burke 1983]. For a comprehensive test of the USM, alloy model systems where the atomic size difference dominates and where the driving forces considered are negligible, should also be investigated.

Finally, in commercial applications of alloys bulk trace impurities exist, or may be introduced with time, and may play important roles in establishing the surface composition. From this study, a qualitative understanding of the effects of C and N has evolved. With the present understanding of the binary system, and since pure ternary Mo-rich Cr-Mo-C and Cr-rich Cr-Mo-N can be prepared with relative ease, the quantification of surface segregation in the ternary systems should now be possible.

7.5 CONCLUDING REMARKS

The work that has been presented establishes a basic framework for a study of binary alloy surfaces. An understanding of surface compositional modifications of binary alloys has evolved through a comprehensive study of the effect of varying the irradiating conditions and sample composition. It has been shown that numerous processes exist which can potentially contribute to the compositional modification of the surface.

The results have shown that AES can provide sufficient surface sensitivity and accuracy for the investigation and documentation of surface compositional modifications. Through careful, and often tedious procedures, the limitations of the technique can be overcome.

Ion bombardment compositional modifications of refractory alloys at room temperature have been interpreted in terms of the phenomenological preferential sputtering model presented, radiation damage recovery literature and theoretical ion and damage range distribution calculations.

Compositional modifications at elevated temperatures, where equilibrium conditions prevail, have been successfully interpreted in terms of the Unified Segregation Model. The results of this study confirm the accuracy of the qualitative predictions of the model and indicate acceptable agreement with quantitative predictions at both ends of the composition range. There is evidence that the procedure used for estimating the elastic strain energy contribution should be re-evaluated. Interpretation of segregation results at elevated temperatures, but under non-equilibrium conditions, must consider the state of the sub-surface and contributions from all activated processes since most defects may be mobile. The

experimental results confirm that any complete treatment of equilibrium surface segregation must consider contributions from surface energies, alloy interactions and elastic strain energy, i.e., minimization of the total free energy of the system must be considered.

In conclusion, the study of the Cr-Mo alloy system, has led to significant contributions in determining and predicting the relationship between surface composition and the externally controllable parameters of irradiating conditions and sample composition. It is through such studies that procedures for obtaining accurate experimental measurements are developed, thereby allowing a test of theoretical models. The ultimate goal being the control of materials performance in applications which depend on surface properties.

APPENDIX

APPENDIX 1: ESTIMATION OF THE 'MOBILE DEPTH' FROM A CONSERVATION OF MASS ANALYSIS (SECTION 6.4)

Consider a sub-surface region of a Mo-rich Cr-Mo alloy, d layers in thickness homogeneously modified by ion-bombardment (Fig. 5.12). Assume that the total number of atoms per layer is constant, then one can write:

$$\sum_{i=1}^{m} n_{i(S)}^{Cr} = \sum_{i=1}^{m} n_{i(A)}^{Cr} \qquad (A1)$$

where m is the effective number of mobile layers such that $d \geq m$; $n_{i(S)}^{Cr}$ and $n_{i(A)}^{Cr}$ are the number of Cr atoms in layer i of the homogeneouly ion-mixed sputtered surface (S) and in the low-temperature annealed surface (A) where the conditions are such that m layers attain 'local equilibrium', respectively; $n_{i(S)}^{T}$ and $n_{i(A)}^{T}$ are the corresponding total number of atoms in layer i assumed to be equal. From (A1),

$$\sum_{i=1}^{m} (n_{i(S)}^{Cr} / n_{i(S)}^{T}) = \sum_{i=1}^{m} (n_{i(A)}^{Cr} / n_{i(A)}^{T})$$

using the definition of mole fraction (eq. 3.6) yields:

$$\sum_{i=1}^{m} x_{i(S)}^{Cr} = \sum_{i=1}^{m} x_{i(A)}^{Cr}$$

separating the first layer in the annealed alloy yields,

$$\sum_{i=1}^{m} x_{i(S)}^{Cr} = x_{i(A)}^{Cr} + \sum_{i=2}^{m} x_{i(A)}^{Cr}$$

Using the homogeneous approximation for the sputtered surface, i.e., $x^{Cr}_{i(S)} = x^{Cr}_{(S)}$ for $i \leq m$, and assuming a composition profile for the annealed surface that has attained 'local equilibrium' to consist of a pure Cr monolayer, i.e., $x^{Cr}_{1(A)} = 1$ and for the underlying layers ($2 \leq i \leq m$), $x^{Cr}_{i(A)} = x^{Cr}_{(A)}$, one obtains,

$$m\, x^{Cr}_{(S)} = 1 + (m-1)\, x^{Cr}_{(A)}$$

isolating for $x^{Cr}_{(A)}$ yields,

$$x^{Cr}_{(A)} = (m\, x^{Cr}_{(S)} - 1) / (m-1) \qquad \text{for } 2 \leq i \leq m$$

which is eq. (6.9a) in Section 6.4.

REFERENCES

Abraham, F.F., Brundle, C.R. (1981),J. Vac. Sci. Technol. 18(2), 506.

Abraham, F.F., Tsai, N.H., and Pound, G.M. (1976), Surf. Sci. 37, 1433.

Abraham, F.F., Tsai, N.H., and Pound, G.M. (1978), Surf. Sci. 77, 465.

Abraham, F.F., Tsai, N.H., and Pound, G.M. (1979a), Scripta Metal. 13, 307.

Abraham, F.F., Tsai, N.H., and Pound, G.M. (1979b), Surf. Sci. 83, 406.

Agarwala, R.P. (1984), in: "Diffusion in Solids", eds. A.L. Laskar, G.P. Tiwari, E.C. SubbaRao and R. Krishnan (Trans Tech Publications, Aedermannsdorf) pp. 15-27.

Andersen, H.H. (1982), in: "Ion Implantation and Beam Processing", eds. J.S. Williams and J.M. Poate (Academic Press, London).

Andersen, H.H. and Bay, H.L. (1981), in: "Sputtering by Particle Bombardment I", Topics Appl. Phys., Vol. 47, ed. R. Behrisch (Springer-Verlag, Berlin, Heidelberg, New York) pp. 145-218.

Andersen, N., Eggleton, P.P. and Keesing, R.G.W. (1967), Rev. Sci. Instrum. 38, 924.

Andersen, N. and Sigmund, P. (1974), K. Dan. Vidensk. Selsk. Mat. Fys. Medd. 39, no. 3.

Askill, J. (1965), in: "Diffusion in Body-Centered Cubic Metals" (ASM, Metals Park) pp. 247-259.

Askill, J. (1970), "Tracer Diffusion Data for Metals, Alloys, and Simple Oxides" (Plenum, New York).

ASM (1965), "Diffusion in Body-Centered Cubic Metals" (ASM, Metals Park).

ASM (1985), "ASM Metals Handbook", 9th ed. (ASM, Metals Park).

Auciello, O. (1981), J. Vac. Sci. Technol. 19, 841

Auciello, O. (1982), Radiat. Eff. 60, 1.

Baird, R.J., Fadley, C.S., Kawamoto, S.K., Mehta, M., Alvarez, R. and Silva, J.A. (1976), Anal. Chem. 48, 843.

Balseiro, C.A. and Moran-Lopez, J.L. (1980), Phys. Rev. B. 21, 349.

Balluffi, R.W. (1978), J. Nucl. Mater. 69&70, 240.

Barrett, C.S. (1966), "The Structure of Metals: Crystallographic Methods, Priciples and Data", 3rd ed. (McGraw-Hill, New-York).

Bearden, J.A. and Burr, A.F. (1967), Rev. Mod. Phys. 39, 125.

Behrisch, R. (1983), in: "Sputtering by Particle Bombardment II", Topics Appl. Phys., Vol. 52, ed. R. Behrisch (Springer-Verlag, Berlin, Heidelberg, New York) pp. 1-10.

Bentley, J., Eyre, B.L. and Loretto, M.H. (1975), in: "Fundamental Aspects of Radiation Damage in Metals", eds. M.T. Robinson and F.W. Young (ERDA Conf. 751006, Washington) p. 925.

Betz, G. (1980), Surf. Sci. 92,283.

Betz, G. and Wehner, G.K. (1983), in: "Sputtering by Particle Bombardment II", Topics Appl. Phys., Vol. 52, ed. R. Behrisch (Springer-Verlag, Berlin, Heidelberg, New York) pp. 11-90.

Biget, M., Vajda, P., Maury, P., Lucasson, A. and Lucasson, P. (1975), in: "Fundamental Aspects of Radiation Damage in Metals", eds. M.T. Robinson and F.W. Young (ERDA Conf. 751006, Washington) p. 66.

Blakely, J.M. and Eizenberg, M. (1981), in: "The Chemical Physics of Solid Surfaces and Heterogeneous Catalysis, Volume 1: Clean Solid Surfaces", eds. D.A. King and D.P. Woodruff (Elsevier, Amsterdam) pp. 1-80.

Borisov, E.V., Grunzin, P.L. and Zemskii, S.V. (1968), Zashch. Pokryt. Metal. 2, 104.

Brunauer, S., Emmett, P.H. and Teller, E. (1938), J. Am. Chem. Soc. 60, 309.

Buck, T.M. (1982), in: "Chemistry and Physics of Solid Surfaces IV", eds. R. Vanselow and R. Howe (Springer-Verlag Berlin) pp. 435-464.

Burton, J.J. and Machlin, E.S. (1976), Phys. Rev. Letts. 37, 1433.

Carter, G., Navinsek, B. and Whitton, J. (1983), in: "Sputtering by Particle Bombardment II", Topics Appl. Phys., Vol. 52, ed. R. Behrisch (Springer, Berlin, Heidelberg, New York) pp. 231-269.

Chang, C.C. (1974), in: "Characterization of Solid Surfaces", eds. P.F. Kane and G.B. Larrabee (Plenumn, New York) pp. 509-575.

Chu, W.K., Howard, J.K. and Lever, R.F. (1976), J. Appl. Phys. 47, 4500.

Coburn, J.W. (1976), J. Vac. Sci. Technol. 13, 1037.

Coburn, J.W. (1979), Thin Solid Films 64, 371.

Crank, J. (1956), "The Mathematics of Diffusion" (Clarendon Press, Oxford).

Cullity, B.D. (1956), "Elements of X-ray Diffraction" (Addison-Wesley, Reading).

Damask, A.C. and Dienes, G.J. (1963), "Point Defects in Metals" (Gordon and Breach, London) p. 145.

Davies, J.A. (private communication).

Davis, L.E., MacDonald, N.C., Palmberg, P.W., Riach, G.E. and Weber, R.E. (1976), "Handbook of Auger Electron Spectroscopy" (Physical Electronics Industries Inc., Minneapolis, Minnesota).

Dawson, P.T. and Burke, N.A. (1983), J. Electron Spectrosc. Relat. Phenom. 31, 355.

Dawson, P.T. and Hu, M.P. (1985), Surf. Sci. 163, 198.

Dawson, P.T. and Petrone, S.A. (1981), J. Vac. Sci. Technol. 18, 529.

Dawson, P.T. and Petrone, S.A. (1985), Surf. Sci. 152/153, 925.

Dawson, P.T. and Petrone, S.A. (in preparation).

Dawson, P.T. and Tzatzov, K.K. (1985), Surf. Sci. 149, 105.

Dawson, P.T. and Tzatzov, K.K. (1986), Surf. Sci. 171, 239.

De Bernardez, L.S., Ferron, J., Goldberg, E.C. and Buitrago, R.H. (1984), Surf. Sci. 139, 541.

Defay, R., Prigogine, I., Bellemans, A. and Everett, D.H. (1966), "Surface Tension and Adsorption" (Wiley, New York).

Dieter, G.E. (1976), "Mechanical Metallurgy", 2nd ed. (McGraw-Hill, New York), pp. 105-110.

Donnelly, R.G. and King, T.S. (1978), Surf. Sci. 74, 89.

Dumke, M.F., Tombrello, T.A., Weller, R.A., Housley, R.M. and Cirlin, E.H. (1983), Surf. Sci. 124, 407.

Elliott, R.P. (1965), "Constitution of Binary Alloys, First Supplement" (McGraw-Hill, New-York).

Eldrup, M., Mogerson, O.E. and Evans, J.H. (1975), in: "Fundamental Aspects of Radiation Damage in Metals", eds. M.T. Robinson and F.W. Young (ERDA Conf. 751006, Washington) p. 1127.

Ertl, G. and Kuppers, J. (1974), "Low Energy Electrons and Surface Chemistry", Monographs in Modern Chemistry, ed. H.F. Ebel (Verlag Chemie, Weinheim) pp. 1-51.

Evans, J.H. (1975), in: "The Physics of Irradiation Produced Voids", ed. R.S. Nelson (AERE-R7934, Harwell UK) pp. 95-100.

Evans, J.H. and Eldrup, M.E. (1975), Nature 254, 685.

Eyre, B.L. (1972), in: "Defects in Refractory Metals", ed. R. deBatist, J. Nihoul and L. Stals (SCK/CEN, Mol) p. 311.

Eyre, B.L. (1973), J. Phys. F: Metal Phys. 3, 422.

Eyre, B.L. and English, C.A. (1974), in: "The Physics of Irradiation Produced Voids", ed. R.S. Nelson (AERE-R7934, Harwell UK) pp. 239-256.

Fadley, C.S., Baird, R.J., Siekhaus, W., Novakov, T. and Bergstrom, S.A. (1974), J. Electron Spectrosc. Relat. Phenom. 4, 93.

Fadley, C.S. (1974), J. Electron Spectrosc. Relat. Phenom. 5, 725.

Fadley, C.S. (1976), Progress in Solid State Chemistry 11, 265.

Farnsworth, H.E., Haque, C.A., Zehner, D.M. and Barton, G. (1969), Surf. Sci. 17, 1.

Fedorov, G.B. and Smirnov, E.A. (1984), "Diffusion in Reactor Materials" (Oxonian Press Pvt. Ltd., New Delhi).

Ferron, J., De Bernardez, L.S. and Buitrago, R.H. (1984), Surf. Sci. 145, L501.

Fine, J., Andreadis, T.D. and Davarya, F. (1983), Nucl. Instr. Meth. 209/210, 521.

Friedel, J. (1954), Advan. Phys. 3, 446.

Gallon, T.E. (1969), Surf. Sci. 17, 486.

Gelatt, C.D. and Ehrenreich, H (1974), Phys. Rev. B 10, 398.

Gibbons, J.F., Johnson, W.S. and Mylroie, S.W. (1975), "Projected Range Statistics, Semiconductors and Related Materials", 2nd ed. (Dowden, Hutchinson and Ross, Stroudsberg).

Gibbs, J.W. (collected works 1961), "The Scientific Papers of J. Willard Gibbs, Vol 1" (Dover, New York).

Gold, R.E. and Harrod, D.L. (1979), J. Nucl. Mater. 85&86, 805.

Goldstein, J.E., Newbury, D.E., Echlin, P., Joy, D.C., Fiori, C. and Lifshin, E. (1981), "Scanning Electron Microscopy and X-ray Microanalysis" (Plenum Press, New York).

Gschneidner, K.A. (1964), Solid State Phys. 16, 276.

Guggenheim, E.A. (1945), Trans. Farad. Soc. 41, 150.

Gvosdover, R.S., Efremenkova, V.M., Shelyakin, L.B. and Yurasova, V.E. (1976), Radiat. Eff. 27, 237.

Hall, P.M. and Morabito, J.M. (1977), Surf. Sci. 67, 373.

Hall, P.M. and Morabito, J.M. (1978), CRC Critical Rev. Solid State Sci. Mater. Sci. 8, 53.

Hall, P.M. and Morabito, J.M. (1979), Surf. Sci. 83, 391.

Hall, P.M., Morabito, J.M. and Conley, D.K. (1977), Surf. Sci. 62, 1.

Hansen, M. (1958), "Constitution of Binary Alloys" (McGraw-Hill, New York).

Harris, L.A. (1969), J. Appl. Phys. 39, 1419.

Hauffe, W. (1971), Phys. Status. Solidi A 4, 111.

Hennesen, H., Keller, H. and Viefhaus, H. (1984), Scripta Met. 18, 1319.

Hermanne, N. (1973), Radiat. Eff. 19, 161.

Hertel, B., Diehl, J. and Gotthardt, R. and Sultze, H. (1974), in: "Application of Ion Beams to Metals", eds. S.T. Picraux, E.P. EerNisse and F.L. Vook (Plenum Publ. Corp., New York) pp. 507-520.

Holloway, P.H. (1975), J. Electron Spectrosc. Relat. Phenom. 7, 215.

Holloway, P.H. (1977), Surf. Sci. 66, 479.

Holloway, P.H. (1978), Scan. Electron Microsc. 1, 361.

Hondros, E.D. (1965), Proc. Roy. Soc. A 286, 479.

Hultgren, R., Desai, P.D., Hawkins, D.T., Gleiser, M., Kelley, K.K. and Wagman, D.D. (1973a), "Selected Values of Thermodynamic Properties of the Elements (ASM, Cleveland).

Hultgren, R., Desai, P.D., Hawkins, D.T., Gleiser, M. and Kelley, K.K. (1973b), "Selected Values of Thermodynamic Properties of Binary Alloys (ASM, Cleveland).

Ichimura, S., Shimuzu, R. and Langeron, J.P. (1983), Surf. Sci. 124, L49.

Joshi, A., Davis, L.E. and Palmberg, P.W. (1975), in: "Methods of Surface Analysis", ed. A.W. Czanderna (Elsevier, Amsterdam) pp.159-222.

Kalinovich, D.F., Kovenskii, I.I. and Smolin, M.D. (1961), Fiz. Metal. Metalloved 11, 307.

Kelley, M.J. and Ponec, V. (1981), Prog. Surf. Sci. 11, 139.

Kelly, R. (1978), Nucl. Instr. Meth. 149, 553.

Kelly, R. (1980), Surf. Sci. 100, 85.

Kelly, R. (1984a), in: "Ion Bombardment Modifications of Surfaces", eds. O. Auciello and R. Kelly (Elsevier, Amsterdam) pp. 27-78.

Kelly, R. (1984b), Radiat. Eff. 80, 273.

Kelly, R. (1984c), in: "Chemistry and Physics of Solid Surfaces V", eds. R. Vanselow and R. Howe (Springer-Verlag, Berlin, Heidelberg, New York) pp. 159-182.

Kelly, R. (1985), Surf. Inter. Anal. 7, 1.

Kerker, G., Moran-Lopez, J.L. and Bennemann, K.H. (1977), Phys. Rev. B 15, 638.

King, H.W. (1966), J. Mater. Sci. 1, 79.

Kittel, C. (1976), in: "Introduction to Solid State Physics", 5th ed. (Wiley, New York). p. 32.

Kretschmeru, M. and Koch, K.H. (1977), Radex-Rundschau 4, 301.

Kumar, V. (1979), Surf. Sci. 84, 231.

Lambin, P.H. and Gaspard, J.P. (1980), J. Phys. F: Metal Phys. 10, 2413.

Lam, N.Q., Hoff, H.A., Wiedersich, H. and Rehn, L.E. (1985), Surf. Sci. 149, 517.

Lam, N.Q. and Rothman, S.J. (1975), in: "Radiation Damage in Metals" (ASM, Metals Park) pp. 125-156.

Langeron, J.P., Minel, L., Vignes, J.L., Bouquet, S., Pellerin, F., Lorang, G., Ailloud, P. and Le Hericy, J. (1984), Surf. Sci. 138, 610.

Lazarus, D. (1960), Solid State Phys. 10, 71.

Lea, C. and Seah, M.P. (1977), Phil. Mag. 35, 213.

Li, R.S., Koshikawa, T. and Goto, K. (1982), Surf. Sci. 121, L561.

Li, R.S. and Koshikawa, T. (1985), Surf. Sci. 151, 459.

Lindhard, J., Nielsen, V., Scharff, M. and Thomsen, P.V. (1963a), K. Dan. Vidensk. Selsk. Mat. Fys. Medd. 33, no. 10.

Lindhard, J., Scharff, M. and Schiott, H.E. (1963b), K. Dan. Vidensk. Selsk. Mat. Fys. Medd. 33, no. 14.

Lindhard, J., Nielsen, V. and Scharff, M. (1968), K. Dan. Vidensk. Selsk. Mat. Fys. Medd. 36, no. 10.

Marwick, A.D. (1983), in: "Surface Modification and Alloying by Laser, Ion and Electron Beams", eds. J. M. Poate, G. Foti and D.C. Jacobson (Plenum, New York and London) pp. 211.240.

Matsunami, N., Yamamura, Y., Itikawa, Y., Itoh, N., Kazumata, Y., Miyagawa, S., Morita, K., Shimuzu, R. and Tawara, H. (1983), "Energy Dependence of the Yields of Ion-Induced Sputtering of Monatomic Solids" (Inst. of Plasma Physics, Nagoya Univ., Nagoya, Japan).

McCargo, M., Davies, J.A. and Brown, F. (1963), Can. J. Phys. 41, 1231.

Mclean, D. (1957), "Grain Boundaries in Metals" (Oxford University Press, London),

Merkle, K.L. (1975), in: "Radiation Damage in Metals" (ASM, Metals Park) pp. 58-94.

Mervyn, D.A., Baird, R.J. and Wynblatt, P. (1979), Surf. Sci. 82, 79.

Miedema, A.R. (1978), Z. Metall. 69, 455.

Miedema, A.R., deChatel, P.F. and deBoer, F.R. (1980), Physica 100B, 1.

Moteff, J. (1967), in: "AIME Symposium on Radiation Effects", Radiation Effects Metallurgical Society Conference Vol 37, ed. W.F. Sheely (Gordon and Breach, New York) p. 267.

Mroczowski, S. and Lichtman, D. (1983a), Surf. Sci. 127, 119.

Mroczowski, S. and Lichtman, D. (1983b), Surf. Sci. 131, 159.

Mroczowski, S. and Lichtman, D. (1985), J. Vac. Sci. Technol. A 3, 1860.

Mrowec, S. (1980), "Defects and Diffusion in Solids" (Polish Scientific Publishers, Warrszawa).

Navinsek, B. (1977), Prog. Surf. Sci. 7, 49.

Nelson, J.B. and Riley, D.P. (1945), Proc. Phys. Soc. 57, 160.

Nihoul, J. (1970), in: "Vacancies and Interstitials in Metals", eds. A. Seeger, D. Schumacher, W. Schilling and J. Diehl (North-Holland, Amsterdam).

Overbury, S.H., Bertrand, P.A. and Somorjai, G.A. (1975), Chemical Reviews 75, 547.

Palmberg, P.W. (1973), Anal. Chem. 45, 549A.

Palmberg, P.W., Riach, G.E., Weber, R.E. and Macdonald, N.C. (1972), "Handbook of Auger Electron Spectroscopy" (Physical Electronics Industries Inc., Minneapolis, Minnesota).

Parkins, W.E., Dienes, G.J. and Brown, F.W. (1951), J. Appl. Phys. 22, 1012.

Pearson, W.B. (1958), "Handbook of Lattice Spacings and Structures of Metals and Alloys", Vol. 1 (Pergamon Press, New York).

Pearson, W.B. (1967), "Handbook of Lattice Spacings and Structures of Metals and Alloys", Vol. 2 (Pergamon Press, New York).

Penn, D.R. (1976), J. Electron Spectrosc. Relat. Phenom. 9, 29.

Petersen, K., Thrane, N. and Cotterill, R.M.J. (1974), Phil. Mag. 29, 9.

Peterson, N.L. (1968), Solid State Phys. 22, 409.

Peterson, N.L. and Siegel, R.W. eds. (1978), "Properties of Atomic Defects in Metals", Proceedings of the International Conference on the Properties of Atomic Defects in Metals (North Holland, Amsterdam).

Powell, C.J. (1985a), J. Vac. Sci. Technol. A 3, 1338.

Powell, C.J. (1985b), Surf. Inter. Anal. 7, 256.

Powell, C.J. (1985c), Surf. Inter. Anal. 7, 263.

Prutton, M. (1975), "Surface Physics" (Clarendon Press, Oxford).

Reimer, L. (1985), "Scanning Electron Microscopy: Physics of Image Formation and Microanalysis" (Springer-Verlag, Berlin, New-York).

Rehn, L.E. and Okamoto, P.R. (1983), in: "Phase Transformations During Irradiation", ed. F.V. Nolfi Jr. (Applied Science Publishers, London and New York) pp. 247-290.

Reuter, W. (1972), in: "Proc. 6th Intern. Conf. on X-ray Optics and Microanalysis", eds. G. Shinoda, K. Kohra and T. Ichinokawa (Univ. of Tokyo Press) p. 121.

Robinson, M.T. (1981), in: "Sputtering by Particle Bombardment I", Topics Appl. Phys., Vol. 47, ed. R. Behrisch (Springer-Verlag, Berlin, Heidelberg, New York) pp. 73-144.

Robinson, M.T. and Young, F.W., eds. (1975), "Fundamental Aspects of Radiation Damage in Metals" (ERDA Conf. 751006, Washington).

Rudy, E. (1969), "Compendium of Phase Diagram Data", U.S. Air Force Tech. Do. AFML-TR-65-2, Part V, Air Force Materials Laboratory.

Samuels, L.E. (1967), "Metallographic Polishing by Mechanical Methods" (Pitman, Melbourne and London).

Schilling, W. and Sonnenberg, K. (1973), J. Phys. F: Metal Phys. 3, 322.

Seah, M.P. (1972), Surf. Sci. 32, 703.

Seah, M.P. (1979), J. Catal. 57, 450.

Seah, M.P. (1980), J. Phys. F: Metal Phys. 10, 1043.

Seah, M.P. (1983a), in: "Practical Surface Analysis by Auger and X-ray Photoelectron Spectroscopy", eds. M.P. Seah and D. Briggs (John Wiley & Sons, Norwich) pp. 181-216.

Seah, M.P. (1983b), Scan. Electron Microsc. 2, 521.

Seah, M.P. and Briggs, D., eds. (1983), "Practical Surface Analysis by Auger and X-ray Photoelectron Spectroscopy" (John Wiley & Sons, Norwich).

Seah, M.P. and Dench, W.A. (1979), Surf. Int. Anal. 1, 2.

Seah, M.P. and Hondros, E.D. (1973), Proc. Roy. Soc. A 335, 191.

Seah, M.P. and Lea, C. (1975), Phil. Mag. 31, 627.

Seeger, A. (1962), in: "Radiation Damage in Solids", Vol. I (International Atomic Energy Agency, Vienna) p. 101.

Seeger, A. (1973), J. Phys. F: Metal Phys. 3, 248.

Seeger, A., Schumacher, D., Schilling, W. and Diehl, J., eds. (1970) "Vacancies and Interstitials in Metals" (North Holland, Amsterdam)

Seidman, D.N. (1973), J. Phys. F: Metal Phys. 3, 393.

Shapiro, M.H., Haff, P.K., Tombrello, T.A., Harrison, D.E. and Webb, R.P. (1985), Radiat. Eff. 89, 243.

Shewmon, P.G. (1963) "Diffusion in Solids" (McGraw-Hill, New York).

Shimuzu, H., Ono, M. and Nakayama, K. (1973), Surf. Sci. 36, 817.

Shimuzu, R. (1983), Jpn. J. Appl. Phys. 22, 1631.

Shunk, F.A. (1969), "Constitution of Binary Alloys" (McGraw-Hill, New York).

Sigmund, P. (1969a), Phys. Rev. 184, 383; 187, 768.

Sigmund, P. (1969b), Appl. Phys. Letts. 14, 114.

Sigmund, P. (1972a), Rev. Roum. Phys. 17, 823, 969, 1079.

Sigmund, P. (1972b), in: "Physics of Ionized Gases", ed. M. Kurepa (Inst. of Physics, Univ. Belgrade) p. 137.

Sigmund, P. (1979), J. Appl. Phys. 50, 7261.

Sigmund, P. (1980), J. Vac. Sci. Technol. 17(1), 396.

Sigmund, P. (1981), in: "Sputtering by Particle Bombardment I", Topics Appl. Phys., Vol. 47, ed. R. Behrisch (Springer-Verlag, Berlin, Heidelberg, New York) pp. 9-71.

Sigmund, P., Oliva, A. and Falcone, G. (1982), Nucl. Instr. Methods 194, 541.

Smallman, R.E. and Harris, J.E., eds. (1977), "Vacancies '76" (The Metals Society, Bristol).

Sully, A.H. and Brandes, E.A. (1967), "Metallurgy of the Rarer Metals I-Chromium" (Butterworth, London).

Sun. T.S., McNamara, D.K., Ahearn, J.S., Chen, J.M., Ditchek, B. and Venables, J.D. (1980), Appl. Surf. Sci. 5, 406.

Suezawa, M. and Kimura, H. (1973), Phil. Mag. 28, 901.

Sundaram, V.S. and Wynblatt, P. (1975), Surf. Sci. 52, 569.

Swalin, R.A. (1972), "Thermodynamics of Solids" (Wiley, New York).

Swartzfager, D.G. and Kelley, M.J. (1980), Phys. Lett. 76A, 86.

Szajman, J., Liesegang, J., Jenkin, J.G. and Leckey, R.C.G. (1981), J. Electron. Spectrosc. Relat. Phenom. 23, 97.

Thompson, M., Baker, M.D., Christie, A. and Tyson, S.F. (1984), "Auger Electron Spectroscopy", Chemical Analysis Vol. 74 (John Wiley & Sons, New York).

Tsai, N.H., Abraham, F.F. and Pound, G.M. (1977), J. Catal. 50, 200.

Van Santen, R.A. and Boersma, M.A.M. (1974), J. Catal. 33, 202.

Wagner, C.D., Davis, L.E. and Riggs, W.M. (1980), Surf. Interf. Anal. 2, 53.

Wehbi, D. and Roques-Carmes, C. (1984), J. Phys. Colloq. C2, 319

Wehner, G.K. (1985), J. Vac. Sci. Technol. A 3, 1821.

Werner, H.W. and Garten, R.P.H. (1984), Rep. Prog. Phys. 47, 221.

White, G., Hall, G.D. and Fisher, R. (1970), BISRA Open Report, MG/D/695/70.

Whitton, J.L., Tanovic, L. and Williams, J.S. (1978), Appl. Surf. Sci. 1, 408.

Wiedersich, H. (1983), in: "Surface Modification and Alloying by Laser, Ion and Electron Beams", eds. J.M. Poate, G. Foti and D.C. Jacobson (Plenum Press, New York) pp. 261-285.

Wiedersich, H. (1985), Nucl. Instr. Meth. B7/8, 1.

Wiedersich, H. and Lam, N.Q. (1983), in: "Phase Transformations During Irradiation", ed. F.V. Nolfi Jr. (Applied Science Publishers, London and New York) pp. 1-46.

Williams, F.L. and Nason, D. (1974), Surf. Sci. 45, 1974.

Wilkens, M. (1970), in: "Vacancies and Interstitials in Metals", eds. A. Seeger, D. Schumacher, W. Schilling and J. Diehl (North-Holland, Amsterdam) pp. 1-58.

Wilkens, M. (1974), in: "Application of Ion Beams to Metals", eds. S.T. Picraux, E.P. EerNisse and F.L. Vook (Plenum Publ. Corp., New York) pp. 441-458.

Wilkens, M. (1975), in: "Fundamental Aspects of Radiation Damage in Metals", eds. M.T. Robinson and F.W. Young (ERDA Conf. 751006, Washington) pp. 98-126.

Winterbon, K.B. (1975), "Ion Implantation Range and Energy Deposition Distributions", Vol. 2 (Plenum Press, New York and London).

Winterbon, K.B., Sigmund, P. and Sanders, J.B. (1970), K. Dan. Vidensk. Selsk. Mat. Fys. Medd. 37, no. 14.

Wynblatt, P. and Ku, R.C. (1977a), Surf. Sci. 65, 511

Wynblatt, P. and Ku, R.C. (1977b), in: "Interfacial Segregation", eds. W.C. Johnson and J.M. Blakely (ASM, Metals Park) pp. 115-136.

Wu, O.K.T. and Butler, E.M. (1982), J. Vac. Sci. Technol. 20, 453.

Wu, O.K.T., Peterson, G.G., LaRocca, W.J. and Butler, E.M. (1982), Appl. Surf. Sci. 11/12, 118.

Yamada, R., Saidoh., M., Sone, K. and Ohtsuka, H. (1979), J. Nucl. Mater. 82, 155.

Young, F.W. (1975), in: "Radiation Damage in Metals" (ASM, Metals Park) pp. 95-124.